The Interaction of Amyloid-β Peptide with Lipid Membranes and Glycosaminoglycans

INAUGURALDISSERTATION

zur

Erlangung der Würde eines Doktors der Philosophie

vorgelegt der

Philosophisch-Naturwissenschaftlichen Fakultät

der Universität Basel

von

Christian Thomas Benedikt Müller

aus

Lengnau AG und Dietikon ZH, Schweiz

Basel, 2012

Originaldokument gespeichert auf dem Dokumentenserver der Universität Basel
edoc.unibas.ch

Dieses Werk ist unter dem Vertrag „Creative Commons Namensnennung-Keine kommerzielle Nutzung-Keine Bearbeitung 2.5 Schweiz“ lizenziert. Die vollständige Lizenz kann unter
creativecommons.org/licences/by-nc-nd/2.5/ch
eingesehen werden.

creative commons

Namensnennung-Keine kommerzielle Nutzung-Keine Bearbeitung 2.5 Schweiz

---

Sie dürfen:

das Werk vervielfältigen, verbreiten und öffentlich zugänglich machen

Zu den folgenden Bedingungen:

Namensnennung. Sie müssen den Namen des Autors/Rechteinhabers in der von ihm festgelegten Weise nennen (wodurch aber nicht der Eindruck entstehen darf, Sie oder die Nutzung des Werkes durch Sie würden entlohnt).

Keine kommerzielle Nutzung. Dieses Werk darf nicht für kommerzielle Zwecke verwendet werden.

Keine Bearbeitung. Dieses Werk darf nicht bearbeitet oder in anderer Weise verändert werden.

- Im Falle einer Verbreitung müssen Sie anderen die Lizenzbedingungen, unter welche dieses Werk fällt, mitteilen. Am Einfachsten ist es, einen Link auf diese Seite einzubinden.
- Jede der vorgenannten Bedingungen kann aufgehoben werden, sofern Sie die Einwilligung des Rechteinhabers dazu erhalten.
- Diese Lizenz lässt die Urheberpersönlichkeitsrechte unberührt.

Die gesetzlichen Schranken des Urheberrechts bleiben hiervon unberührt.

Die Commons Deed ist eine Zusammenfassung des Lizenzvertrags in allgemeinverständlicher Sprache: http://creativecommons.org/licenses/by-nc-nd/2.5/ch/legalcode.de

Haftungsausschluss:
Die Commons Deed ist kein Lizenzvertrag. Sie ist lediglich ein Referenztext, der den zugrundeliegenden Lizenzvertrag übersichtlich und in allgemeinverständlicher Sprache wiedergibt. Die Deed selbst entfaltet keine juristische Wirkung und erscheint im eigentlichen Lizenzvertrag nicht. Creative Commons ist keine Rechtsanwaltsgesellschaft und leistet keine Rechtsberatung. Die Weitergabe und Verlinkung des Commons Deeds führt zu keinem Mandatsverhältnis.

Quelle: http://creativecommons.org/licenses/by-nc-nd/2.5/ch/ Datum: 3.4.2009

Genehmigt von der Philosophisch-Naturwissenschaftlichen Fakultät auf Antrag von

Prof. Dr. Joachim Seelig

Prof. Dr. Jörg Huwyler

Basel, den 26.06.2012

Prof. Dr. Martin Spiess (Dekan)

Table of Contents

1. Introduction

1.1. Amyloidosis

Proteins are macromolecules, composed of the 20 naturally occurring L-amino acids, which are involved in almost all biological processes. In order to function, proteins fold from a random coil state to their three-dimensional native conformation. Considering the prominent role of proteins and the complexity of their folding process, it is not surprising that protein misfolding might result in diseases (*1*). Several human protein misfolding diseases have been reported, of which the amyloidoses represent the largest group, including Alzheimer's disease, Parkinson's disease, Huntington's disease and type II diabetes (*2*). Amyloidoses are characterized by the deposits of amyloid fibrils, which are composed of a single peptide or protein. In general, these deposits are extracellular, although also intracellular deposits of amyloid fibrils have been observed (*3*). Although the precursor peptides/proteins of amyloid firbrils differ substantially with respect to size, sequence and structure, the corresponding amyloid fibrils show high similarity in both external morphology and internal structure (*4*). Amyloid fibrils are long, unbranched filaments with diameters of 60-120Å and composed of 2-6 subunits, named protofilaments, which are often twisted around one another (*5, 6*). In these protofilaments, the peptides/proteins exhibit the characteristic cross-β structure, in which the individual β-strands run perpendicular to the fibril axis (*7*). Interestingly, it has been observed that also non-amyloidogenic proteins can form amyloid fibrils under specific conditions (*8*). These observations support the idea that the formation of amyloid fibrils is a basic property

of the polypeptide chains. Although amyloid fibrils are strongly linked to diseases, there are also examples of nonpathological, functional amyloid fibrils (*2*)

1.2. Alzheimer's disease (AD)

In 1906, the German psychiatrist Alois Alzheimer (1864-1915) gave a talk at the 37th Conference of South-West German Psychiatrists in Tübingen, reporting on a new form of dementia. In his talk, he described the psychiatric symptoms and the changes in brain histology of an earlier patient Auguste Deter, who died at the age of 56 (*9*). Although Alzheimer's talk attracted very little attention from the audience, Emile Kraepelin, a famous German professor of psychiatry and Alzheimer's superior, introduced only four years later this newly discovered form of dementia in his textbook of psychiatry for students and practitioners and named it Alzheimer's disease (AD) (*10*).

Today, AD is the major form of dementia, responsible for nearly 60 to 80% of all dementia case (*11*). In 2005, the worldwide prevalence of dementia was estimated to be 24.3 million, with the highest predicted increase rates in China, India and Latin America (*12*). Two forms of AD are distinguished: the familial form (FAD), which accounts only for less than 5% of all cases, and the more prevalent sporadic form (*13*). FAD is caused by mutations in genes of amyloid precursor protein (APP) (*14*), presenilin 1 (*15*) and presenilin 2 (*16*) , and is characterized by the early onset of the disease (<60 years), whereas the sporadic form of AD (henceforth called AD) is rarely observed under the age of 65 years (*17*). Several risk factors have been reported for AD, including age (*18*), genetic factors (*19*), including apolipoprotein E

(*20*), type 2 diabetes mellitus (*21, 22*), depression (*23, 24*), body weight (*25, 26*), midlife hypertension (*27, 28*) and smoking (*29, 30*).

However, the major risk factor of the disease is age, as indicated by the increase of the age-specific incidence rate of AD from 0.1% at the age 60-65 to 12.1% for individuals aged over 95 years (*31*). Due to the expected increase in life expectancy, the impact of the disease will even increase in the future. For the year 2050, a worldwide prevalence of 106.2 million is predicted, meaning that 1 in 85 persons living with AD (*32*). Therefore, AD represents a major future challenge for the society, including the enormous financial burden of the disease. In 2008, the total cost of dementia in the European Union has been estimated to be € 160 billion, of which 56% were costs of informal care (*33*).

The core clinical features of AD is the gradual and progressive decline in cognitive functions, including memory (particular the short-term memory), orientation, language and executive function, and noncognitive and behavioral symptoms, such as unawareness of deficits, apathy, psychosis and agitation (*34*). The patients lose their ability to cope with daily activities and become dependent on caregivers. Although symptoms and rate of the disease vary considerable among different individuals, the end stage is associated with the almost complete loss of all cognitive functions, and death occurs usually by complications of aspiration, infection and inanition (*35*). The two major pathological hallmarks of AD are intracellular neurofibrillary tangles (NFTs), composed of the hyperphosphorylated tau protein (*36*), and extracellular senile plaques, which are mainly formed by the amyloid-β peptide (Aβ) (*37*). Further neuropathological changes include the loss of neurons and white matter, congophilic (amyloid) angiophaty and oxidative damage (*38*).

Despite enormous research effort, the exact pathological processes responsible for AD are still not completely understood. Although currently under debate (*39, 40*), the amyloid-beta hypothesis is the most accepted hypothesis for AD. The hypothesis states that the formation, aggregation and deposition of Aβ is the primary pathological event in AD (*41, 42*). Alternative hypothesis are the presenilin (*43, 44*) and the dual pathway hypothesis (*45*). Unfortunatly, there is currently still no drug available, which would prevent, stop or reverse the disease. Drugs approved by the FDA for the treatment of AD are cholinesterase inhibitors and N-methyl D-aspartate (NMDA), which regulates acetylcholine and glutamate in the brain (*46*). However, the benefits of these drugs are considered as only modest and transient (*47, 48*). The lack of an effective medication for AD emphasizes the importance of the prevention. Several of the above described risk factors of AD are partly or fully modifiable, such as body weight, hypertension and smoking. Several other factors have been reported to have preventive effect, such as physical activity (*49*), mediterranean diet (*50*) and extracts from turmeric, grapes and green tea (*51*). However, a national institute of health conference statement of 2010 concluded that there is not sufficient scientific evidence for the existence of modifiable factors (i.e. dietary factors, social or economic factors, or environmental exposures), which are associated with a reduced risk for AD (*52*)

AD is a slow, progressive disorder, which lacks a defined event which can be considered as the onset of the disease. The disease is divided into three stages with defined diagnosis guidelines: the preclinical statge (*53*), mild cognitive impairement (MCI) (*54*) and dementia (*55*). A growing body of evidence indicates that the pathological processes of AD begin years before the clinical symptoms emerge (*56*).

Therefore, the reliable diagnosis of the so-called preclinical stage of the disease is a prerequisite for the better understanding of AD and the development and testing of effective drugs.

1.3. Amyloid-β peptide (Aβ)

The 39 to 42 amino acids long amyloid-β peptide (Aβ) has an amphiphilic character with a hydrophilic N-terminus (residues 1-28) and a hydrophobic C-terminal domain (residues 29-40/42). As displayed in figure X, the hydrophilic part contains 6 acidic amino acids (D^{1}, E^{3}, D^{7}, E^{11}, E^{22} and D^{23}) with pKa values of 4.3-4.5, 3 basic amino acids (R^{5}, K^{16} and K^{18}) with pKa values of 10.2 and 3 histidine residues (H^{6}, H^{13} and H^{14}) with a pKa value of 6.5 (*57*). Therefore, the isoelectric point is 5.6, and the peptide has a net charge of -3.05 at pH 7.4.

Figure 1. Amino acid sequence of Aβ peptides in one letter code. Blue and red symbolize negatively and positively charged residues, whereas amino acids in grey correspond to the former membrane domain of the precursor protein of Aβ, the amyloid precursor protein (APP).

Aβ is formed by proteolytical processing of its precursor protein, the amyloid precursor protein (APP). APP is a type 1 transmembrane glycoprotein with a single membrane-spanning domain. Alternative splicing of the APP gene located on chromosome 21 leads to several isoforms, of which APP-695 is the most abundant in neurons (*58*). Although APP is present in many human tissues, its physiological role is poorly understood. In vitro and knockout studies (APP-deficient mice) suggested that APP may play a role in cell-cell adhesion (*59*), neurite outgrowth (*60*) and copper homeostasis (*61*). However, the further study of the physiological functions of APP is

considered as one of the major topic in future AD research (*62*). APP processing involves three types of proteases, termed α-, β-, and γ-secretases. Two principal processing pathways for APP are described: the amyloidogenic pathway and the non-amyloidogenic pathway. In the amyloidogenic pathway, the consecutive action of the β-, and γ-secretase leads to the formation of Aβ. β-secretase cleaves APP at the N-terminus of Aβ, generating a large N-terminal ectodomain APPsβ and the membrane-bound fragment C99. This cleavage process is considered as the initial and rate-limiting process (*63*). BACE 1, a membrane-bound aspartyl protease, was identified as β-secretase (*64-66*), and knockout studies demonstrated that it is the sole β-secretase (*67, 68*). This exclusivity makes the β-secretase to a promising target of drug development. As BACE 1 has an activity optimum at pH 4.5, this cleavage step occurs in the endosomes. The fragment C99 is intramembranously cleaved by the γ-secretase generating Aβ and APP intracellular domain (AICD). γ-secretase is a multi-subunit protease complex composed of minimal four membrane proteins: presenilin, nicastrin (Nct), APH-1 and PEN-2 (*69*). As the site of γ-cleavage is not precise, several isoforms of Aβ are generated, of which Aβ(1-40) and Aβ(1-42) are the most abundant (*70*). The subcellular site of γ-cleavage is the plasma membrane and the endosomal/lysosomal system (*70*).

Alternatively, in the non-amyloidogenic pathway the initial proteolysis step is processed by the α-secretase, which cleaves APP between Lys16 and Leu 17 in the Aβ domain (*71*). The α-cleavage occurs mainly at the cell surface, generating a large amino (N)-terminal ectodomain (sAPPα), which is released into the extracellular space, and a membrane-bound C-terminal fragment (C83). The fragment C83 is

further processed by γ-secretase, producing a truncated Aβ peptide named p3 and AICD (*72*), and therefore precluding the formation of Aβ.

Aβ show polymorphic structures in solution, depending on the peptide concentration (*73*) and the environmental conditions, such as pH (*74*), salt (*75*), temperature (*76*) and solvent (*77*). In aqueous solution, monomeric Aβ exhibits a predominant random coil structure (*73*), whereas in organic solvent and membrane-mimicking systems Aβ favors an α-helical structure (*78, 79*). Aβ is prone to aggregate, forming oligomers, protofibrils and amyloid fibrils. In vitro, the aggregation process occurs in a nucleation-dependent reaction, similar to crystallization (*80*). A close link between the aggregation state and the neurotoxicity of Aβ has been established, although the exact molecular mechanisms of the Aβ toxicity are still unknown. In the beginning, the amyloid fibrils of Aβ were considered as the main source of Aβ toxicity (*81, 82*). However, recent studies indicated that non-fibrillar structure of Aβ, such as oligomers, amyloid-derived diffusible ligands (ADDLs) and protofibrils are more toxic (*83-85*). On the other hand, the monomeric Aβ has a very low toxic activity (*86*).

Aβ has termed as "peptide from hell" not only because its putative toxic effect on neurons, but particular because the biophysical and biochemical handling is full of difficulties (*87*). A major problem is the low reproducibility in studies, investigating the kinetics of Aβ fibrillization and its neurotoxicity activity (*88*). Differences arise not only between Aβ purchased from different suppliers, but also between batches from the same manufacturer. In this respect, starting conformation and the aggregational state of the lyophilized peptide is seen as the major source of irreproducibility (*87*). Pre-existing aggregates can act as seeds in the Aβ fibrillization,

and therefore affect both the kinetic of fibrillization process and the neurotoxic activity (*80, 89*). To remove any pre-existing aggregates, Aβ are usually treated with strong acids and organic solvents, such as hexafluoroisopropanol (HFIP), trifluoroacetic acid (TFA) and dimethylsulfoxide (DMSO). Furthermore, stock solutions of Aβ in aqueous buffer systems (higher than the corresponding critical concentration) should be avoided due to time-dependence of the Aβ aggregation process. Quantitative research with Aβ is moreover complicated by the lack of a tryptophan in the peptide sequence. UV absorbance is therefore precluded as a method to determine the peptide concentration. However, amino acid analysis is an accurate technique to determine the Aβ concentration.

1.4. Biological membranes

An important step in the origin of the first cellular life was the formation of a boundary structure, which separates the inside from the outside (*90*). In addition to their (selective) permeability barrier function, early membranes were assigned for further functions, including the capture of energy and its conversion into a suitable energy currency (*91*). These early membranes were composed of simple amphiphiles, such as fatty acids, fatty alcohols or monoglycerides (*92*). These molecules were formed under the prebiotic conditions on earth (*93*), and/or could be brought to earth via meteorites (*94*). However, it is still an unsolved mystery in the origins of cells, how the complex cytoplasm, containing ribosomes, nucleotides, RNA and even DNA got enclosed by the membrane. In the first scenario, the cellular system have evolved within the membrane boundary (*95*). Cellular precursor molecules would have crossed the early membrane, which, mainly composed of simple amphiphiles, have a

lower permeability compared to phospholipid bilayers (*96*). Alternatively, the second scenario suggests that the cytoplasm evolved to a large extent outside from a membrane shell, before it was engulfed by a lipid layer (*97*).

Membranes of contemporary cells are involved in even more cellular processes, which is reflected in an more complex composition. These membranes are mainly composed of lipids and proteins, with a minor fraction of carbohydrates, which are covalently attached to either lipids (glycolipids) or proteins (glycoproteins) (*98*). In membrane, lipids are arranged in a bilayer structure, in which the hydrophobic domains constitute the hydrophobic core, whereas their hydrophilic domains interact with water (*99*). Mammalian membrane lipids can be divided into phospholipids, sphingolipids and the sterols (*100*). While cholesterol is almost the sole sterol in mammalian membranes, there exists a large diversity of phospho-and sphingolipids, by variations of the headgroup, chain length and extent of cis-unsaturations. As the lipid composition is tightly regulated in the different parts of the human body, it is not surprising that several diseases are associated with an aberrant lipid metabolism (*101*).

1.5. Literature

1. Dobson, C. M. (2004) Principles of protein folding, misfolding and aggregation, *Semin Cell Dev Biol 15*, 3-16.
2. Chiti, F., and Dobson, C. M. (2006) Protein misfolding, functional amyloid, and human disease, *Annu Rev Biochem 75*, 333-366.
3. Serpell, L. C., Berriman, J., Jakes, R., Goedert, M., and Crowther, R. A. (2000) Fiber diffraction of synthetic alpha-synuclein filaments shows amyloid-like cross-beta conformation, *Proc Natl Acad Sci U S A 97*, 4897-4902.
4. Stefani, M., and Dobson, C. M. (2003) Protein aggregation and aggregate toxicity: new insights into protein folding, misfolding diseases and biological evolution, *J Mol Med (Berl) 81*, 678-699.
5. Shirahama, T., and Cohen, A. S. (1967) High-resolution electron microscopic analysis of the amyloid fibril, *J Cell Biol 33*, 679-708.
6. Serpell, L. C., Sunde, M., Benson, M. D., Tennent, G. A., Pepys, M. B., and Fraser, P. E. (2000) The protofilament substructure of amyloid fibrils, *J Mol Biol 300*, 1033-1039.
7. Sunde, M., Serpell, L. C., Bartlam, M., Fraser, P. E., Pepys, M. B., and Blake, C. C. (1997) Common core structure of amyloid fibrils by synchrotron X-ray diffraction, *J Mol Biol 273*, 729-739.
8. Fandrich, M., Fletcher, M. A., and Dobson, C. M. (2001) Amyloid fibrils from muscle myoglobin, *Nature 410*, 165-166.
9. Alzheimer, A. (1906) Über einen eigenartigen schweren Erkrankungsprozeß der Hirnrinde, *Neurologisches Centralblatt 23*, 1129-1136.
10. Kraepelin, E. (1910) *Psychiatrie: Ein Lehrbuch für Studierende und Ärzte.*, Leipzig: Barth.
11. Barnes, D. E., and Yaffe, K. (2011) The projected effect of risk factor reduction on Alzheimer's disease prevalence, *Lancet Neurol 10*, 819-828.
12. Ferri, C. P., Prince, M., Brayne, C., Brodaty, H., Fratiglioni, L., Ganguli, M., Hall, K., Hasegawa, K., Hendrie, H., Huang, Y., Jorm, A., Mathers, C., Menezes, P. R., Rimmer, E., and Scazufca, M. (2005) Global prevalence of dementia: a Delphi consensus study, *Lancet 366*, 2112-2117.
13. Hutton, M., and Hardy, J. (1997) The presenilins and Alzheimer's disease, *Hum Mol Genet 6*, 1639-1646.
14. Goate, A., Chartier-Harlin, M. C., Mullan, M., Brown, J., Crawford, F., Fidani, L., Giuffra, L., Haynes, A., Irving, N., James, L., and et al. (1991) Segregation of a missense mutation in the amyloid precursor protein gene with familial Alzheimer's disease, *Nature 349*, 704-706.
15. Sherrington, R., Rogaev, E. I., Liang, Y., Rogaeva, E. A., Levesque, G., Ikeda, M., Chi, H., Lin, C., Li, G., Holman, K., Tsuda, T., Mar, L., Foncin, J. F., Bruni, A. C., Montesi, M. P., Sorbi, S., Rainero, I., Pinessi, L., Nee, L., Chumakov, I., Pollen, D., Brookes, A., Sanseau, P., Polinsky, R. J., Wasco, W., Da Silva, H. A., Haines, J. L., Perkicak-Vance, M. A., Tanzi, R. E., Roses, A. D., Fraser, P. E., Rommens, J. M., and St George-Hyslop, P. H. (1995) Cloning of a gene bearing missense mutations in early-onset familial Alzheimer's disease, *Nature 375*, 754-760.

16. Rogaev, E. I., Sherrington, R., Rogaeva, E. A., Levesque, G., Ikeda, M., Liang, Y., Chi, H., Lin, C., Holman, K., Tsuda, T., and et al. (1995) Familial Alzheimer's disease in kindreds with missense mutations in a gene on chromosome 1 related to the Alzheimer's disease type 3 gene, *Nature 376*, 775-778.
17. Reitz, C., Brayne, C., and Mayeux, R. (2011) Epidemiology of Alzheimer disease, *Nat Rev Neurol 7*, 137-152.
18. Katzman, R., and Saitoh, T. (1991) Advances in Alzheimer's disease, *Faseb J 5*, 278-286.
19. Daw, E. W., Payami, H., Nemens, E. J., Nochlin, D., Bird, T. D., Schellenberg, G. D., and Wijsman, E. M. (2000) The number of trait loci in late-onset Alzheimer disease, *Am J Hum Genet 66*, 196-204.
20. Corder, E. H., Saunders, A. M., Strittmatter, W. J., Schmechel, D. E., Gaskell, P. C., Small, G. W., Roses, A. D., Haines, J. L., and Pericak-Vance, M. A. (1993) Gene dose of apolipoprotein E type 4 allele and the risk of Alzheimer's disease in late onset families, *Science 261*, 921-923.
21. Ott, A., Stolk, R. P., van Harskamp, F., Pols, H. A., Hofman, A., and Breteler, M. M. (1999) Diabetes mellitus and the risk of dementia: The Rotterdam Study, *Neurology 53*, 1937-1942.
22. Biessels, G. J., Staekenborg, S., Brunner, E., Brayne, C., and Scheltens, P. (2006) Risk of dementia in diabetes mellitus: a systematic review, *Lancet Neurol 5*, 64-74.
23. Jorm, A. F. (2001) History of depression as a risk factor for dementia: an updated review, *Aust N Z J Psychiatry 35*, 776-781.
24. Ownby, R. L., Crocco, E., Acevedo, A., John, V., and Loewenstein, D. (2006) Depression and risk for Alzheimer disease: systematic review, meta-analysis, and metaregression analysis, *Arch Gen Psychiatry 63*, 530-538.
25. Gustafson, D., Rothenberg, E., Blennow, K., Steen, B., and Skoog, I. (2003) An 18-year follow-up of overweight and risk of Alzheimer disease, *Arch Intern Med 163*, 1524-1528.
26. Razay, G., and Vreugdenhil, A. (2005) Obesity in middle age and future risk of dementia: midlife obesity increases risk of future dementia, *Bmj 331*, 455; author reply 455.
27. Launer, L. J., Ross, G. W., Petrovitch, H., Masaki, K., Foley, D., White, L. R., and Havlik, R. J. (2000) Midlife blood pressure and dementia: the Honolulu-Asia aging study, *Neurobiol Aging 21*, 49-55.
28. Qiu, C., Winblad, B., and Fratiglioni, L. (2005) The age-dependent relation of blood pressure to cognitive function and dementia, *Lancet Neurol 4*, 487-499.
29. Ott, A., Slooter, A. J., Hofman, A., van Harskamp, F., Witteman, J. C., Van Broeckhoven, C., van Duijn, C. M., and Breteler, M. M. (1998) Smoking and risk of dementia and Alzheimer's disease in a population-based cohort study: the Rotterdam Study, *Lancet 351*, 1840-1843.
30. Merchant, C., Tang, M. X., Albert, S., Manly, J., Stern, Y., and Mayeux, R. (1999) The influence of smoking on the risk of Alzheimer's disease, *Neurology 52*, 1408-1412.
31. Brookmeyer, R., Gray, S., and Kawas, C. (1998) Projections of Alzheimer's disease in the United States and the public health impact of delaying disease onset, *Am J Public Health 88*, 1337-1342.

32. Brookmeyer, R., Johnson, E., Ziegler-Graham, K., and Arrighi, H. M. (2007) Forecasting the global burden of Alzheimer's disease, *Alzheimers Dement 3*, 186-191.
33. Wimo, A., Jonsson, L., Gustavsson, A., McDaid, D., Ersek, K., Georges, J., Gulacsi, L., Karpati, K., Kenigsberg, P., and Valtonen, H. (2011) The economic impact of dementia in Europe in 2008-cost estimates from the Eurocode project, *Int J Geriatr Psychiatry 26*, 825-832.
34. David S. Geldmacher, M. D. (2009) Alzheimer Disease, In *The American Psychiatric Publishing Textbook of Alzheimer Disease and Other Dementias* (Myron F. Weiner, M. D., and Anne M. Lipton, M.D., Ph.D., Ed.), American Psychiatric Publishing, Inc., Arlington, VA, USA.
35. Tarawneh, R., and Holtzman, D. M. (2012) The clinical problem of symptomatic Alzheimer disease and mild cognitive impairment, *Cold Spring Harb Perspect Med 2*, a006148.
36. Grundke-Iqbal, I., Iqbal, K., Quinlan, M., Tung, Y. C., Zaidi, M. S., and Wisniewski, H. M. (1986) Microtubule-associated protein tau. A component of Alzheimer paired helical filaments, *J Biol Chem 261*, 6084-6089.
37. Glenner, G. G., and Wong, C. W. (1984) Alzheimer's disease and Down's syndrome: sharing of a unique cerebrovascular amyloid fibril protein, *Biochem Biophys Res Commun 122*, 1131-1135.
38. Querfurth, H. W., and LaFerla, F. M. (2010) Alzheimer's disease, *N Engl J Med 362*, 329-344.
39. Golde, T. E., Schneider, L. S., and Koo, E. H. (2011) Anti-abeta therapeutics in Alzheimer's disease: the need for a paradigm shift, *Neuron 69*, 203-213.
40. Holtzman, D. M., Morris, J. C., and Goate, A. M. (2011) Alzheimer's disease: the challenge of the second century, *Sci Transl Med 3*, 77sr71.
41. Hardy, J. A., and Higgins, G. A. (1992) Alzheimer's disease: the amyloid cascade hypothesis, *Science 256*, 184-185.
42. Hardy, J., and Selkoe, D. J. (2002) The amyloid hypothesis of Alzheimer's disease: progress and problems on the road to therapeutics, *Science 297*, 353-356.
43. Sambamurti, K., Suram, A., Venugopal, C., Prakasam, A., Zhou, Y., Lahiri, D. K., and Greig, N. H. (2006) A partial failure of membrane protein turnover may cause Alzheimer's disease: a new hypothesis, *Curr Alzheimer Res 3*, 81-90.
44. Shen, J., and Kelleher, R. J., 3rd. (2007) The presenilin hypothesis of Alzheimer's disease: evidence for a loss-of-function pathogenic mechanism, *Proc Natl Acad Sci U S A 104*, 403-409.
45. Small, S. A., and Duff, K. (2008) Linking Abeta and tau in late-onset Alzheimer's disease: a dual pathway hypothesis, *Neuron 60*, 534-542.
46. Salloway, S., and Correia, S. (2009) Alzheimer disease: time to improve its diagnosis and treatment, *Cleve Clin J Med 76*, 49-58.
47. Lleo, A., Greenberg, S. M., and Growdon, J. H. (2006) Current pharmacotherapy for Alzheimer's disease, *Annu Rev Med 57*, 513-533.
48. van Marum, R. J. (2008) Current and future therapy in Alzheimer's disease, *Fundam Clin Pharmacol 22*, 265-274.
49. Etgen, T., Sander, D., Huntgeburth, U., Poppert, H., Forstl, H., and Bickel, H. (2010) Physical activity and incident cognitive impairment in elderly persons: the INVADE study, *Arch Intern Med 170*, 186-193.

50. Scarmeas, N., Stern, Y., Tang, M. X., Mayeux, R., and Luchsinger, J. A. (2006) Mediterranean diet and risk for Alzheimer's disease, *Ann Neurol 59*, 912-921.
51. Kim, J., Lee, H. J., and Lee, K. W. (2010) Naturally occurring phytochemicals for the prevention of Alzheimer's disease, *J Neurochem 112*, 1415-1430.
52. Daviglus, M. L., Bell, C. C., Berrettini, W., Bowen, P. E., Connolly, E. S., Jr., Cox, N. J., Dunbar-Jacob, J. M., Granieri, E. C., Hunt, G., McGarry, K., Patel, D., Potosky, A. L., Sanders-Bush, E., Silberberg, D., and Trevisan, M. (2010) National Institutes of Health State-of-the-Science Conference statement: preventing alzheimer disease and cognitive decline, *Ann Intern Med 153*, 176-181.
53. Sperling, R. A., Aisen, P. S., Beckett, L. A., Bennett, D. A., Craft, S., Fagan, A. M., Iwatsubo, T., Jack, C. R., Jr., Kaye, J., Montine, T. J., Park, D. C., Reiman, E. M., Rowe, C. C., Siemers, E., Stern, Y., Yaffe, K., Carrillo, M. C., Thies, B., Morrison-Bogorad, M., Wagster, M. V., and Phelps, C. H. (2011) Toward defining the preclinical stages of Alzheimer's disease: recommendations from the National Institute on Aging-Alzheimer's Association workgroups on diagnostic guidelines for Alzheimer's disease, *Alzheimers Dement 7*, 280-292.
54. Albert, M. S., DeKosky, S. T., Dickson, D., Dubois, B., Feldman, H. H., Fox, N. C., Gamst, A., Holtzman, D. M., Jagust, W. J., Petersen, R. C., Snyder, P. J., Carrillo, M. C., Thies, B., and Phelps, C. H. (2011) The diagnosis of mild cognitive impairment due to Alzheimer's disease: recommendations from the National Institute on Aging-Alzheimer's Association workgroups on diagnostic guidelines for Alzheimer's disease, *Alzheimers Dement 7*, 270-279.
55. McKhann, G. M., Knopman, D. S., Chertkow, H., Hyman, B. T., Jack, C. R., Jr., Kawas, C. H., Klunk, W. E., Koroshetz, W. J., Manly, J. J., Mayeux, R., Mohs, R. C., Morris, J. C., Rossor, M. N., Scheltens, P., Carrillo, M. C., Thies, B., Weintraub, S., and Phelps, C. H. (2011) The diagnosis of dementia due to Alzheimer's disease: recommendations from the National Institute on Aging-Alzheimer's Association workgroups on diagnostic guidelines for Alzheimer's disease, *Alzheimers Dement 7*, 263-269.
56. Morris, J. C. (2005) Early-stage and preclinical Alzheimer disease, *Alzheimer Dis Assoc Disord 19*, 163-165.
57. Ma, K., Clancy, E. L., Zhang, Y., Ray, D. G., Wollenberg, D., and Zagorski, M. G. (1999) Residue-Specific pKa Measurements of the β-Peptide and Mechanism of pH-Induced Amyloid Formation, *J. Am. Chem. Soc. 121*, 8698 - 8706.
58. Ponte, P., Gonzalez-DeWhitt, P., Schilling, J., Miller, J., Hsu, D., Greenberg, B., Davis, K., Wallace, W., Lieberburg, I., and Fuller, F. (1988) A new A4 amyloid mRNA contains a domain homologous to serine proteinase inhibitors, *Nature 331*, 525-527.
59. Mattson, M. P. (1997) Cellular actions of beta-amyloid precursor protein and its soluble and fibrillogenic derivatives, *Physiol Rev 77*, 1081-1132.
60. Muller, U., Cristina, N., Li, Z. W., Wolfer, D. P., Lipp, H. P., Rulicke, T., Brandner, S., Aguzzi, A., and Weissmann, C. (1994) Behavioral and anatomical deficits in mice homozygous for a modified beta-amyloid precursor protein gene, *Cell 79*, 755-765.

61. White, A. R., Reyes, R., Mercer, J. F., Camakaris, J., Zheng, H., Bush, A. I., Multhaup, G., Beyreuther, K., Masters, C. L., and Cappai, R. (1999) Copper levels are increased in the cerebral cortex and liver of APP and APLP2 knockout mice, *Brain Res 842*, 439-444.
62. Hardy, J. (2009) The amyloid hypothesis for Alzheimer's disease: a critical reappraisal, *J Neurochem 110*, 1129-1134.
63. Vassar, R. (2004) BACE1: the beta-secretase enzyme in Alzheimer's disease, *J Mol Neurosci 23*, 105-114.
64. Hussain, I., Powell, D., Howlett, D. R., Tew, D. G., Meek, T. D., Chapman, C., Gloger, I. S., Murphy, K. E., Southan, C. D., Ryan, D. M., Smith, T. S., Simmons, D. L., Walsh, F. S., Dingwall, C., and Christie, G. (1999) Identification of a novel aspartic protease (Asp 2) as beta-secretase, *Mol Cell Neurosci 14*, 419-427.
65. Sinha, S., Anderson, J. P., Barbour, R., Basi, G. S., Caccavello, R., Davis, D., Doan, M., Dovey, H. F., Frigon, N., Hong, J., Jacobson-Croak, K., Jewett, N., Keim, P., Knops, J., Lieberburg, I., Power, M., Tan, H., Tatsuno, G., Tung, J., Schenk, D., Seubert, P., Suomensaari, S. M., Wang, S., Walker, D., Zhao, J., McConlogue, L., and John, V. (1999) Purification and cloning of amyloid precursor protein beta-secretase from human brain, *Nature 402*, 537-540.
66. Vassar, R., Bennett, B. D., Babu-Khan, S., Kahn, S., Mendiaz, E. A., Denis, P., Teplow, D. B., Ross, S., Amarante, P., Loeloff, R., Luo, Y., Fisher, S., Fuller, J., Edenson, S., Lile, J., Jarosinski, M. A., Biere, A. L., Curran, E., Burgess, T., Louis, J. C., Collins, F., Treanor, J., Rogers, G., and Citron, M. (1999) Beta-secretase cleavage of Alzheimer's amyloid precursor protein by the transmembrane aspartic protease BACE, *Science 286*, 735-741.
67. Cai, H., Wang, Y., McCarthy, D., Wen, H., Borchelt, D. R., Price, D. L., and Wong, P. C. (2001) BACE1 is the major beta-secretase for generation of Abeta peptides by neurons, *Nat Neurosci 4*, 233-234.
68. Roberds, S. L., Anderson, J., Basi, G., Bienkowski, M. J., Branstetter, D. G., Chen, K. S., Freedman, S. B., Frigon, N. L., Games, D., Hu, K., Johnson-Wood, K., Kappenman, K. E., Kawabe, T. T., Kola, I., Kuehn, R., Lee, M., Liu, W., Motter, R., Nichols, N. F., Power, M., Robertson, D. W., Schenk, D., Schoor, M., Shopp, G. M., Shuck, M. E., Sinha, S., Svensson, K. A., Tatsuno, G., Tintrup, H., Wijsman, J., Wright, S., and McConlogue, L. (2001) BACE knockout mice are healthy despite lacking the primary beta-secretase activity in brain: implications for Alzheimer's disease therapeutics, *Hum Mol Genet 10*, 1317-1324.
69. Edbauer, D., Winkler, E., Regula, J. T., Pesold, B., Steiner, H., and Haass, C. (2003) Reconstitution of gamma-secretase activity, *Nat Cell Biol 5*, 486-488.
70. Dries, D. R., and Yu, G. (2008) Assembly, maturation, and trafficking of the gamma-secretase complex in Alzheimer's disease, *Curr Alzheimer Res 5*, 132-146.
71. Esch, F. S., Keim, P. S., Beattie, E. C., Blacher, R. W., Culwell, A. R., Oltersdorf, T., McClure, D., and Ward, P. J. (1990) Cleavage of amyloid beta peptide during constitutive processing of its precursor, *Science 248*, 1122-1124.
72. Haass, C., Hung, A. Y., Schlossmacher, M. G., Teplow, D. B., and Selkoe, D. J. (1993) beta-Amyloid peptide and a 3-kDa fragment are derived by distinct cellular mechanisms, *J Biol Chem 268*, 3021-3024.

73. Terzi, E., Holzemann, G., and Seelig, J. (1995) Self-association of beta-amyloid peptide (1-40) in solution and binding to lipid membranes, *J Mol Biol 252*, 633-642.
74. Huang, T. H., Yang, D. S., Plaskos, N. P., Go, S., Yip, C. M., Fraser, P. E., and Chakrabartty, A. (2000) Structural studies of soluble oligomers of the Alzheimer beta-amyloid peptide, *J Mol Biol 297*, 73-87.
75. Klement, K., Wieligmann, K., Meinhardt, J., Hortschansky, P., Richter, W., and Fandrich, M. (2007) Effect of different salt ions on the propensity of aggregation and on the structure of Alzheimer's abeta(1-40) amyloid fibrils, *J Mol Biol 373*, 1321-1333.
76. Gursky, O., and Aleshkov, S. (2000) Temperature-dependent beta-sheet formation in beta-amyloid Abeta(1-40) peptide in water: uncoupling beta-structure folding from aggregation, *Biochim Biophys Acta 1476*, 93-102.
77. Serpell, L. C. (2000) Alzheimer's amyloid fibrils: structure and assembly, *Biochim Biophys Acta 1502*, 16-30.
78. Barrow, C. J., and Zagorski, M. G. (1991) Solution structures of beta peptide and its constituent fragments: relation to amyloid deposition, *Science 253*, 179-182.
79. Coles, M., Bicknell, W., Watson, A. A., Fairlie, D. P., and Craik, D. J. (1998) Solution structure of amyloid beta-peptide(1-40) in a water-micelle environment. Is the membrane-spanning domain where we think it is?, *Biochemistry 37*, 11064-11077.
80. Harper, J. D., and Lansbury, P. T., Jr. (1997) Models of amyloid seeding in Alzheimer's disease and scrapie: mechanistic truths and physiological consequences of the time-dependent solubility of amyloid proteins, *Annu Rev Biochem 66*, 385-407.
81. Pike, C. J., Walencewicz, A. J., Glabe, C. G., and Cotman, C. W. (1991) In vitro aging of beta-amyloid protein causes peptide aggregation and neurotoxicity, *Brain Res 563*, 311-314.
82. Roher, A. E., Ball, M. J., Bhave, S. V., and Wakade, A. R. (1991) Beta-amyloid from Alzheimer disease brains inhibits sprouting and survival of sympathetic neurons, *Biochem Biophys Res Commun 174*, 572-579.
83. Walsh, D. M., Klyubin, I., Fadeeva, J. V., Cullen, W. K., Anwyl, R., Wolfe, M. S., Rowan, M. J., and Selkoe, D. J. (2002) Naturally secreted oligomers of amyloid beta protein potently inhibit hippocampal long-term potentiation in vivo, *Nature 416*, 535-539.
84. Lambert, M. P., Barlow, A. K., Chromy, B. A., Edwards, C., Freed, R., Liosatos, M., Morgan, T. E., Rozovsky, I., Trommer, B., Viola, K. L., Wals, P., Zhang, C., Finch, C. E., Krafft, G. A., and Klein, W. L. (1998) Diffusible, nonfibrillar ligands derived from Abeta1-42 are potent central nervous system neurotoxins, *Proc Natl Acad Sci U S A 95*, 6448-6453.
85. Hartley, D. M., Walsh, D. M., Ye, C. P., Diehl, T., Vasquez, S., Vassilev, P. M., Teplow, D. B., and Selkoe, D. J. (1999) Protofibrillar intermediates of amyloid beta-protein induce acute electrophysiological changes and progressive neurotoxicity in cortical neurons, *J Neurosci 19*, 8876-8884.
86. Ono, K., Condron, M. M., and Teplow, D. B. (2009) Structure-neurotoxicity relationships of amyloid beta-protein oligomers, *Proc Natl Acad Sci U S A 106*, 14745-14750.

87. Zagorski, M. G., Yang, J., Shao, H., Ma, K., Zeng, H., and Hong, A. (1999) Methodological and chemical factors affecting amyloid beta peptide amyloidogenicity, *Methods Enzymol 309*, 189-204.
88. Fezoui, Y., Hartley, D. M., Harper, J. D., Khurana, R., Walsh, D. M., Condron, M. M., Selkoe, D. J., Lansbury, P. T., Jr., Fink, A. L., and Teplow, D. B. (2000) An improved method of preparing the amyloid beta-protein for fibrillogenesis and neurotoxicity experiments, *Amyloid 7*, 166-178.
89. Snyder, S. W., Ladror, U. S., Wade, W. S., Wang, G. T., Barrett, L. W., Matayoshi, E. D., Huffaker, H. J., Krafft, G. A., and Holzman, T. F. (1994) Amyloid-beta aggregation: selective inhibition of aggregation in mixtures of amyloid with different chain lengths, *Biophys J 67*, 1216-1228.
90. Szostak, J. W., Bartel, D. P., and Luisi, P. L. (2001) Synthesizing life, *Nature 409*, 387-390.
91. Deamer, D. W., and Dworkin, J. P. (2005) Chemistry and physics of primitive membranes, *Top Curr Chem 259*, 1-27.
92. Monnard, P. A., and Deamer, D. W. (2002) Membrane self-assembly processes: Steps toward the first cellular life, *Anat Record 268*, 196-207.
93. Deamer, D. W., and Oro, J. (1980) Role of lipids in prebiotic structures, *Biosystems 12*, 167-175.
94. Mautner, M., Leonard, R. L., and Deamer, D. W. (1985) Meteorite organics in planetary envrionments: hydrothermal release, surface activity and microbial utilization, *Planet Space Sci 43*, 139-147.
95. Luisi, P. L., Ferri, F., and Stano, P. (2006) Approaches to semi-synthetic minimal cells: a review, *Naturwissenschaften 93*, 1-13.
96. Griffiths, G. (2007) Cell evolution and the problem of membrane topology, *Nat Rev Mol Cell Biol 8*, 1018-1024.
97. Blobel, G. (1980) Intracellular protein topogenesis, *Proc Natl Acad Sci U S A 77*, 1496-1500.
98. Seelig, A., and Seelig, J. (2002) Membrane Structure, In *Encyclopedia of Physical Science and Technology* (Meyers, R. A., Ed.) 3rd ed., pp 355-367, N.Y.: Academic Press.
99. Wilkins, M. H., Blaurock, A. E., and Engelman, D. M. (1971) Bilayer structure in membranes, *Nat New Biol 230*, 72-76.
100. Simons, K., and Sampaio, J. L. (2011) Membrane organization and lipid rafts, *Cold Spring Harb Perspect Biol 3*, a004697.
101. Wenk, M. R. (2005) The emerging field of lipidomics, *Nat Rev Drug Discov 4*, 594-610.

2. Thermodynamics of the random-coil-to-β-sheet transition of Aβ(1-40) in a membrane environment

Summary

Alzheimer's disease (AD) is the most common form of dementia with a worldwide prevalence of 20 to 30 million. The amyloid-β peptide (Aβ) is the main component of the amyloid plaques, which are considered as the major pathological hallmark of the disease. Aβ(1-40) reveals a random-coil-to-β-structure transition in the presence of anionic small unilamellar vesicles (SUVs). An additional structural transition of Aβ(1-40) to an α-helical structure can be observed at high lipid-to-peptide molar ratios. Here, we present a method to quantitatively determine the thermodynamic parameters of the random-coil-to-β-structure transition in the membrane environment. We have used Aβ(1-40) and four double-d isomers, in which two adjacent amino acids are replaced by their d-enantiomers. Double-d substitution has shown to result in a local disturbance of secondary structure without modifying other characteristics such as hydrophobicity and side-chain functionality. Circular dichroism (CD) spectroscopy provides the content of β-structure in solution and upon binding to anionic lipid membranes. By the use of anionic lipid vesicles containing 5mol% PEG-PE, the transition to α-helix is inhibited and a conformational endpoint is observed. Thermodynamic parameters of membrane binding were determined with isothermal titration calorimetry. Linear regression analysis yields a linear correlation between the thermodynamic binding parameters and the extent of β-structure. β-structure formation of Aβ(1-40) at the membrane surface is thermodynamically characterized

by enthalpy change of $\Delta H_\beta = -1.01 kcal/mol$ per residue, an entropy change of $\Delta S_\beta = -3.62 cal/molK$ residue and a free energy change of $\Delta G_\beta = -0.04 kcal/mol$ residue.

Manuscript: Thermodynamics of the random-coil-to-β-sheet transition of Aβ(1-40) in a membrane environment

Introduction

Alzheimer's disease (AD) is the major form of dementia, affecting estimated 25 million people worldwide in 2005 (*1*). Predictions for the future indicate an dramatic increase of the worldwide prevalence of AD (106.2 million in 2050) (*2*). Despite enormous efforts, there is still no effective cure available for the disease. Besides the personal suffering of patients and their families, AD caused indirect and direct cost of $422 billion (*3*). Therefore, AD must be considered as a major future challenge for the society.

Major pathological hallmarks of AD are extracellular neuritic plaques and intracellular neurofibrillary tangles. The core of neuritic plaques consists of amyloid fibrils, which are composed of the 39-43 amino acids long amyloid-β peptide (Aβ). In amyloid fibrils, Aβ exhibit a characteristic cross β-structure, in which the individual β-strands run perpendicular to the fibril axis (*4*). Aβ is formed by proteolytical cleavage of the amyloid precursor protein (APP), a type 1 transmembrane glycoprotein, by the consecutive action of β-, and γ-secretase (for review (*5*)). Aβ is in its solube, monomeric form a normal component of the cerebro spinal fluid (CSF) and the blood plasma (*6-8*). In vitro studies demonstrated that Aβ fibrilization is a nucleation-dependent process, comparable with crystallization (*9, 10*). Many factors

have been reported to influence the Aβ fibrillization, including pH (*11, 12*), salt (*13*), temperature (*14*) and seeds, such as preformed fibrils (*15, 16*) or glycosaminoglycans (*17*). However, the exact mechanism by which Aβ fibrillization occurs in vivo is still largely unknown.

Originally, the Aβ fibrils were considered as the source of the putative neurotoxicity of Aβ (*18, 19*). More recent studies indicated that non-fibrillar structure of Aβ, including oligomers and protofibrils, are more neurotoxic (*20*). On the other hand, monomeric Aβ have a very low toxic activity (*21*). In aqueous solution, monomeric Aβ exhibits a predominant random-coil structure (*22*). However, Aβ exhibits β-structure in in the fibrillar oligomers (*23*) and amyloid fibrils (*4*). Therefore, the structural conversion of Aβ from random-coil-to-β-structure is considered as crucial event in the pathology of the disease.

Emerging evidences indicate that the lipid membrane plays a particular role in the course of AD. Several models for the membrane-mediated toxicity of Aβ were proposed, including the formation of ion-channel and pores in membranes, which leads to membrane depolarization and disruption of ionic homeostasis (*24*). Therefore, it is of particular interest to investigate the random-coil to β-structure transition in a membrane environment. Thermodynamic studies investigating the membrane-induced β-structure formation are relatively rare. Recent studies on the model peptide $(KIGAKI)_3$ yielded in the thermodynamic characterization of the β-structure formation in a membrane environment (*25*), which has been demonstrated to be dependent on the peptide chain length (*26*).

In this study, we aimed to characterize the thermodynamics of the membrane-induced β-structure formation of Aβ(1-40). For this purpose, we have used four double d-isomers of Aβ(1-40) (d5, 6; d13, 14; d19, 20 and d35, 36 Aβ(1-40)), in which two adjacent amino acids are substituted by the corresponding d-enantiomers. Double-d substitution has shown to result in a local disturbance of secondary structure without modifying other characteristics such as hydrophobicity and side-chain functionality (*27, 28*). Circular dichroism (CD) spectroscopy was used to quantify the content of β-structure upon binding to anionic lipid membrane. Isothermal titration calorimetry (ITC) was applied to study the thermodynamic parameters of the binding process. The obtained thermodynamic parameters entail contributions of two different processes: (i) the adsorption of the peptide to the lipid membrane surface and (ii) conformational changes of the peptide from random-coil-to-β-structure. By correlating the thermodynamic binding parameters with the extent of membrane-induced β-structure of the studied peptides, it was possible to separate these two different processes, deducing the thermodynamics of the β-structure formation of Aβ(1-40) in a membrane environment

Material and Methods

All lipids such as 1-palmitoyl-2-oleoyl-sn-glycero-3-phosphocholine (POPC), 1-palmitoyl-2-oleoyl-sn-glycero-3-phospho-rac-glycerol (POPG), and 1,2-dioleoyl-sn-glycero-3-phosphoethanolamine-N[methoxy(polyethylene glycol)-2000] (mPEG 2000 PE) were purchased from Avanti Polar Lipds (Alabaster, AL). Aβ(1-40) was obtained from rPeptide (Bogart, GA, USA). The double-d-isomers were kindly provided by Dr. M. Beyermann of the Leibniz-Institute für Molekulare

Pharmakologie, 13125 Berlin, Germany. All other chemical were purchased from commercial sources at the highest purity.

Preparation of Lipid Vesicles

Small unilamellar vesicles (SUVs) composed of ternary lipid mixture were prepared as follows. A defined amount of the first lipid was dried from a chloroform stock solution with a soft stream of nitrogen and then overnight in high vacuum. The amount of the first lipid was weighed and a defined amount of the second lipid was added. The mixture was treated as before and the same procedure was applied for the third lipid. Typically, a buffer volume of 2-3 ml was added to the dried lipid film and the dispersion was extensively vortexed. Then, the lipid dispersion was sonicated with a G112SP1 Special Ultrasonic Cleaner (Laboratory Supplies CO., Inc) for 25 min. Metal debris from the titanium tip was removed by centrifugation at 14,000 rpm for 4 min using an Eppendorf 5415 C benchtop centrifuge (Vaudaux-Eppendorf AG, Schonenbuch, Switzerland). The size and ζ-potential of the SUVs were measured by dynamic light scattering (DLS).

Preparation of Aβ(1-40) solution

Aβ(1-40) has been repeatedly reported to differ in fibrillogenic properties within different lots and suppliers, possibly caused by pre-existing aggregates. Therefore, it was crucial to establish a chemical starting point of the peptide. Treatment of Aβ(1-40) with hexafluoroisopropanol (HFIP) dissolves pre-existing aggregates. Aβ(1-40) samples were prepared as follows. First, the peptides were dissolved in HFIP (at a concentration of 0.5 mg peptide/ ml HFIP) and equilibrated for one hour at room temperature. Then, an appropriate amount of the Aβ(1-40)-HFIP solution was aliquoted in 4ml glass tubes, and the solvent was removed by soft stream of nitrogen

and subsequent high vacuum overnight. The peptide samples were then stored at -20 °C. Immediately prior to use, the peptide was dissolved in appropriate buffer (1min sonication). In general, a Aβ(1-40) concentration below 30 μM were used due to the confirmed structural stability within the time range of experiments. The peptide concentration was obtained by amino acid analysis (University of Bern).

Circular Dichroism (CD) Spectroscopy

All measurements were performed on a Chirascan CD spectrometer (Applied Photophysics Ltd., Leatherhead, UK). CD spectra were recorded from 190 nm to 250 nm at 25 °C, with resolution of 1 nm, a bandwidth of 2 nm and a response time of 25 s. A quartz cuvette with a path length of 1 mm was used for all measurements. The percentage of peptide secondary structure was estimated from a computer simulation based on the reference spectra obtained by Reed and Reed (*29*).

Isothermal Titration Calorimetry (ITC)

Isothermal Titration Calorimetry (ITC) measurements were performed on a VP ITC calorimeter (MicroCal, Northampton, MA). All measurements were made at 25 °C in 5 mM Hepes (pH 7.0, 7.4 and 8.0). For the lipid-into-peptide titrations, the calorimeter cell contained the peptide solution at a concentration of below $25\,\mu M$. Lipid vesicles were suspended in the same buffer as the peptide (~15mM lipid) and $10\,\mu l$ aliquots were injected every $300\,s$ via a $300\,\mu l$ syringe. As a control, every lipid vesicle suspension was injected into pure buffer. Raw data were processed using a Origin software provided with the instrument.

Results

Thermodynamics of peptide binding

The thermodynamic characterization of a peptide-lipid binding reaction can be determined by high-sensitivity isothermal calorimetry (ITC). The general term "binding" is used in the following to describe the peptide adsorption from the bulk solution to the lipid membrane. Figure 1 show a representative example of an ITC experiment. The calorimetric cell contained a 25 µM Aβ(1-40) solution, which was titrated every 300 s with 10 µl aliquots of a 15 mM SUV suspension composed of 1-palmitoyl-2-oleoyl-sn-glycero-3-phosphocholine (POPC), 1-palmitoyl-2-oleoyl-sn-glycero-3-phosphoglycerol (POPG), and 1,2-dioleoyl-sn-glycero-3-phosphoethanolamine-N[methoxy(polyethylene glycol)-2000] (mPEG 2000 PE) (50/45/5 mol%) at 25 °C. Each injection caused an exothermic reaction as illustrated by the calorimetric trace. The heat of reaction h_j corresponds to the integral of the titration peak and decreased with increasing number of injections as less peptide was available for binding (figure 1B). After about 27 injections all peptide was bound to the lipid membrane and further injections of lipid vesicles entailed only heats of dilution h_{dilute}. As a control, lipid-into-buffer injections were conducted (data not shown). No significant heats were observed providing good evidence for a proper experimental set-up. The molar binding enthalpy, ΔH^0, can be calculated according to :

$$\Delta H^0 = \sum_{j=1}^{n} (h_j - h_{dilute}) / n_{pep}^0 \qquad (1)$$

where n^0_{pep} is the total molar amount of peptide in the calorimetric cell and h_{dilute} is the heat of dilution. The molar binding enthalpies for Aβ(1-40) and its double d-isomers are listed in table 1. They were dependent on the position of the double-d substitution and varied between $-17.5 kcal/mol$ for d13, 14 Aβ(1-40) and $-1.1 kcal/mol$ for d35, 36 Aβ(1-40). Binding isotherm of the peptide-lipid interaction can be derived from the lipid-into-peptide calorimetric experiment as described elsewhere (*30*). Figure 2 displays the binding isotherm for the ITC data of figure 1. The binding isotherm describes the dependence of the degree of binding, X_b, on the equilibrium concentration of free peptide, c_f. X_b is defined as the molar ratio of bound peptide, $n_{p,bound}$, to lipid n_L. Since Aβ(1-40) does not penetrate the lipid membrane, only the outer lipid layer is available for binding and n_L corresponds to 60% of the total lipid, n^0_L (*31*). The molar amount of bound peptide, $n^i_{pep,bound}$, after i injections is linked to the calorimetric data according to

$$n^i_{pep,bound} = \sum_{j=1}^{i} h_j / (\Delta H^0 \cdot V_{cell} \cdot c_{0,pep}) \qquad (2)$$

where V_{cell} is the volume of the calorimetric cell and $c_{0,pep}$ is the total peptide concentration in the cell. The molar amount of lipid available for binding is given by $n_L = i \cdot V_{inj} \cdot c_{L,0}$, where V_{inj} is the injection volume ($10 \mu l$) and $c_{L,0}$ is the concentration of the lipid suspension in the syringe. While the binding isotherm can be derived in a model-independent manner from the calorimetric data, the thermodynamic analysis of the binding isotherm requires the assumption of a specific binding model. The model used in the following is a surface partition model which states that peptide binding is

linearly correlated with the peptide concentration, c_M , found immediately above the plane of binding (*32*):

$$X_b = K_0 \cdot c_M \tag{3}$$

The binding constant K_0 corresponds to the transfer of the peptide from the plane of binding into the membrane. The model takes into account that an anionic lipid membrane attract molecule bearing cationic groups such as Aβ(1-40). The peptide surface concentration c_M is therefore increased and an expression is given by the Boltzmann relation according to:

$$c_M = c_f \cdot e^{-z_p \cdot F_0 \cdot \psi / RT} \tag{4}$$

where z_p is the effective peptide charge (charge which is exposed to the lipid membrane), F_0 is the Faraday constant, ψ is the membrane surface potential and RT the thermal energy. The application of the Gouy-Chapman theory allows the calculation of the surface potential ψ and the surface concentration c_M for each data point of the binding isotherm, leading to surface partition constant K_0. The solid line in figure 2 is the best theoretical fit to the experimental data. For all peptides a good agreement between the model and the experimental data could be established. The binding constant K_0 and the effective charge z_p for all peptides are summarized in table 1. The free energy of binding, ΔG^0, is then given by

$$\Delta G^0 = -RT \cdot \ln 55.5 \cdot K \tag{5}$$

where the factor 55.5 is the molar concentration of water. Next, the entropy of binding, ΔS^0, is given by $\Delta G^0 = \Delta H^0 - T\Delta S^0$. The thermodynamic parameters of all peptides are summarized in table 1.

Isothermal titration calorimetry was also used to study the pH dependence of Aβ(1-40)-lipid interaction. Experiments were performed at three different pH values (7.0, 7.4 and 8.0) in 5mM Hepes at 25 °C. Lipid-into-peptide titrations and theirs analysis were conducted as described above, and the binding parameters are summarized in table 2. At pH 8.0, no heats of reaction could be detected, and no binding constant K_0 , and therefore no ΔG^0, could be derived (n.d. in table 2). The molar binding enthalpy ΔH^0 increased with increasing pH values from $-18.9 kcal/mol$ at 7.0 to $-13.5 kcal/mol$ at 7.4 and reached $0 kcal/mol$ at 8.0. Further, the increases of pH form 7.0 to 7.4 lead to an small increase of the binding constant K_0 from $0.04 M^{-1}$ to $0.06 M^{-1}$, whereas the effective charge z_p is decreased from 1.1 to 0.2.

Structural transition of Aβ(1-40) peptides upon lipid binding

Circular dichroism (CD) spectroscopy was performed to monitor structural changes of Aβ(1-40) and the double-d isomers upon binding to anionic lipid membrane. CD spectra of the peptides in buffer are shown in figure 3. All spectra revealed a predominantly random coil conformation. To obtain the fraction of secondary structure, the spectra are analyzed as described in the material and method section. Analysis revealed a nearly identical random coil content of 65.5 to 69.1% for all peptides. The contribution of β-structure varied from 21.7 to 33.4% and the content of α-helix was in the range of 0 to 11.4%. The detailed analysis is given in table 3. Upon addition of anionic lipid vesicles, the peptides were bound to the membrane surface

and experienced a conformational transition to β-structure as demonstrated in figure 3B. As an example, figure 4 displays the CD spectra of Aβ(1-40) in presence of various concentration of lipid SUV composed of POPG/POPC/mPEG 2000 PE (45/50/5 mol%). The lipid-to-peptide ratio was gradually increased from 0 to 344. CD spectra recorded at high lipid-to-peptide ratio ensure complete peptide binding. An isosbestic point could be observed at $\lambda = 213nm$ indicating a simple two-state equilibrium. The CD spectra were analyzed and the corresponding fractions of secondary structure are plotted versus the molar lipid-to-peptide ratio in figure 4B. The content of α-helix remained nearly constant and is not shown. The increase of the lipid-to-peptide ratios by 150 resulted in an increase of β-structure by 37%, while the random coil content decreased by the same magnitude. However, above a lipid-to-peptide ratio of 150 the fractions of secondary structure elements remained constant which suggests a conformational endpoint. The existence of a conformational endpoint allows us to quantify the lipid-induced transition from random coil to β-structure of Aβ(1-40). For this purpose, the change of β-structure, Δf_β (%), is defined as $\Delta f_\beta = f_\beta(lipid) - f_\beta(buffer)$, where $f_\beta(lipid)$ is the fraction of β-structure at the conformational endpoint and $f_\beta(buffer)$ in buffer. Next, the number of amino acids, $\Delta\beta(aa)$, which transfer from random coil to β-structure, can be calculated according to $\Delta\beta(aa) = \Delta f_\beta \cdot n_{aa}$, where n_{aa} is the number of amino acids (40). The corresponding values for all peptides are summarized in table 3. The values of $\Delta\beta(aa)$ varied from 1.4 to 15.8, depending on the position of the double-d-substitution.

Correlation of thermodynamics and structural changes of Aβ(1-40) peptides

The binding of Aβ(1-40) and its double-d isomers to lipid membranes comprises two processes: (i) the adsorption to the membrane surface and (ii) conformational changes of the peptides. Similar adsorption energies can be assumed for all peptides as they possess nearly identical structure in solution. (~70% random coil, ~30% β-structure). Differences in the thermodynamic parameters are then caused by the conformational change upon binding to the membrane surface. A correlation between the thermodynamic parameters $\Delta G^0, \Delta H^0$, and ΔS^0 of the peptide binding reaction and the change in β-structure can be established as displayed in figure 5. Regression analysis yields a linear dependence of the thermodynamics on the change in β-structure with the following expressions:

$$\Delta H^0 = -1.01 \cdot \Delta n_\beta + 1.18 (kcal / mol) \tag{6}$$

$$\Delta G^0 = -0.04 \cdot \Delta n_\beta - 0.06 (kcal / mol) \tag{7}$$

$$T\Delta S^0 = -1.08 \cdot \Delta n_\beta + 2.92 (kcal / mol) \tag{8}$$

where Δn_β is the number of amino acid residues that change from random coil to β-structure. The contribution of the β-structure formation to the binding process corresponds to the slopes of the regression lines:

$$\Delta H_\beta = -1.01 (\pm 0.1) kcal / mol \; per \; residue$$

$$\Delta G_\beta = -0.04 (\pm 0.002) kcal / mol \; per \; residue$$

$$\Delta S_\beta = -3.62 (\pm 0.5) cal / molK \; per \; residue$$

From the intercept with the ordinate (0% β-structure) the thermodynamic binding parameters of a hypothetical Aβ(1-40) peptide with no conformational change can be estimated as:

$$\Delta H^0 = 1.18 kcal / mol$$

$$\Delta G^0 = -0.06 kcal / mol$$

$$\Delta S^0 = 9.8 cal / mol\, K$$

Discussion

Structural aspect of membrane-peptide interactions

Aβ(1-40) and four double-d isomers were used to derive information on the thermodynamics of the lipid-induced random coil-to-β-structure transition of Aβ(1-40). For all peptides, CD spectroscopy provides evidence for a simple random coil-to-β-structure transition induced by anionic PEGylated lipid vesicles. The incorporation of PEG into lipid vesicles avoids close contact between the vesicles and therefore prevents vesicle aggregation. Along with the prevention of vesicle aggregation, the addition of PEG-lipid in the lipid mixture inhibits the β-structure-α-helix transition observed at high lipid-to-peptide ratios in the case of nonPEGylated lipid vesicles (*31*). Therefore, it can be speculated that the β-structure-α-helix transition is due to dilution effect of a single Aβ(1-40) peptide induced by close contact of the lipid vesicles. Similar observations were made in the studies of the interaction of the cell-penetrating peptide penetratin with lipid membranes (*33*). The interaction of penetratin with LUVs composed of either pure DOPG or DOPC/DOPG (60/40mol%) lead above a specific lipid-to-peptide ratio to vesicles aggregation followed by

spontaneous disaggregation (*34*). Both processes are strongly linked to a conformational transition of penetration: an α-helix-to-β-sheet transition during aggregation and then back to α-helix during the disaggregation process. The use of PEGylated lipid vesicles inhibits these conformational transitions.

In a β-sheet structure, the side chains of involved amino acids are either above or below the plane of the β-sheet. The incorporation of a d-amino acid would then change the orientation of the side chain from perpendicular to the plane of backbone-backbone hydrogen bonds into a parallel alignment. The presence of an adjacent pair of d-amino acids causes local disturbance in structure and flexibility (*27*). The degree of structural disturbance has been shown to be correlated with the magnitude of the secondary structure of the replaced region in the all-L-amino acid peptide (*35*). Table 3 summarizes the lipid-induced change in β-structure for all peptides. The largest decrease in the magnitude of β-structure formation are observed for the double d-isomers d19, 20 Aβ(1-40) and d35, 36 Aβ(1-40). Only a minor decrease can be observed for d5, 6 Aβ(1-40), which indicates that these amino acids are probably not involved in β-structure formation. However, d13, 14 Aβ(1-40) is an exception, revealing a slightly increased magnitude of β-structure formation. Our results can now compared with structural studies on Aβ(1-40) fibrils. Amyloid fibrils of Aβ(1-40) are characterized by a specific intermolecular polypeptide assemblies, named cross-β structural motif (*36*). Cross-β structures are defined as extended β-sheet in which the plane of β-sheet and the backbone-backbone hydrogen bonds are in linear orientation to the fibril axis, while the individual β-strands run perpendicular to the fibril axis. The secondary structure of Aβ(1-40) fibrils have been studied by several biophysical techniques such as solid-state NMR, hydrogen/deuterium (H/D) exchange

and proline-scanning mutagenesis (*37-39*). In general, the N-terminal residues (1-10/14) are commonly seen as unordered and are not involved in the fibrils. Another common feature of the Aβ(1-40) are 2 β-sheet structure around residues 17-20 and 30-35. A domain which is different in various models of Aβ(1-40) fibrils is the C-terminus. While solid-state NMR data suggests that the C-terminus is involved in the β-sheet structure (*38*), proline-scanning mutagenesis analysis and H/D exchange indicate a more flexible structure (*37, 39*).

Thermodynamic of the Aβ(1-40)-lipid interaction

All peptides employed have the same sequence with respect to side-chain functionality and, in turn similar intrinsic hydrophobicities. In buffer, they adopt a predominant random-coil conformation (70%) with minor content of β-structure (30%). The electrostatic attraction between the peptides and the anionic lipid membrane increases the peptide surface concentration, c_M, probably leading to peptide aggregates on the membrane surface as indicated by the increase of β-structure upon membrane binding. This was previously observed for the Aβ(1-40) interaction with nonPEGylated anionic lipid vesicles (*22*). The incorporation of 5mol% PEG-lipid in the lipid mixture leads to a polymer brush on the lipid membrane surface, which diminishes protein adsorption (*40*). However, the present calorimetric data provide evidence that the peptides penetrate the PEG polymer layer and adsorb to the underlying anionic lipid membrane. A useful parameter to evaluate the electrostatic effect on the membrane binding is the apparent binding constant, K_{app}, comprising both electrostatic attraction to the lipid membrane and the hydrophobic binding into the lipid membrane. K_{app} is defined according to

$$K_{app} = X_b / c_{eq} \tag{9}$$

where X_b is the molar ratio of bound peptide to total available lipid and c_{eq} is the free equilibrium peptide concentration. K_{app} is dependent on the peptide concentration, and in turn not constant. Furthermore K_{app} can now compared with the surface partition constant K_0, which correspond to the transfer of the peptide from the water-membrane interface into the lipid membrane. For the Aβ(1-40)-membrane interaction, K_{app} varies between $3 \cdot 10^6 - 1.2 \cdot 10^7 M^{-1}$, whereas K_0 is in the range of $2.7 - 6.2 \cdot 10^{-2} M^{-1}$. The large difference between K_0 and K_{app} indicates that the main factor of membrane binding is the electrostatic attraction of the peptide to the negatively charged membrane.

The hydrophobic peptide binding is purely driven by enthalpy $(\Delta H^0 < 0)$ and is almost fully opposed by entropy $(\Delta S^0 < 0)$. This phenomenon is denoted as non-classical hydrophobic effect which has been also observed for other peptides and amphiphilic molecules (*41, 42*). The large negative entropy contribution is remarkable and can be explained by the formation of β-structure associated with aggregation on the membrane surface, leading to a higher order of the system. A distinct binding thermodynamics was observed for the membrane binding of the β-structure forming $(KIGAKI)_3$ peptide, which revealed an endothermic binding enthalpy $(\Delta H^0 > 0)$ and a positive entropic contribution (*25*).

The intercepts of the regression analysis (figure 5) provide the thermodynamic binding parameters of a hypothetical Aβ(1-40) peptide that binds to the membrane

without conformational change and is given by $\Delta H^0 = 1.18\,kcal/mol$, $\Delta G^0 = -0.06\,kcal/mol$ and $\Delta S^0 = 9.8\,cal/molK$. The enthalpy ΔH^0 is endothermic, and the adsorption to the membrane is therefore exclusively driven by entropy. Similar results were observed for membrane binding of the (random coil) $(KIGAKI)_3$ peptide (*25*). The positive entropy term can be explained by the release of hydration water

The ITC experiments further demonstrated pH-dependence of the thermodynamics of the Aβ(1-40)-lipid interactions. pH affects the charge of both binding partners. Thus, lower bulk pH leads to a lower membrane surface potential ψ, and in turn to a lower electrostatic attraction of cationic molecules. On the other hand, the net charge of Aβ(1-40) decreases from -2.47 at pH 7.0 to -3.6 at pH 8.0 as calculated by the pK_a values of the charged residues. However, the cluster of basic residues of Aβ(1-40) $(H_{13}H_{14}\,and\,K_{16})$ is supposed to be mainly responsible for the electrostatic attraction to the anionic lipid membrane. The charge of the cluster decreases from 1.47 at pH 7.0, 1.21 at pH 7.4 to 1.05 at pH 8.0, indicating a higher electrostatic interaction with the anionic lipid membrane at lower bulk pH. As outlined above, pH has a conflictive effect on the oppositely charged binding partners. However, pH dependence of the electrostatic interaction can be studied by the contribution of the electrostatic free energy to peptide binding which can be calculated according to

$$\Delta G_{el} = -RT\ln(K_{app}/K_0) \tag{10}$$

At pH 7.0, ΔG_{el} varies between $10.8-11.3\,kcal/mol$, whereas at pH 7.4 ΔG_{el} varies between $10.8-14.4\,kcal/mol$. This demonstrates that pH dependence of peptide

(cluster) charge has a greater effect on the electrostatic interaction compared to the changes in the membrane surface potential. Further, pH affects the aggregation behavior of Aβ(1-40) with a reported maximum in the pH range of 4 to 7. However, CD experiments have demonstrated a nearly identical conformation of Aβ(1-40) in the pH range of 7.0 to 8.0 (data not shown). Changes in the thermodynamic must therefore not be ascribed to conformational changes prior the membrane binding. Table 2 summarizes the thermodynamic binding parameters of the Aβ(1-40)-lipid interaction measured at the three pH values. The molar binding enthalpy ΔH^0 is highly pH-dependent. Regression analysis yielded a significant linear correlation in the studied pH range with the following equation: $\Delta H^0(pH) = 1.8*(pH - 7.0) - 18.5 kcal/mol$. A pH deviation of ± 0.1 leads therefore to a theoretical change in ΔH^0 of $\pm 1.8 kcal/mol$, which is significantly higher than the standard deviations at each point. Next, we observed a slightly higher binding constant K_0 at pH 7.4 than pH 7.0, whereas the effective charge of the peptide is decreased. This can be explained by the fact that less charged molecule bind more easily into the hydrophobic lipid membrane.

Thermodynamics of the β-sheet formation in a membrane environment

The method of double-d substitution combined with isothermal titration calorimetry and CD spectroscopy allows to determine the thermodynamics of β-structure formation of Aβ(1-40). Analogous studies were conducted for the membrane-induced α-helix formation of magainin and the membrane-induced β-structure formation of the KIGAKI peptide (*25, 43*). The thermodynamics of β-structure formation of Aβ(1-40) could now be compared with the results obtained for the KIGAKI peptide. However, it has been shown that the thermodynamics of the β-structure formation of

the KIGAKI peptide is dependent of length of the peptide (*26*). Therefore, it is more revealing to compare the obtained results for Aβ(1-40) with those of a hypothetical KIGAKI peptide composed of 40 amino acids. In this case, the thermodynamic parameters of the β-structure formation are obtained by extrapolation, revealing $\Delta H_\beta = -1.02\,kcal/mol\,residue$, $\Delta S_\beta = -0.86\,cal/molK\,residue$ and $\Delta G_\beta = -0.14 kcal/mol\ residue$. The slope of the regression lines in figure 5 corresponds to the incremental thermodynamic parameters for β-structure formation of Aβ(1-40), and is given by $\Delta H_\beta = -1.01 kcal/mol\ residue$, $\Delta S_\beta = -3.62 cal/molK\ residue$ and $\Delta G_\beta = -0.04 kcal/mol\ residue$. A comparison with the values of the 40 amino acids long KIGAKI peptide reveals almost identical ΔH_β values, whereas small deviations can be observed for ΔS_β and ΔG_β. However, the good numerical agreement between Aβ(1-40) and the (hypothetical) corresponding long KIGAKI peptide is a strong indication that primarily the peptide length than its sequence determine the thermodynamics of the random-coil-to-β-structure transition in a membrane environment.

References

1. Ferri, C. P., Prince, M., Brayne, C., Brodaty, H., Fratiglioni, L., Ganguli, M., Hall, K., Hasegawa, K., Hendrie, H., Huang, Y., Jorm, A., Mathers, C., Menezes, P. R., Rimmer, E., and Scazufca, M. (2005) Global prevalence of dementia: a Delphi consensus study, *Lancet 366*, 2112-2117.
2. Brookmeyer, R., Johnson, E., Ziegler-Graham, K., and Arrighi, H. M. (2007) Forecasting the global burden of Alzheimer's disease, *Alzheimers Dement 3*, 186-191.
3. Wimo, A., Winblad, B., and Jonsson, L. (2010) The worldwide societal costs of dementia: Estimates for 2009, *Alzheimers Dement 6*, 98-103.
4. Kirschner, D. A., Abraham, C., and Selkoe, D. J. (1986) X-ray diffraction from intraneuronal paired helical filaments and extraneuronal amyloid fibers in Alzheimer disease indicates cross-beta conformation, *Proc Natl Acad Sci U S A 83*, 503-507.
5. Haass, C., Kaether, C., Thinakaran, G., and Sisodia, S. (2012) Trafficking and Proteolytic Processing of APP, *Cold Spring Harb Perspect Med 2*, a006270.
6. Haass, C., Schlossmacher, M. G., Hung, A. Y., Vigo-Pelfrey, C., Mellon, A., Ostaszewski, B. L., Lieberburg, I., Koo, E. H., Schenk, D., Teplow, D. B., and et al. (1992) Amyloid beta-peptide is produced by cultured cells during normal metabolism, *Nature 359*, 322-325.
7. Seubert, P., Vigo-Pelfrey, C., Esch, F., Lee, M., Dovey, H., Davis, D., Sinha, S., Schlossmacher, M., Whaley, J., Swindlehurst, C., and et al. (1992) Isolation and quantification of soluble Alzheimer's beta-peptide from biological fluids, *Nature 359*, 325-327.
8. Shoji, M., Golde, T. E., Ghiso, J., Cheung, T. T., Estus, S., Shaffer, L. M., Cai, X. D., McKay, D. M., Tintner, R., Frangione, B., and et al. (1992) Production of the Alzheimer amyloid beta protein by normal proteolytic processing, *Science 258*, 126-129.
9. Jarrett, J. T., and Lansbury, P. T., Jr. (1993) Seeding "one-dimensional crystallization" of amyloid: a pathogenic mechanism in Alzheimer's disease and scrapie?, *Cell 73*, 1055-1058.
10. Lomakin, A., Chung, D. S., Benedek, G. B., Kirschner, D. A., and Teplow, D. B. (1996) On the nucleation and growth of amyloid beta-protein fibrils: detection of nuclei and quantitation of rate constants, *Proc Natl Acad Sci U S A 93*, 1125-1129.
11. Fraser, P. E., Nguyen, J. T., Surewicz, W. K., and Kirschner, D. A. (1991) pH-dependent structural transitions of Alzheimer amyloid peptides, *Biophys J 60*, 1190-1201.
12. Wood, S. J., Maleeff, B., Hart, T., and Wetzel, R. (1996) Physical, morphological and functional differences between ph 5.8 and 7.4 aggregates of the Alzheimer's amyloid peptide Abeta, *J Mol Biol 256*, 870-877.
13. Klement, K., Wieligmann, K., Meinhardt, J., Hortschansky, P., Richter, W., and Fandrich, M. (2007) Effect of different salt ions on the propensity of aggregation and on the structure of Alzheimer's abeta(1-40) amyloid fibrils, *J Mol Biol 373*, 1321-1333.
14. Gursky, O., and Aleshkov, S. (2000) Temperature-dependent beta-sheet formation in beta-amyloid Abeta(1-40) peptide in water: uncoupling beta-structure folding from aggregation, *Biochim Biophys Acta 1476*, 93-102.

15. Snyder, S. W., Ladror, U. S., Wade, W. S., Wang, G. T., Barrett, L. W., Matayoshi, E. D., Huffaker, H. J., Krafft, G. A., and Holzman, T. F. (1994) Amyloid-beta aggregation: selective inhibition of aggregation in mixtures of amyloid with different chain lengths, *Biophys J 67*, 1216-1228.
16. Harper, J. D., and Lansbury, P. T., Jr. (1997) Models of amyloid seeding in Alzheimer's disease and scrapie: mechanistic truths and physiological consequences of the time-dependent solubility of amyloid proteins, *Annu Rev Biochem 66*, 385-407.
17. Castillo, G. M., Ngo, C., Cummings, J., Wight, T. N., and Snow, A. D. (1997) Perlecan binds to the beta-amyloid proteins (A beta) of Alzheimer's disease, accelerates A beta fibril formation, and maintains A beta fibril stability, *J Neurochem 69*, 2452-2465.
18. Pike, C. J., Walencewicz, A. J., Glabe, C. G., and Cotman, C. W. (1991) In vitro aging of beta-amyloid protein causes peptide aggregation and neurotoxicity, *Brain Res 563*, 311-314.
19. Roher, A. E., Ball, M. J., Bhave, S. V., and Wakade, A. R. (1991) Beta-amyloid from Alzheimer disease brains inhibits sprouting and survival of sympathetic neurons, *Biochem Biophys Res Commun 174*, 572-579.
20. Walsh, D. M., Klyubin, I., Fadeeva, J. V., Rowan, M. J., and Selkoe, D. J. (2002) Amyloid-beta oligomers: their production, toxicity and therapeutic inhibition, *Biochem Soc Trans 30*, 552-557.
21. Ono, K., Condron, M. M., and Teplow, D. B. (2009) Structure-neurotoxicity relationships of amyloid beta-protein oligomers, *Proc Natl Acad Sci U S A 106*, 14745-14750.
22. Terzi, E., Holzemann, G., and Seelig, J. (1995) Self-association of beta-amyloid peptide (1-40) in solution and binding to lipid membranes, *J Mol Biol 252*, 633-642.
23. Stroud, J. C., Liu, C., Teng, P. K., and Eisenberg, D. (2012) Toxic fibrillar oligomers of amyloid-beta have cross-beta structure, *Proc Natl Acad Sci U S A 109*, 7717-7722.
24. Arispe, N., Rojas, E., and Pollard, H. B. (1993) Alzheimer disease amyloid beta protein forms calcium channels in bilayer membranes: blockade by tromethamine and aluminum, *Proc Natl Acad Sci U S A 90*, 567-571.
25. Meier, M., and Seelig, J. (2007) Thermodynamics of the coil <==> beta-sheet transition in a membrane environment, *J Mol Biol 369*, 277-289.
26. Meier, M., and Seelig, J. (2008) Length dependence of the coil <--> beta-sheet transition in a membrane environment, *J Am Chem Soc 130*, 1017-1024.
27. Rothemund, S., Beyermann, M., Krause, E., Krause, G., Bienert, M., Hodges, R. S., Sykes, B. D., and Sonnichsen, F. D. (1995) Structure effects of double D-amino acid replacements: a nuclear magnetic resonance and circular dichroism study using amphipathic model helices, *Biochemistry 34*, 12954-12962.
28. Wieprecht, T., Dathe, M., Schumann, M., Krause, E., Beyermann, M., and Bienert, M. (1996) Conformational and functional study of magainin 2 in model membrane environments using the new approach of systematic double-D-amino acid replacement, *Biochemistry 35*, 10844-10853.
29. Reed, J., and Reed, T. A. (1997) A set of constructed type spectra for the practical estimation of peptide secondary structure from circular dichroism, *Anal Biochem 254*, 36-40.

30. Seelig, J. (1997) Titration calorimetry of lipid-peptide interactions, *Biochim Biophys Acta 1331*, 103-116.
31. Terzi, E., Holzemann, G., and Seelig, J. (1997) Interaction of Alzheimer beta-amyloid peptide(1-40) with lipid membranes, *Biochemistry 36*, 14845-14852.
32. Wenk, M. R., and Seelig, J. (1998) Magainin 2 amide interaction with lipid membranes: calorimetric detection of peptide binding and pore formation, *Biochemistry 37*, 3909-3916.
33. Persson, D., Thoren, P. E., Lincoln, P., and Norden, B. (2004) Vesicle membrane interactions of penetratin analogues, *Biochemistry 43*, 11045-11055.
34. Persson, D., Thoren, P. E., and Norden, B. (2001) Penetratin-induced aggregation and subsequent dissociation of negatively charged phospholipid vesicles, *FEBS Lett 505*, 307-312.
35. Krause, E., Beyermann, M., Dathe, M., Rothemund, S., and Bienert, M. (1995) Location of an amphipathic alpha-helix in peptides using reversed-phase HPLC retention behavior of D-amino acid analogs, *Anal Chem 67*, 252-258.
36. Sunde, M., Serpell, L. C., Bartlam, M., Fraser, P. E., Pepys, M. B., and Blake, C. C. (1997) Common core structure of amyloid fibrils by synchrotron X-ray diffraction, *J Mol Biol 273*, 729-739.
37. Morimoto, A., Irie, K., Murakami, K., Masuda, Y., Ohigashi, H., Nagao, M., Fukuda, H., Shimizu, T., and Shirasawa, T. (2004) Analysis of the secondary structure of beta-amyloid (Abeta42) fibrils by systematic proline replacement, *J Biol Chem 279*, 52781-52788.
38. Petkova, A. T., Ishii, Y., Balbach, J. J., Antzutkin, O. N., Leapman, R. D., Delaglio, F., and Tycko, R. (2002) A structural model for Alzheimer's beta -amyloid fibrils based on experimental constraints from solid state NMR, *Proc Natl Acad Sci U S A 99*, 16742-16747.
39. Kheterpal, I., Chen, M., Cook, K. D., and Wetzel, R. (2006) Structural differences in Abeta amyloid protofibrils and fibrils mapped by hydrogen exchange--mass spectrometry with on-line proteolytic fragmentation, *J Mol Biol 361*, 785-795.
40. Marsh, D., Bartucci, R., and Sportelli, L. (2003) Lipid membranes with grafted polymers: physicochemical aspects, *Biochim Biophys Acta 1615*, 33-59.
41. Seelig, J., and Ganz, P. (1991) Nonclassical hydrophobic effect in membrane binding equilibria, *Biochemistry 30*, 9354-9359.
42. Beschiaschvili, G., and Seelig, J. (1992) Peptide binding to lipid bilayers. Nonclassical hydrophobic effect and membrane-induced pK shifts, *Biochemistry 31*, 10044-10053.
43. Wieprecht, T., Apostolov, O., Beyermann, M., and Seelig, J. (1999) Thermodynamics of the alpha-helix-coil transition of amphipathic peptides in a membrane environment: implications for the peptide-membrane binding equilibrium, *J Mol Biol 294*, 785-794.

Table 1. Thermodynamic parameters for the binding of Aβ(1-40) and four double-d-isomers to anionic PEGylated lipid vesicles at 25°C.

Peptide	ΔH° (kcal/mol)	$K_0(M^{-1})$	z_p	ΔG° (kcal/mol)	TΔS° (kcal/mol)
Aβ(1-40)	-13.5 ± 0.7	0.059 ± 0.004	0.19	-0.70 ± 0.04	-12.7 ± 0.8
d5, 6 Aβ(1-40)	-5.7 ± 0.2	0.046 ± 0.001	0.19	-0.55 ± 0.02	-5.0 ± 0.1
d13, 14 Aβ(1-40)	-17.5 ± 0.5	0.062 ± 0.003	0.18	-0.73 ± 0.03	-16.4 ± 0.5
d19, 20 Aβ(1-40)	-4.0 ± 0.2	0.027 ± 0.001	0.18	-0.25 ± 0.02	-3.5 ± 0.3
d35, 36 Aβ(1-40)	-1.1 ± 0.1	n.d.	n.d.	n.d.	n.d.

Measurements were performed in triplicate or higher.

Table 2. pH dependence of the thermodynamic binding parameters of Aβ(1-40) to anionic PEGylated lipid vesicles at 25°C.

pH	ΔH° (kcal/mol)	$K_0(M^{-1})$	z_p	ΔG° (kcal/mol)	TΔS° (kcal/mol)
7.0	-18.9 ± 1.5	0.04 ± 0.007	1.13	-0.46 ± 0.1	-18.4± 1.6
7.4	-13.5± 0.7	0.06 ± 0.004	0.19	-0.70 ± 0.04	-12.7 ± 0.8
8.0	0	n.d.	n.d.	n.d.	n.d.

Measurements were performed in triplicate or higher.

Table 3. Analysis of CD spectra of Aβ(1-40) and its double-d isomers in buffer and when bound to anionic PEGylated lipid vesicles at 25°C.

	Peptide in buffer			Peptide with excess lipid			Change of β-structure	
Peptide	Random coil (%)	β-Structure (%)	α-helix (%)	Random coil (%)	β-Structure (%)	α-helix (%)	$\Delta f_\beta(\%)^{(a)}$	$\Delta\beta(aa)^{(b)}$
Aβ(1-40)	66.0	32.6	1.4	29.0	68.6	2.4	36.0	14.4
d 5, 6 Aβ(1-40)	69.1	23.2	7.7	41.2	50.8	8.0	27.6	11.0
d 13, 14 Aβ(1-40)	65.5	32.4	2.1	27.9	71.8	0.3	39.4	15.8
d 19, 20 Aβ(1-40)	66.9	21.7	11.4	58.4	32.6	9.0	10.9	4.4
d 35, 36 Aβ(1-40)	66.6	33.4	0	62.0	36.9	1.1	3.5	1.4

[(a), (b)] Δf_β, $\Delta\beta(aa)$ are calculated as described in the text.

Figure Captions

Figure 1. Isothermal titration calorimetry of Aβ(1-40) with SUVs composed of POPC/POPG/mPEG 2000 PE (45/50/5mol%). (A) Calorimetric trace obtained by titration of 15 mM lipid SUV suspension into 12 µM Aβ(1-40) solution (5mM Hepes (pH 7.4)) at 25 °C. Each peak corresponds to the injection of 10 µl SUV suspension. (B) Heats of reaction h_j are plotted versus the injection number n_j. The solid line correspond to calculations using the surface partition model combined with electrostatic interactions as discussed above $(K_0 = 0.055M^{-1}, z_p = 0.18 \; and \; \Delta H^0 = -14.6 kcal/mol)$.

Figure 2. Binding isotherm of the binding reaction of Aβ(1-40) to lipid SUVs composed of POPC/POPG/mPEG 2000 PE (45/50/5mol%) derived from ITC experiments. The degree of binding X_b, i.e. molar ratio of bound peptide to lipid available for binding, is plotted against the peptide equilibrium concentration c_f. The solid line corresponds to the theoretical binding calculated by combining the Gouy-Chapman theory with a surface partition model using the binding constant $K_0 = 0.055M^{-1}$ and the effective charge $z_p = 0.18$.

Figure 3. (A) CD spectra of Aβ(1-40) and the double d-isomers dissolved in 5mM Hepes (pH 7.4). The spectra were recorded at peptide concentrations between $16.0 - 25.0 \mu M$. (B) CD spectra of Aβ(1-40) and the double d-isomers recorded in excess of lipid SUVs composed of POPC/POPG/mPEG 2000 (45/50/5mol%).

Figure 4. (A) Lipid-induced random coil-to-β-structure transition of Aβ(1-40) monitored by circular dichroism (CD) spectroscopy. CD spectra were recorded at

lipid-to-peptide molar ratios from 0 to 340. (B) Plot of secondary structure of Aβ(1-40) versus the lipid-to-peptide molar ratio: β-structure (■) and random coil (●). A conformational endpoint of the Aβ(1-40)-lipid interaction could be observed at a lipid-to-peptide ratio of 150.

Figure 5. The thermodynamic parameters of the peptide-lipid interactions are plotted against the magnitude of β-structure formation expressed by $\Delta\beta(aa)$. (A) The molar binding enthalpy ΔH^0 (■). (B) Free energy of binding ΔG^0 (■) and $T\Delta S^0$ (●). The solid lines (in (A) and (B)) correspond to the regression line. All data were recorded at 25 C° in 5mM Hepes (pH 7.4).

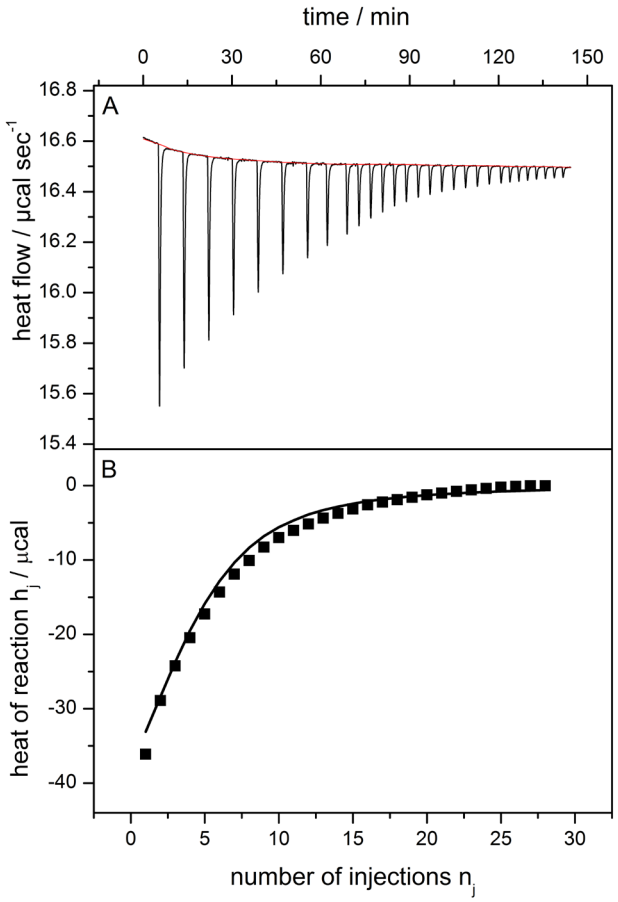
time / min
0
30
60
90
120
150
A
heat flow / µcal sec^{-1}
16.8
16.6
16.4
16.2
16.0
15.8
15.6
15.4
B
heat of reaction h_j / µcal
0
-10
-20
-30
-40
0
5
10
15
20
25
30
number of injections n_j

Figure 1

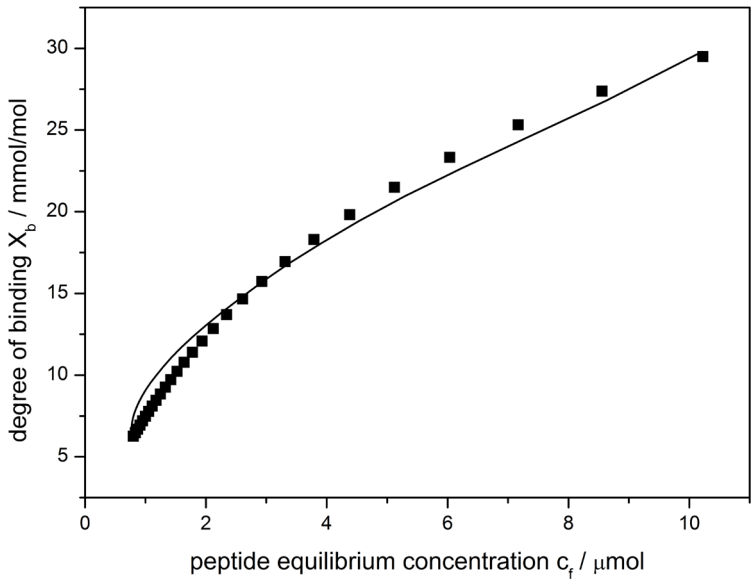
degree of binding X_b / mmol/mol
peptide equilibrium concentration c_f / μmol
30
25
20
15
10
5
0
2
4
6
8
10

Figure 2

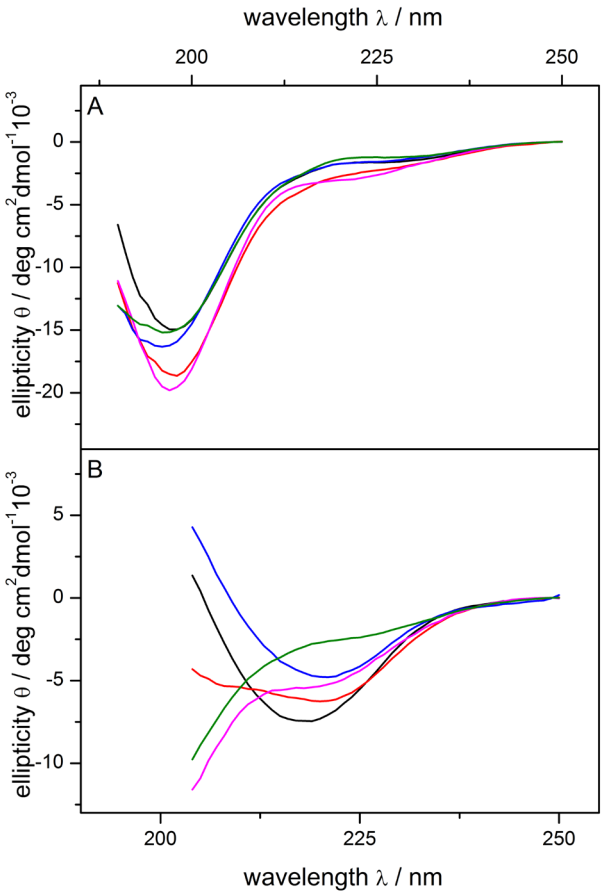
wavelength λ / nm
200
225
250
A
ellipticity θ / deg cm²dmol⁻¹10⁻³
0
-5
-10
-15
-20
B
ellipticity θ / deg cm²dmol⁻¹10⁻³
5
0
-5
-10
200
225
250
wavelength λ / nm

Figure 3

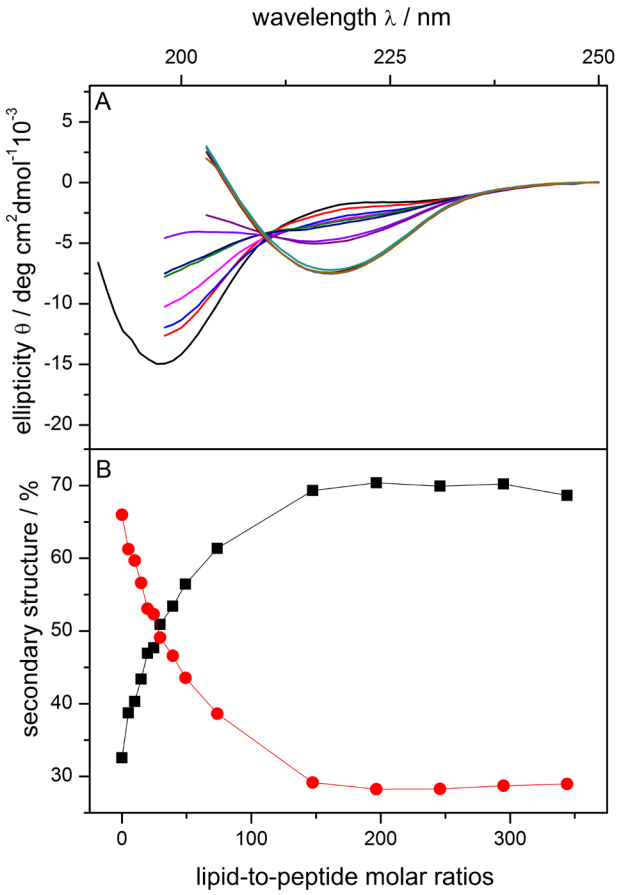
wavelength λ / nm
200
225
250
A
ellipticity θ / deg cm²dmol⁻¹10⁻³
5
0
-5
-10
-15
-20
B
secondary structure / %
70
60
50
40
30
0
100
200
300
lipid-to-peptide molar ratios

Figure 4

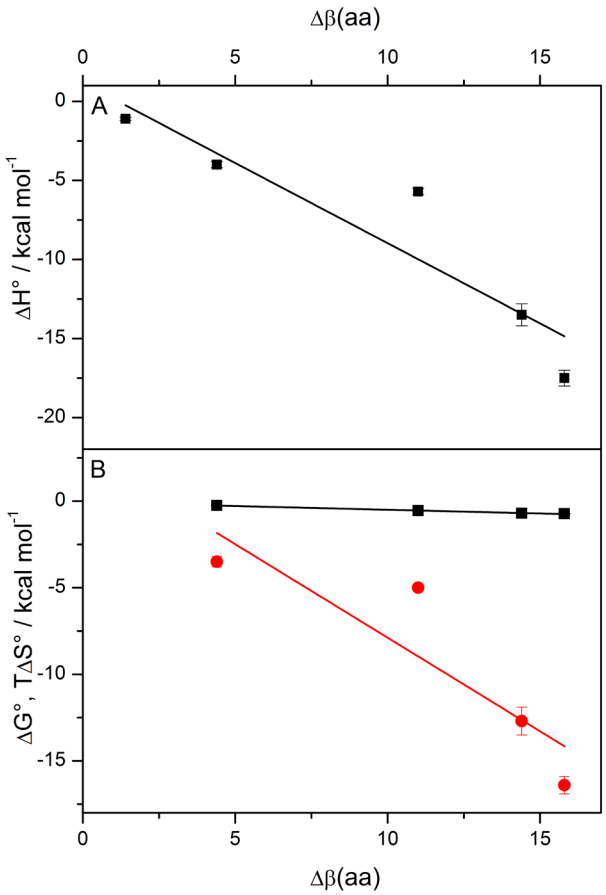
Δβ(aa)
0
5
10
15
A
0
-5
-10
-15
-20
ΔH° / kcal mol-1
B
0
-5
-10
-15
ΔG°, TΔS° / kcal mol-1
0
5
10
15
Δβ(aa)

Figure 5

Appendix

In this appendix, we show a representative example of a calorimetric and CD spectroscopy measurements of the interaction of the four studied double d-isomers of Aβ(1-40) with anionic PEGylated lipid vesicles.

Appendix figure captions

Appendix figure 1. Structural transition of d5, 6 Aβ(1-40) upon binding to SUVs composed of POPC/POPG/PEG (50/45/5 mol%) as monitored by CD spectroscopy. CD spectra were recorded in 5 mM Hepes (pH 7.4) at 25 °C. (A) CD spectra with varying lipid-to-peptide molar ratios between 0 and 396. (B) Fraction of secondary structure was plotted vs. the corresponding lipid-to-peptide molar ratios: (■) β-structure and (●) random coil and (▲) α-helix.

Appendix figure 2. (A) Experimental heat flow obtained by the injection of anionic SUVs (POPC/POPG/ mPEG 2000 PE (50/45/5 mol%) into a 6.2 μM d5, 6 Aβ(1-40) solution at 25 °C. (B) Binding isotherm derived from the ITC experiment displayed in (A). The solid line corresponds to the best fit of the surface partition model.

Appendix figure 3. Conformational change of d13, 14 Aβ(1-40) upon binding to SUVs composed of POPC/POPG/ mPEG 2000 PE (50/45/5 mol%) as measured by CD spectroscopy. CD spectra were recorded in 5 mM Hepes (pH 7.4) at 25 °C. (A) CD spectra with varying lipid-to-peptide molar ratios between 0 and 543. (B) Fraction of secondary structure was plotted vs. the corresponding lipid-to-peptide molar ratios: (■) β-structure and (●) random coil and (▲) α-helix.

Appendix figure 4. (A) Heat flow obtained by the injection of anionic SUVs (POPC/POPG/ mPEG 2000 PE (50/45/5 mol%)) into a 10.1 μM d13, 14 Aβ(1-40)

solution at 25 °C. (B) Binding isotherm derived from the ITC experiment displayed in (A). The solid line corresponds to the best fit of the surface partition model.

Appendix figure 5. Conformational change of d19, 20 Aβ(1-40) upon binding to SUVs composed of POPC/POPG/ mPEG 2000 PE (50/45/5 mol%) as observed by CD spectroscopy. CD spectra were recorded in 5 mM Hepes (pH 7.4) at 25 °C. (A) CD spectra with varying lipid-to-peptide molar ratios between 0 and 495. (B) Fraction of secondary structure was plotted vs. the corresponding lipid-to-peptide molar ratios: (■) β-structure and (●) random coil and (▲) α-helix.

Appendix figure 6. (A) Heat flow obtained by the injection of anionic SUVs (POPC/POPG/ mPEG 2000 PE (50/45/5 mol%) into a 12.5 µM d19, 20 Aβ(1-40) solution at 25 °C. (B) Binding isotherm derived from the ITC experiment displayed in (A). The solid line corresponds to the best fit of the surface partition model.

Appendix figure 7. Conformational change of d35, 36 Aβ(1-40) upon binding to SUVs composed of POPC/POPG/ mPEG 2000 PE (50/45/5 mol%) as observed by CD spectroscopy. CD spectra were recorded in 5 mM Hepes (pH 7.4) at 25 °C. (A) CD spectra with varying lipid-to-peptide molar ratios between 0 and 325. (B) Fraction of secondary structure was plotted vs. the corresponding lipid-to-peptide molar ratios: (■) β-structure and (●) random coil and (▲) α-helix.

Appendix figure 8. (A) Heat flow obtained by the injection of anionic SUVs (POPC/POPG/ mPEG 2000 PE (50/45/5 mol%)) into a 10.9 µM d19, 20 Aβ(1-40) solution at 25 °C. (B) Heats of reaction h_j derived from the ITC experiment displayed in (A) were plotted vs. the injection number n_j.

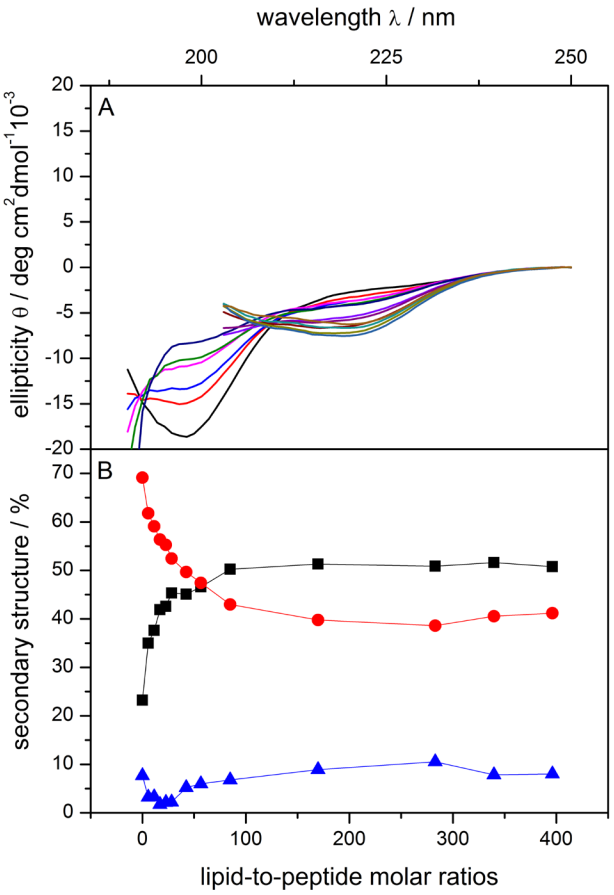

Appendix Figure 1

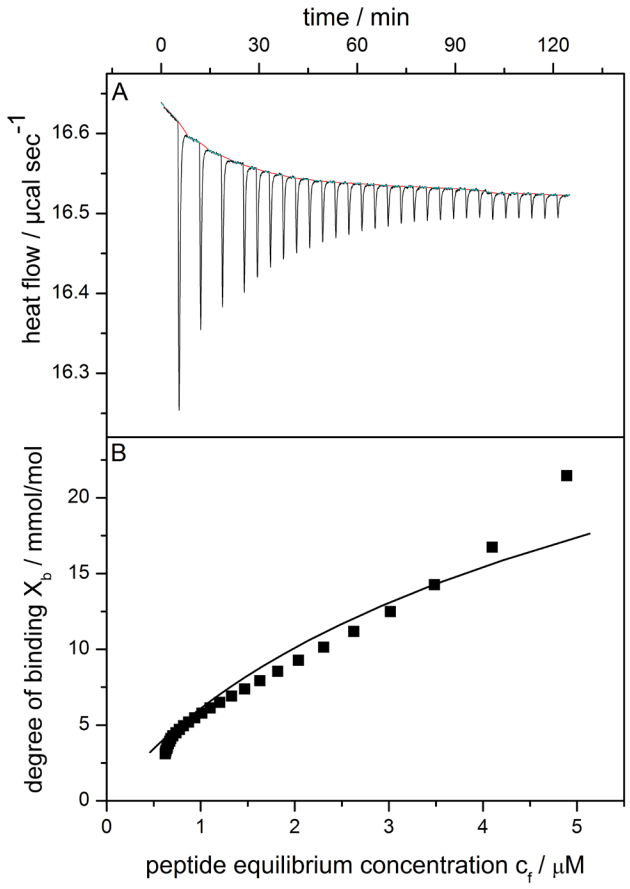

Appendix figure 2

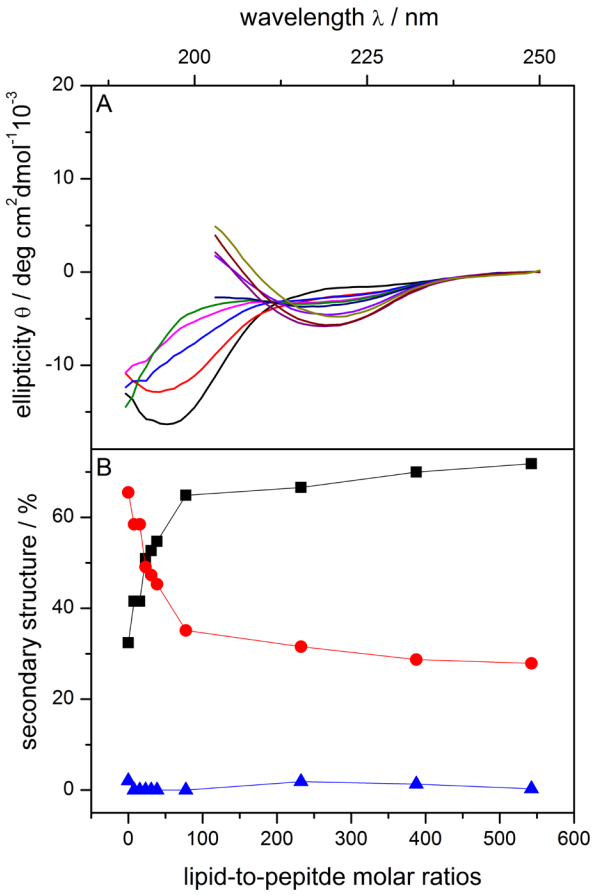

Appendix figure 3

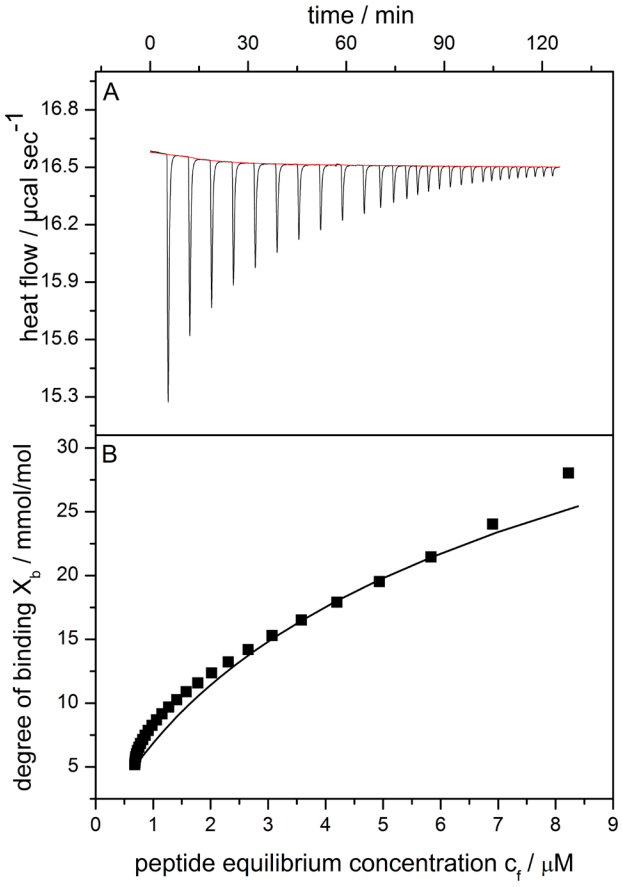

Appendix figure 4

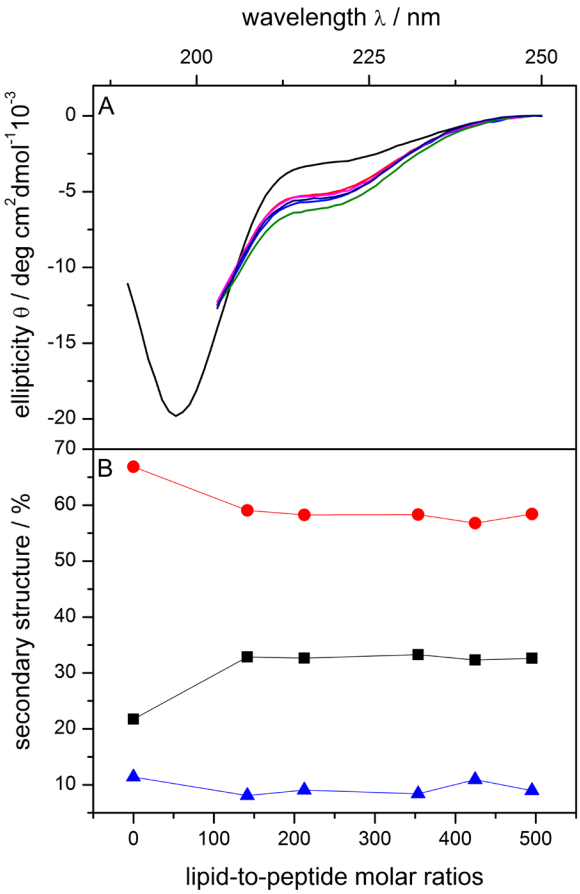

Appendix figure 5

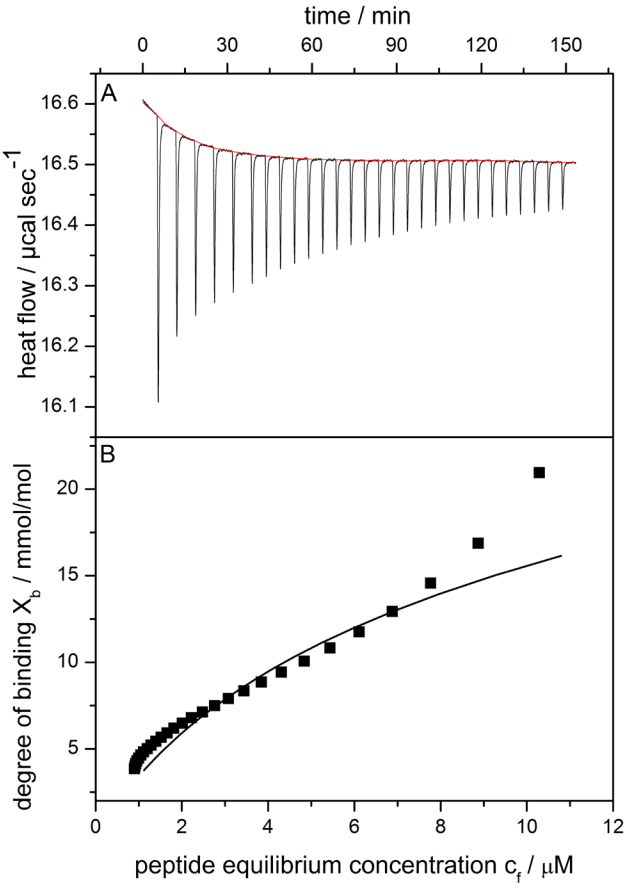

Appendix figure 6

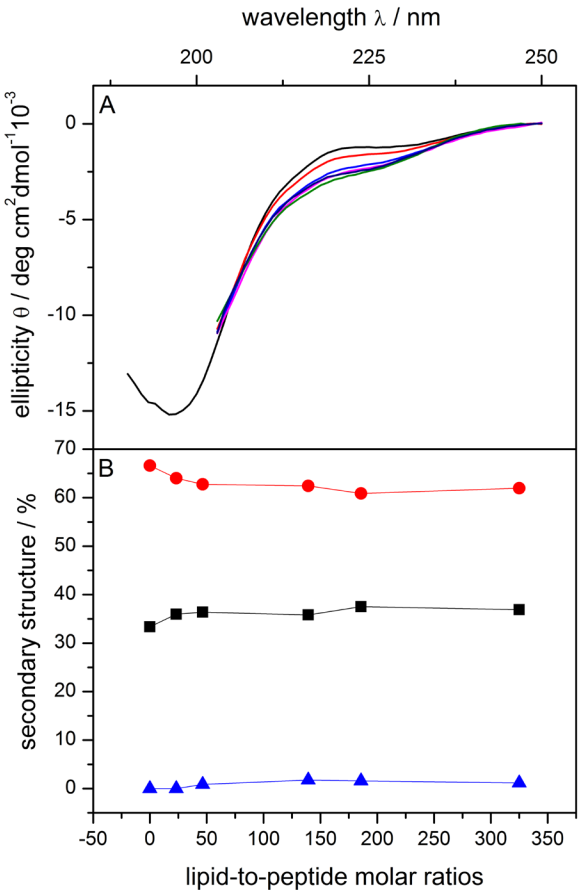

Appendix figure 7

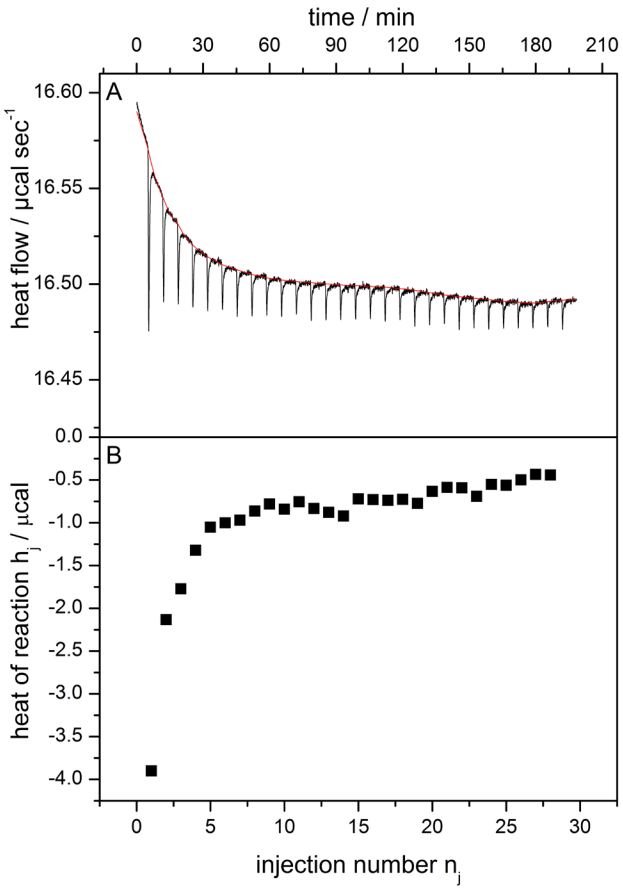

Appendix figure 8

3. Amyloid-β peptide interaction with glycosaminoglycans

Summary

Alzheimer's disease (AD) is a progressive, neurodegenerative disorder affecting around 25 million people worldwide. A major pathological hallmark of the disease are extracellular amyloid plaques, mainly composed of aggregated amyloid-β peptide (Aβ). Several other components are colocalized with the amyloid plaques, including glycosaminoglycans (GAGs) and proteoglycans (PG). GAGs are long, unbranched polysaccharides composed of a repeating disaccharide unit, which are covalently attached to the core protein of PGs. In vitro, GAGs and PGs have the ability to accelerate Aβ aggregation, suggesting the involvement of the Aβ-GAG/PG interaction in the Aβ aggregation process in vivo. Here, we have studied the binding equilibrium between Aβ(1-40) and heparin with isothermal titration calorimetry. Calorimetric data reveals a high affinity of Aβ(1-40) to heparin with a microscopic dissociation constant $K_d = 12.1 nM$, a reaction enthalpy $\Delta H^0_{A\beta} = -6.3 kcal/mol$ and a peptide-to-heparin stoichiometry $n = 16.1$ under the present experimental conditions (5 mM sodium acetate (pH 3.7)) at 25 °C. The obtained binding stoichiometry equals charge neutralization, which emphasize the electrostatics of the Aβ(1-40)-heparin interaction. However, temperature dependence studies reveals a negative heat capacity change of $\Delta c^0_p = -167 cal/molK$, indicating that also hydrophobic and other interactions are involved in the binding equilibrium. Circular dichroism (CD) spectroscopy reveals a conformational change of Aβ(1-40) from random-coil to β-

structure in the presence of heparin at pH 3.7. Studies with double d-isomers of Aβ(1-40) demonstrates that cluster of basic amino acids in the N-terminal domain, His_{13}-His_{14}-Gln_{15}-Lys_{16}, plays an important role in the Aβ(1-40)-heparin interaction. At physiological pH, CD measurements reveal no heparin-induced structural change of Aβ(1-40), suggesting that interaction is abolished at this pH.

Manuscript: Amyloid-β peptide interaction with glycosaminoglycans

Introduction

Alzheimer's disease (AD) is the major form of dementia with an estimated worldwide prevalence of 24 million people in 2005 (*1*). The increase of the life expectancy and the fact that a major risk factor for AD is age will even increase the impacts of the disease. In 2040, 81 million affected people are predicted with the highest increase rates in India, China, and their south Asian and western Pacific neighbours (*1*). Clinically, AD is characterized by the progressive loss of cognitive abilities and behavioral changes. One pathological hallmark of AD are extracellular amyloid plaques in the brain, mainly composed of amyloid fibrils formed by the amyloid-β peptide (henceforth called Aβ). Aβ is a 39-42 amino acid long peptide, derived from proteolytic cleavage of the membrane-bound amyloid precursor protein (APP) (*2*). In fibrils, Aβ exhibit a characteristic cross β-structure, in which the individual β-strands run perpendicular to the fibril axis (*3*). Soluble, monomeric Aβ has been demonstrated to be a normal component of the cerebro spinal fluid (CSF) and the blood plasma (*4-6*). In vitro, Aβ tends to aggregate into a polymorphic solution, including monomers, oligomers and fibrils. The aggregation process occurs in a nucleation-dependent manner (*7*), such as crystallization, and is highly dependent on pH (*8*), salt concentration (*9*) and nature of buffer (*10*). A nucleation-dependent

process is characterized by a nucleation phase, in which the peptide undergoes a series of thermodynamically unfavorable association steps to form a nucleus. After the nucleus is formed, further association steps become thermodynamically favorable, resulting in a rapid growth phase. Typically, oligomers are not observed until the monomer concentration exceeds the so-called critical concentration. In literature, different values of the critical concentration of Aβ are reported, probably due to differences in the chemical treatment of the peptide, physicochemical conditions such as pH and salt concentrations and the applied measurement techniques. At pH 7.4, critical concentration values of $6-9\,\mu M$ (*11*) and $40\,\mu M$ (*12*) were reported. However, the concentration of Aβ in vivo has found to be in the low subnanomolar range both in the healthy and diseased brain (*4-6*). Thus, the discrepancy between the in vivo concentration of Aβ and its critical concentration in vitro is at least four orders of magnitude. Several mechanisms are proposed to overcome this concentration discrepancy, including the interaction of Aβ to proteoglycans (PG) and glycosaminoglycans (GAGs). GAGs are long, unbranched polysaccharide composed of a repeating disaccharide unit, which are covalently attached to the core protein of PGs. The involvement of PG and GAGs in AD is mainly based on the findings that both components are found in amyloid plaques (*13*). In vitro experiments demonstrated that Aβ binds with high affinity to GAG (*14*) and that this interaction is dependent on both the pH and the fibrillar state of the Aβ (*15, 16*). To what extent Aβ interacts with GAGs or PG at physiological pH is still controversial. While some investigators report that Aβ interacts with GAG at physiological relevant (7.0) or even higher pH (*17, 18*), others claim that Aβ interacts with GAG only in its fibrillar state at physiological pH (*15*). Therefore, the question remains open whether Aβ-

GAG interaction is an putative nucleation mechanism or that if follows only after Aβ fibrillization. However, the interaction of PG with Aβ inhibits the proteolytic breakdown of amyloid fibrils, contributing to the accumulation and persistence of amyloid plaques (*15*). Further, it was demonstrated that the Aβ fibrillization is accelerated by the presence of PG, and that this acceleration is mainly mediated by the sulphate groups of the GAG (*19*)

In this study, we investigated the Aβ(1-40)-GAG interaction, using heparin as GAG molecule. Using isothermal titration calorimetry (ITC), we investigated the thermodynamic details of the binding reaction, and report here the microscopic binding constant K, the stoichiometry n and the reaction enthalpy ΔH^0. CD spectroscopy was applied to give insights into the structural aspects of the binding interaction. Finally, double d-isomers of Aβ(1-40) were used to study the existence of a molecular recognition site for the Aβ(1-40)-GAG interaction.

Material and Methods

Aß(1-40) was purchased from rPeptide (Bogart, GA, USA). The double d-isomers were kindly provided by Dr. M. Beyermann from the Leibniz-Institute of Molecular Pharmacology, 13125 Berlin, Germany. Unfractionated heparin (sodium salt, from porcine intestinal mucosa, average $M_r \sim 13000$) was purchased from Celsus Laboratories (Cincinnati, OH). All other chemicals were purchased from commercial sources at the highest purity.

Peptide solution preparation

Aβ(1-40) has been observed to exhibit significant experimental differences, depending on the manufacturer and even between different batches of the same

supplier. To decrease the variation between different batches, Aβ(1-40) and its double d-isomers were dissolved in hexafluoroisopropanol (HFIP) at 0.5 mg/ml and the stock solution was equilibrated for 1 h. The treatment with HFIP removes any pre-existing aggregates and defines a common chemical starting point. Aliquots of the stock solution were stored in glass tubes. HFIP is first removed by the means of gentle stream of nitrogen and by subsequent overnight vacuum. The samples were stored at a temperature of -20°C. For measurements, the appropriate volume of buffer was added. To accelerate the peptide solubilization, the peptide solution was sonicated for a short period of time.

Circular dichroism (CD) spectroscopy

CD measurements were performed on a Chirascan CD spectrometer (Applied Photophysics Ltd., Leatherhead, UK). Spectra were recorded from 250 nm to 190 nm, with a resolution of 1 nm, a response time of 20 s and a bandwidth of 1 nm. Unless noted otherwise, a quartz cuvette with a path length of 0.1 cm was used. Results are reported as mean molar residue ellipticities in units of deg cm^2 $dmol^{-1}$. The percentage of peptide secondary structure was estimated from a computer simulation based on the reference spectra obtained by Reed and Reed (*20*).

Isothermal titration calorimetry (ITC)

ITC was performed on a VP ITC calorimeter (MicroCal, Northampton, MA). To avoid air bubbles, all solutions were degassed in vacuum for ~10 min immediately prior use. Raw data were processed using the Origin software provided with the instrument.

Evaluation of calorimetric data

Calorimetric data were analyzed by a three-parameter nonlinear least-squares fitting (NLSF) in which the sum of squared residuals (SSR) is minimized. The fitting procedure was conducted in a Microsoft Excel worksheet using the Solver add-in. The confidence of the fitted parameters were determined with the help of SSR plots as described elsewhere (*21*). The parameters ΔH° and n exhibit SSR plots with a clear minimum and steep slopes on both sides and can therefore be determined with high confidence. However, the SSR plot of the parameter K generally reveal a minimum with a smooth slope to higher K values (maximal calculated K of $10^9 M^{-1}$), which preclude the determination of the parameter K with high confidence. For the best fit values of K we quote the minimum of the SSR plot.

Peptide concentration determination

Aβ(1-40) and its double-d-isomers do not contain a Trp residue, therefore the peptide concentration cannot be calculated using UV absorbance at 280 nm. Alternatively, the peptide concentration was determined by amino acid analysis. The amino acid analysis was conducted by the Protein Analytical Service facility of the University of Bern. The tubes for the analysis contain 50µl of the peptide-HFIP solution (0.5mg/ml). The tubes were first dried at RT and then overnight in vacuum.

Results

Conformation of Aβ(1-40) in aqueous solution

The aggregation of Aβ(1-40) is dependent on the peptide concentration itself and the physical-chemical environment such as pH, temperature, pressure, buffer and salt. Using Circular dichroism (CD) spectroscopy, we tested the effect of physical-

chemical parameters on the conformation of freshly dissolved Aβ(1-40). First, the effect of low pH values was studied. Figure 1 displays CD spectra of Aβ(1-40) dissolved in 5 mM sodium acetate with varying pH values from 3.7 to 4.2. At pH 3.7, CD spectrum exhibits a minimum at 198 nm indicating a mainly random coil conformation. As shown in figure 1A, the ellipicity at 198 nm is decreased with increasing pH values. An isobestic point could be observed at 211 nm indicating a two state transition. CD spectra were analyzed as described in the method section and the resulting fractions of secondary structure are displayed in Figure 1B. The content of α-helix remained constant at around 3% (not shown). The increase of pH from 3.7 to 4.2 resulted in an increase of β-structure by 13.2%, while the random coil content decreased by the same magnitude.

Figure 2 shows the salt influence of increasing NaCl concentrations on the CD spectra of Aβ(1-40) in 5 mM sodium acetate (pH 3.7) . The NaCl concentration was gradually increased from 0 to 20 mM and finally up to 100 mM. With the addition of NaCl, the elliptictiy at 198 nm decreased and became positive. A new minimum at 220 nm was observed, which is a characteristic of β-structure. The isosbestic point observed at 212 nm indicates again a two-state random coil-to-β-structure transition. Figure 2B shows a plot of secondary structure against the NaCl concentration. The addition of 20 mM NaCl increased β-structure content by 22%, while additional 80 mM NaCl only led to a further increase of 8%. Compared to NaCl, even stronger effects were observed with $NaSO_4$ whereas KCl induced a less pronounced effect (at identical ionic strength, data not shown).

Finally, the effect of both temperature and increasing concentration of sodium acetate (pH 3.7) on the secondary structure of Aβ(1-40) were studied. CD spectra revealed no

significant structural changes within the measured range of buffer (5 mM to 25 mM) (figure 3) and temperature (18-32°C) (data not shown). Further, the CD spectrum of Aβ(1-40) in 25 mM sodium acetate (pH 3.7) remains constant within 12 hours.

Heparin-induced conformational change of Aβ(1-40)

We performed CD measurements to monitor the structural changes of Aβ(1-40) upon binding to heparin. CD spectra were recorded in 5 mM sodium acetate (pH 3.7) at a peptide concentration of 15 µM and were titrated with a 28 µM heparin solution. The corresponding spectra are displayed in figure 4. An isosbestic point could not be observed for all spectra, indicating the involvement of more than two structural species.

CD spectra were divided depending on their heparin-to-Aβ(1-40) ratio (r) in into a low, intermediate and high heparin region. In absence of heparin, CD spectra of Aβ(1-40) shows a predominant random-coil conformation (66%) with some β-structure (33%). The addition of low amount of heparin (r=0-0.05) induced a random-coil-to-β-structure transition with an observed isosbestic point at 211 nm as shown in figure 4A. At a heparin-to-Aβ(1-40) ratio of 0.05, the CD spectra of Aβ(1-40) reveals a high content of β-structure (70%), while the content of random coil is 29%. This corresponds to an increase of β-structure by 37%. For heparin-to-Aβ(1-40) ratios of r=0.06-0.12, the spectral minimum is increased from $-3855\ to\ -1258\ \mathrm{deg}\,cm^2dmol^{-1}$ and shifted from 222 nm to 225 nm as displayed in figure 4B. In this intermediate region, the CD spectra could not be used to calculate the secondary structure. A possible explanation for this phenomena could be the interfering scattering by the presence of aggregates formed by the cross-linking of heparin molecules via Aβ(1-40), which was previously observed for the interaction of the peptide TAT-PTD with

heparan sulfate (*22*). Further addition of heparin brings the aggregates again in solution, as indicated by the CD spectra exhibiting a minimum at 220 nm and with ellipticities of $-4700\ to\ -5870 \deg cm^2 dmol^{-1}$. This corresponds to an increase of β-structure from 80% to 85% within this region.

Binding of Aβ(1-40) to heparin

Isothermal titration calorimetry (ITC) is an established method for the thermodynamic characterization of a binding reaction. Here ITC was applied to study the binding of Aβ(1-40) to heparin. A typical ITC experiment is shown in figure 5A. The ITC cell contained a 15 μM Aβ(1-40) solution which was titrated with 4 μl aliquots of a 28 μM heparin solution. Aβ(1-40) and heparin were both dissolved in 5 mM sodium acetate (pH 3.7). The heat flow of the injection peaks was integrated yielding the heat of reaction h_i for the i injection. As illustrated in figure 5A, h_i are initially exothermic, with an abrupt change to zero, before becoming endothermic. In the end of the calorimetric experiment, h_i approaches slowly zero. We assume that the all Aβ(1-40) were bound to heparin, as the heats of reaction become first zero. The endothermic heats in the end of the ITC experiment are assigned to lateral aggregation of small fibrils and/or crosslinking of heparin molecules. As a control experiment, heparin solution was titrated in buffer solution obtaining small heat peaks (not shown), which were included in the evaluation. For a better analysis of the calorimetric data, the maximal endothermic heat of reaction was subtracted from all h_i. The corrected heats of reaction are denoted as δh_i and can be plotted against the heparin-to-Aβ(1-40) molar ratio as displayed in figure 5B. The molar binding

enthalpy of Aβ(1-40), $\Delta H^0_{A\beta}$, can be directly derived from the ITC experiment and is calculated according to,

$$\Delta H^0_{A\beta} = \sum_{i=1}^{n} \delta h_i / n_{A\beta} \quad (1)$$

where $n_{A\beta}$ is the molar amount of Aβ(1-40) in the calorimetric cell and $\sum \delta h_i$ is the cumulative heat of reaction (the final endothermic heats of reaction were not considered). For the ITC measurement in figure 5, a molar binding enthalpy of $\Delta H^0_{A\beta} = -5.9 kcal / mol$ was determined.

As shown in figure 5B, the first few injections of heparin lead to rather constant heats of reaction with $\delta h_i = -11 \mu cal$. In the beginning of the ITC measurement Aβ(1-40) is in excess over heparin and complete binding of the injected heparin to Aβ(1-40) can be assumed. The molar heat of reaction of heparin can be calculated as $\Delta H^0_{Hep} = \delta h_i / n_{hep,injected} = -98.2 kcal / mol\, heparin$, where $n_{hep,injected}\,(112\, pmol)$ is the molar amount of injected heparin. The number of bound Aβ(1-40) per heparin molecule can be derived by the ratio $\Delta H^0_{Hep} / \Delta H^0_{A\beta}$, yielding a binding stoichiometry n of 16.6. To obtain the binding constant K and therefore complete the thermodynamic characterization of the Aβ(1-40)-heparin interaction, the binding isotherm was analyzed using the multisite binding model. In the multisite binding model, a macromolecule such heparin has n binding sites of identical affinity to a ligand and binding occurs in a noncooperative way. The characteristic equation of the model is (*23*):

$$\frac{[A\beta]_{bound}}{[H]_{total}} = \frac{nK[A\beta]_{free}}{1+K[A\beta]_{free}} \quad (2)$$

where n is the average number of Aβ(1-40) bound to a heparin molecule, K is the microscopic binding constant to each binding site of heparin. In the following, the indices t, f and b stand for the total, free and bound concentration of the compound in parentheses. In equation , the concentration of free Aβ(1-40), $[A\beta]_f$, can be replaced by the term $[A\beta]_f = [A\beta]_t - [A\beta]_b$ using the mass conservation. Simple mathematical rearrangements lead to a quadratic equation,

$$K[A\beta]_b^{\,2} - \left(1+K[A\beta]_t + nK[H]_t\right)[A\beta]_b + nK[H]_t[A\beta]_t = 0 \quad (3)$$

, which gives us the following expression of the concentration of bound Aβ(1-40), $[A\beta]_b$,

$$[A\beta]_b = \frac{\left(1+K[A\beta]_t + nK[H]_t\right) - \sqrt{\left(\left(1+K[A\beta]_t + nK[H]_t\right)^2 - 4nK^2[H]_t[A\beta]_t\right)}}{2K} \quad (4)$$

The total concentration of Aβ(1-40), $[A\beta]_t$, is adjusted after each injection. The concentration of bound Aβ(1-40), $[A\beta]_b$, is linked to the experimental ITC data according the following equation,

$$\delta h_i = \Delta H^0_{A\beta} \cdot \delta[A\beta]_{b,i} \cdot V_{cal} \quad (5)$$

where $\Delta H^0_{A\beta}$ is the molar binding enthalpy of Aβ(1-40) , $\delta[A\beta]_{b,i}$ is the change of concentration of bound Aβ(1-40) in the ith injection and V_{cal} is the volume of the calorimetric cell.

The data in figure 5 can now be fit using a three-parameter nonlinear least-square fitting (NLSF), obtaining the following parameters for the best fit: $K = 9.9 \cdot 10^7 M^{-1}; n = 16.1; \Delta H^0_{A\beta} = -6.3 kcal/mol$. The fit values of n and $\Delta H^0_{A\beta}$ are in good agreement to those determined by simple calculations from the calorimetric data ($n = 16.6; \Delta H^0_{A\beta} = -5.9 kcal/mol$. see above). The knowledge of the binding constant K allows the calculation of the free energy of binding ($\Delta G^0 = -10.9\ kcal/mol$) and the change in entropy ($T\Delta S^0 = 4.6 kcal/mol$).

A sulfur content of 12.4% was determined for a different batch of heparin obtained from the same manufacturer (*24*). Based on this sulfur content, the average disaccharide unit of the used heparin has a molecular weight of $M_r = 481.8$ and bears a charge of $+3.13$. Therefore, an average heparin molecule has an estimated charge of $+84.3$. On the other hand, Aβ(1-40) has a net charge of +5.14 at pH 3.7. Charge neutralization is fulfilled at a binding stoichiometry n of 16.4. The binding stoichiometry obtained from the calorimetric data therefore equals charge neutralization.

ITC measurements were also performed at 18 °C and 32 °C. Within this temperature range conformation of Aβ(1-40) is nearly constant as shown previously. Differences in the thermodynamics are thus not caused by structural differences of Aβ(1-40). All thermodynamic parameters measured at the three temperatures are summarized in

table 1. The binding stoichiometry of the Aβ(1-40)-heparin varied between 14.1 to 18.2 with increasing values at higher temperature. Moreover, the reaction enthalpy became more negative at higher temperature. The decrease was linearly dependent on temperature as displayed in figure 6. The molar heat capacity change is $\Delta C^0_{P,A\beta} = -167 cal\, mol^{-1}\, K^{-1}$ (slope of the regression line) and indicates a hydrophobic contribution to the binding process. The temperature dependence of the binding constant can be calculated with vant't Hoff's law, $\frac{d \ln K}{dT} = \Delta H^0_{A\beta} / RT^2$, using the experimentally determined temperature dependence of the molar reaction enthalpy as $\Delta H^0_{A\beta}(T) = \Delta H^0_{A\beta}(298.13K) + \Delta c^0_P (T - T_0)$. In figure 7, the dots correspond to the experimentally determined constants whereas the solid line shows the predicted temperature-dependence of the binding constant (using the experimentally determined binding constant at 25 °C). At 32 °C, the experimental binding constant is in good agreement with the predictions. However, a large discrepancy is found at 18 °C, which must be ascribed to particular difficulty in determine the binding constant from the calorimetric data at this temperature.

Comparision of Aβ(1-40) with double-d isomers

We have used a set of four double d-isomers of Aβ(1-40) to study the structural aspect of the Aβ(1-40)-heparin interaction. In the sequence of the double d-isomers two adjacent amino acids are substituted by their corresponding d-enantiomers. The double-d-amino acid substitution has been shown to lead to local disturbance of their secondary structure without altering other physical characteristics such as hydrophobicity or side-chain functionality (*25*). Figure 8 displays the CD spectra of the peptides in buffer (5mM sodium acetate (pH 3.7)) and upon binding to heparin.

While all peptides adopt a mainly random coil structure in aqueous solution, they fold to β-structure upon binding to heparin**.** Further, ITC measurements were performed for Aβ(1-40) and its double d-isomers in 5mM sodium acetate (pH 3.7) at 25°C and the thermodynamic binding parameters are summarized in table 2. All double d-isomers of Aβ(1-40) bind with high affinity to heparin as indicated by high binding constants (the corresponding dissociation constants are in the nanomolar range). Three double d-isomers, namely d5, 6, d19, 20 and d35, 36 Aβ(1-40), have dissociation constants which are slightly lower than the measured $K_d = 5.6 \pm 0.8 nM$ for Aβ(1-40). In contrast, d13, 14 Aβ(1-40) has a less high affinity to heparin indicated by a higher K_d-value of 14.0 ± 7.4 nM. All double d-isomers reveal a smaller stoichiometry n in comparison to Aβ(1-40), with n varying between 7.0 *to* 13.9. The binding of all double d-isomers to heparin is an exothermic reaction as indicated by negative binding enthalpies ΔH^0. Compared to Aβ(1-40), the double d-isomer d5, 6 exhibits identical $\Delta H^0_{A\beta}$-values, while the d13, 14 has smaller, and d19, 20 and d35, 36 larger negative $\Delta H^0_{A\beta}$-values.

Electrostatic of Aβ(1-40) –heparin interaction

Protein-polyelectrolyte interactions, such as the interaction of Aβ(1-40) with heparin, are strongly dependent on the salt concentration of the solution (*26*). A popular model to describe the salt dependence of the binding constant of protein to polyelectrolyte is the oligolysine model (*27*). The basis of this model is the counterion condensation which predicts that the charge of a polyelectrolyte such as heparin is partly neutralized by counterion condensation (*28*). The oligolysine model states that when ligand binding to a polyelectrolyte is accompanied by the penetration of z-charged

residues into the condensed counterion layer, in turn, z condensed counterions are released into the bulk solution. For ligand-heparin interaction, the salt-dependence of the observable binding constant is expressed by the following equation (*27*),

$$\log K_{obs} = \log K_0 + 0.01z - 0.434 - z\log\left[M^+\right] \quad (6)$$

where $\log K_0$ contains all physical contribution to binding other than counterion release and is assumed to be independent on the salt-concentration. $\log K_{obs}$ is predicted to be linearly dependent on the logarithm of the salt concentration with slope $d\log K_{obs} / d\log\left[salt\right] = -z$. The value of z is obtained by determining the slope in a log-log plot of the experimentally determined binding constant K_{obs} versus the salt concentration $\left[salt\right]$. To test the electrostatic effect on the thermodynamic parameters, the usual procedure is to gradually increase the salt concentration of the buffer solution. In the case of Aβ(1-40) at pH 3.7, the presence of salt immediately induces the aggregation process of Aβ(1-40), as indicated by the observed random-coil to β-structure transition of Aβ(1-40). As discussed above, the binding constant K can only be properly derived from the calorimetric data when Aβ(1-40) is in a monomeric state. Therefore, this approach is not suitable to study the salt-dependence of the Aβ(1-40)-heparin interaction. However, at pH 3.7, we observed that CD spectra of Aβ(1-40) are identical in a sodium acetate concentration range of 5 to 25 mM. Sodium acetate is formed by dissolving acetic acid into water with subsequent adjusting of pH by addition of NaOH. Using the pK_a value of acetic acid ($pK_a = 4.79$), the concentration of sodium ions in the buffer solution can be calculated, resulting in 0.07, 0.28 and 0.43 mM for 5, 15 and 25 mM sodium acetate

(pH 3.7). Although the concentration range of sodium is very small, ITC measurements were performed for three buffer concentrations (5, 15 and 25 mM) and the thermodynamic parameters are summarized in table 1. However, regression analysis of a $\log K_{obs} - \log\left[Na^{+}\right]$ plot yields a linear correlation with slope -0.75 (not significant). Nevertheless, the obtained z value of -0.75 is used as a rough prediction for the number of positively charged residues of Aβ(1-40) penetrating the condensed counterion layer of heparin. However, this z value is much smaller than the nominal net charge of Aβ(1-40) at pH 3.7 (+5.14). Discrepancy between z values and the nominal peptide charge were observed for oligolysine and to a much greater degree for the 26-amino-acid long peptide mellitin and can be ascribed to the flexibility of the peptide main and side chains(*27, 29*). By using equation (6) and $z = -0.75$, the salt-dependence of the binding constant of Aβ(1-40)-heparin interaction can now calculated and is displayed in figure 9. The binding constant decreases with increasing salt concentration and is reduced to $K_{obs} = 8.74 \cdot 10^{5} M^{-1}$ at physiological salt concentration (140mM). Same calculations were performed for z-values of 2.5 and 5, which corresponds to half and the whole net charge of the peptide at pH 3.7 and are also displayed in figure 9.

Aβ(1-40)-heparin interaction at physiological pH

CD spectroscopy was applied to examine the abiltiy of heparin to induce a structural transition of Aβ(1-40) at physiological pH. Aβ(1-40) was dissolved in 5mM Hepes (pH 7.4) containing 0 or 140 mM NaF. Hepes buffer was used instead of phosphate buffer, as phosphate buffer was reported to specifically shield electrostatic interactions which are important for the Aβ(1-40)-heparin interaction (*17*). NaF was preferred to NaCl in order to avoid excessive light absorption by the chloride ions

below 200 nm. Aβ(1-40) and heparin were mixed (1:1, m:m) and CD spectra of the peptide and the mixture were recorded at 0, 24, 48 and 96 hr for the two buffer conditions. In the absence of salt, CD spectra of Aβ(1-40) showed a predominant random-coil conformation and remained constant over the observed time range, as displayed in figure 10A. For the Aβ(1-40)-heparin mixture, virtually identical CD spectra were observed (figure 10B), leading to the conclusion that heparin cannot induce a structural transition of Aβ(1-40) at physiological pH.

In the presence of NaF, CD spectra of Aβ(1-40) exhibit a minimum at 200 nm, indicating a mainly disordered conformation as displayed in figure 10C. However, the spectra show a high variation, which is best illustrated by the varying values of the minimal ellipticity at 200 nm from $-17569\ to\ -11608 \deg cm^2 dmol^{-1}$. These variations, however, cannot be correlated with the time point of recording, as e.g. the spectra recorded at 72 hr shows the lowest minimal ellipticity at 198 nm. Similar results were obtained for the Aβ(1-40)-heparin mixtures (figure 10D). Here, CD spectra showed a minimum at 200 nm which are slightly increased in comparison to the spectra of Aβ(1-40) alone. However, the differences are not large enough to conclude that addition of heparin lead to a structural conformation change of Aβ(1-40).

Discussion

We studied the interaction of Aβ(1-40) with heparin over a broad range of pH and salt concentrations, including the physiological range. Isothermal titration calorimetry (ITC) is a valid and often used method to study binding interactions, including

peptide-glycosaminoglycan interactions (*24, 30*). ITC experiments provide the whole binding isotherm in a single experiment. However, the binding constant K, and therefore ΔG^0, can only be derived from the calorimetric data by using a specific binding model. Binding models, including the multisite binding model applied here, require the exact concentrations of both binding partners. While the handling of heparin is uncomplicated, Aβ(1-40) tends to aggregate in aqueous solution forming a polydispersed solution, including monomers, oligomers and fibrils. The concentration of such a solution cannot be determined. Therefore, Aβ(1-40) must be monomeric in order to obtain the binding constant from the calorimetric data. As a typical ITC experiments is normally finished in 60 to 90 min (including the calibration time), Aβ(1-40) should be monomeric and stable over this time range.

Aβ(1-40) in aqueous solution

The effect of varying pH and salt content on the conformation of freshly dissolved Aβ(1-40) was investigated by CD spectroscopy. Monomeric Aβ(1-40) produces a CD spectrum which is characterized by a high content of random coil and minor content of β-structure (*31*). Our CD measurements indicate that even small pH changes (0.1) in the pH range of 3.7 to 4.2 immediately change the Aβ(1-40) aggregation pattern, as illustrated by the increase of β-structure content of the freshly dissolved peptide. Analogous results were obtained when the pH was gradually decreased from 7.2 to 6.4 (phosphate buffer, data not shown). These data are consistent with previous observations of a more pronounced aggregation of Aβ(1-40) in the pH range of 4 to 7 (*8*). Specific charge-charge interactions between carboxylate groups of glutamate and aspartate residues and imidazolium of histidine residues have been proposed to account for the pH dependence of the Aβ(1-40) fibrillization (*32, 33*). Additionally,

salt bridges between D23 and K28 and K16 and E22 have been identified in amyloid fibrils, supporting the importance of charge-charge interactions (*34*). However, it was also claimed that these favorable charge-charge interactions are not essential for the Aβ(1-40) fibrillization (*35*). Here, we suggest that the diminishing electrostatic repulsion of the peptides near the isoelectric point plays the major role in the pH dependence of the Aβ(1-40) fibrillization.

We have also shown that the addition of salt induces a conformational transition from random coil to β-structure at pH 3.7. This indicates that the presence of salt favors the aggregation of Aβ(1-40) even at relative low salt concentration (5 mM). Our observations are in line with a previous study showing the positive effect of salt on the Aβ(1-40) aggregation process (*9*). It was concluded that salt affects the aggregation of Aβ(1-40) by a combination of specific ion-peptide interactions and a change of water structure, whereas unspecific Debye-Hückel screening was excluded. However, no change of the conformation of the freshly dissolved peptide was observed in the corresponding study (*9*). It is noteworthy to mention that all data of this study were measured at pH 9.0. To exclude differences due to differences in peptide source and sample preparations, similar CD measurements were conducted at pH 7.0 and 8.0. Indeed, CD experiments do not show any conformational change of Aβ(1-40) within 24 hr. Therefore, salt increases the kinetic of the aggregation process in a much greater extent at pH 3.7 compared to pH 7.0 (or 8.0). Both pH values represent the edge of the pH-dependent aggregation maximum of Aβ(1-40), and can be seen as equal vulnerable for aggregation. The reason for the immediate salt-induced conformational transition at pH 3.7 remains elusive.

However, our data clearly demonstrate that pH and salt can affect the aggregation properties of an Aβ(1-40) solution. In the pH range between 3.8 and 7.0, the Aβ(1-40) cannot be assumed as monomeric. This might be insignificant for certain questions and techniques, however, it is not for the study of the thermodynamics of the heparin-Aβ(1-40) interaction. As discussed above, the binding constant K can only be derived from the calorimetric data, when Aβ(1-40) is monomeric. Therefore, the strong dependence of the Aβ(1-40) aggregation on its physical-chemical environment, particular pH and salt concentration, limits the condition, in which we can properly study the Aβ(1-40)-heparin interaction by ITC.

Binding of Aβ(1-40) to heparin

Isothermal titration calorimetry shows that under the present experimental conditions (pH 3.7, no salt) monomeric Aβ(1-40) binds with high affinity to heparin with a dissociation constant of $K_d = 12.1 nM$ at 25 °C. Further, calorimetric data also demonstrate that heparin has multiple independent binding site for Aβ(1-40). Both negative ΔH^0 and positive $T\Delta S^0$ contribute to the free energy of binding reaction in the studied temperature range (18-32 °C). At 18 °C, the entropic contribution amounts to 56% of the total free energy, which decrease with increasing temperature to 40% at 32 °C. The positive entropy can be explained by the release of hydration water, which is further supported by the negative molar heat capacity $\Delta C^0_{P,A\beta}$. A negative molar heat capacity generally indicates the involvement of hydrophobic interaction. However, the obtained stoichiometry is equivalent to charge neutralization of heparin by Aβ(1-40), which indicates the importance of electrostatic interactions. Generally, the interaction of ligands to glycosaminoglycans is

considered to be electrostatic in nature, although other types of interactions may also occur (*36*).

The binding of Aβ(1-40) to heparin entails two processes: 1) association with the GAG molecule and 2) the structural transition to β-structure. Membrane binding studies using double d-isomers of Aβ(1-40) have demonstrated that the membrane-induced β-structure formation of Aβ(1-40) is an exothermic process with a ΔH_β-value of $-1.0\,kcal/mol\,per\,residue$ (chapter 2). Structural data have shown that he binding of Aβ(1-40) to heparin is associated with an increase of β-structure of 36% which corresponds to 14 amino acids changing from random coil to β-structure. Therefore, the contribution of the β-structure formation to the binding enthalpy is in the range of $-14\,kcal/mol$. An additional exothermic contribution to the enthalpy comes from the electrostatic interactions between the positively charged amino acids and the sulfur groups. Thus, the theoretically expected enthalpy is much lower than the experimentally determined $\Delta H^0 = -6.3\,kcal/mol$. However, a possible explanation for this differences could be that the β-structure formation in the heparin-Aβ(1-40) system is less exothermic compared to the membrane environment. This could be possible, since the thermodynamic of the β-structure formation has been shown to be highly dependent on the solvent (*37*). A similar observation was made for the GAG binding of the melittin (*29*). The binding of the peptide is accompanied by a structural transition from random-coil-to-α-helix. In aqueous solution, the helix formation is an exothermic process with an enthalpy of $\Delta H_\alpha^0 = -0.9\ to -1.1 kcal/mol$, whereas in the melittin-GAG system it was reported close to zero.

In the case of Aβ(1-40), the cluster of basic amino acids in the N-terminal domain, His13-His14-Gln15-Lys16, has been suggested to interact with glycosaminoglycans. This is primarily due to the cluster of positive charged amino acids, but also to its resemblance with the proposed consensus motif, BBXB (B is basic residue) for the heparin binding site on proteins (*38*). Further, it has proposed that the basic amino acids of Aβ(1-40) has to assume a specific conformation for glycosaminoglycans binding (*39*). However, to examine the existence of a molecular recognition for the Aβ(1-40)-heparin interaction, double d-isomers of Aβ(1-40) were studied. The main advantage of double-d substitution is that it does not alter important physical-chemical properties such as net charge, hydrophobicity and side-chain functionality (*25*). The site of double-d-substitutions were located in the N-terminal domain in the case of d5, 6 Aβ(1-40), in the putative glycosaminoglycan-binding site (d13, 14 Aβ(1-40)) and in region presumably involved in the β-structure (d19, 20 and d35, 36 Aβ(1-40)). Table 2 showed that all peptide binds with high affinity to heparin, as demonstrated by dissociation constants in the nanomolar range. However, d13, 14 Aβ(1-40) shows a slightly lower binding constant compared to the other peptides. The double d-isomers d5, 6 Aβ(1-40) exhibits nearly identical thermodynamic binding parameters, suggesting that N-terminal domain is not important for GAG binding. Double-d substitutions in regions involved in the β-structure do not affect the binding constant of the Aβ(1-40)-heparin interaction, but lead to smaller binding stoichiometry and larger binding enthalpies. This indicates the importance of the basic cluster of H13-K16 for the GAG-binding and that binding is maximal when the residues assume a specific conformation

The salt dependence of the binding of Aβ(1-40) to heparin cannot be directly measured, but can be predicted using the oligolysine model for the salt-dependence of protein-polyelectrolyte interactions (*27*). At 100 mM NaCl, we predict a binding constant of $K = 5 \cdot 10^6 M^{-1}$, which is similar to reported binding constant of $K = 3 \cdot 10^6 M^{-1}$ for the melittin-heparin interaction under similar conditions (100 mM NaCl, net charge of the peptide +5) (*29*).

The binding constant derived from the calorimetric data using the multisite binding model is the microscopic binding constant. For statistical reason, the binding constant for a specific binding step i to a macromolecule with n independent binding sites varies according to (*40*)

$$K_j = \frac{n+1-j}{j} K \tag{7}$$

Therefore, the binding constant for the first binding step correspond to $K_1 = nK$, whereas the last peptide binds with $K_n = K / n$. For the Aβ(1-40)-heparin interaction with a measured stoichiometry of ~ 17, the K_1 / K_n ratio is 289. . Thus, the first peptide has a 289 times higher binding constant as the last peptide. Such a high differences can be misinterpreted in terms two types of binding sites with high and low affinity, respectively (*22*). In vivo, the concentration of glycosaminoglycans can be assumed as in excess over Aβ(1-40), for which reason $K_1 = 17 \cdot K_0 = 1.7 \cdot 10^{10} M^{-1}$ is applied, which corresponds to a dissociation constant of $K_d = 0.6 nM$.

Physiological relevance of Aβ(1-40)-GAG interaction

To our knowledge, this study is the first thermodynamic characterization of the interaction of monomeric Aβ(1-40) to glycosaminoglycans (GAGs). ITC experiments revealed a dissociation constant of $K_d = 12.1 nM$ for the Aβ(1-40)-heparin interaction under the given experimental condition (low ionic strength, pH 3.7). Heparin naturally occurs in the granules of mast cells, and is therefore not directly available for Aβ(1-40) binding. However, heparin possesses a similar structure of the basic dissacharide unit compared to the physiologic more relevant heparan sulfate, but has a higher degree of sulfation (*41*). Earlier studies demonstrated that the dissociation constant of small cationic peptide to heparin was equal or only slightly lower (by one magnitude) compared to that of heparan sulfate, mainly due to the higher negative charge of heparin (*22, 29*). The involvement of GAGs in the Aβ fibrillization is based on findings that GAGs are colocalized in amyloid plaques (*13*) and that GAGs can accelerate the fibrillization process (*14*). Further, it was postulated that the Aβ-GAG interaction is a putative nucleation mechanism of the Aβ fibrillization in vivo (*17*). Indeed, CD experiments demonstrated that the presence of heparin at pH 3.7 induces a random-coil-to-β-structure transition in Aβ(1-40) (figure 4). However, no heparin-induced conformational change in Aβ(1-40) was observed at pH 7.4 within 96 hr, as illustrated in figure 10. Even salt has a larger effect on the conformation of Aβ(1-40) than the presence of heparin. Therefore, we conclude that it is rather unlikely that an extracellular Aβ(1-40) binds to GAGs on the cellular membrane, representing a putative nucleation mechanism in vivo. This results are in line with previous study, reporting that monomeric Aβ(1-40) interacts with GAGs only in the pH range of 4 to 6, whereas a fibrillar Aβ(1-40)-GAGs interaction was observed between pH 4 to 9

(*15*). However, it was found that a small portion of Aβ is indeed bound to the membrane (*42*). A part of these membrane-bound Aβs could be bound to GAGs attached at the cell surface. Neuronal membranes have a negative surface potential, leading to a lower pH at the surface compared to the bulk pH, which facilitate a Aβ(1-40)-GAG interaction. However, an alternative site of interaction emerges from the observation that Aβ(1-40) is formed not only at the plasma membrane, but also in the endosomes/lysosomes (*42*). The endosomal pH is ~ 5.5, and therefore favoring the Aβ-GAG interaction. As the Aβ oligomerization was shown to start intracellularly (*43*), the interaction of Aβ to GAG could play a role in the nucleation process.

References

1. Ferri, C. P., Prince, M., Brayne, C., Brodaty, H., Fratiglioni, L., Ganguli, M., Hall, K., Hasegawa, K., Hendrie, H., Huang, Y., Jorm, A., Mathers, C., Menezes, P. R., Rimmer, E., and Scazufca, M. (2005) Global prevalence of dementia: a Delphi consensus study, *Lancet 366*, 2112-2117.
2. Selkoe, D. J. (1994) Normal and abnormal biology of the beta-amyloid precursor protein, *Annu Rev Neurosci 17*, 489-517.
3. Kirschner, D. A., Abraham, C., and Selkoe, D. J. (1986) X-ray diffraction from intraneuronal paired helical filaments and extraneuronal amyloid fibers in Alzheimer disease indicates cross-beta conformation, *Proc Natl Acad Sci U S A 83*, 503-507.
4. Haass, C., Schlossmacher, M. G., Hung, A. Y., Vigo-Pelfrey, C., Mellon, A., Ostaszewski, B. L., Lieberburg, I., Koo, E. H., Schenk, D., Teplow, D. B., and et al. (1992) Amyloid beta-peptide is produced by cultured cells during normal metabolism, *Nature 359*, 322-325.
5. Seubert, P., Vigo-Pelfrey, C., Esch, F., Lee, M., Dovey, H., Davis, D., Sinha, S., Schlossmacher, M., Whaley, J., Swindlehurst, C., and et al. (1992) Isolation and quantification of soluble Alzheimer's beta-peptide from biological fluids, *Nature 359*, 325-327.
6. Shoji, M., Golde, T. E., Ghiso, J., Cheung, T. T., Estus, S., Shaffer, L. M., Cai, X. D., McKay, D. M., Tintner, R., Frangione, B., and et al. (1992) Production of the Alzheimer amyloid beta protein by normal proteolytic processing, *Science 258*, 126-129.
7. Jarrett, J. T., and Lansbury, P. T., Jr. (1993) Seeding "one-dimensional crystallization" of amyloid: a pathogenic mechanism in Alzheimer's disease and scrapie?, *Cell 73*, 1055-1058.
8. Wood, S. J., Maleeff, B., Hart, T., and Wetzel, R. (1996) Physical, morphological and functional differences between ph 5.8 and 7.4 aggregates of the Alzheimer's amyloid peptide Abeta, *J Mol Biol 256*, 870-877.
9. Klement, K., Wieligmann, K., Meinhardt, J., Hortschansky, P., Richter, W., and Fandrich, M. (2007) Effect of different salt ions on the propensity of aggregation and on the structure of Alzheimer's abeta(1-40) amyloid fibrils, *J Mol Biol 373*, 1321-1333.
10. Garvey, M., Tepper, K., Haupt, C., Knupfer, U., Klement, K., Meinhardt, J., Horn, U., Balbach, J., and Fandrich, M. (2011) Phosphate and HEPES buffers potently affect the fibrillation and oligomerization mechanism of Alzheimer's Abeta peptide, *Biochem Biophys Res Commun 409*, 385-388.
11. Jarrett, J. T., Berger, E. P., and Lansbury, P. T., Jr. (1993) The carboxy terminus of the beta amyloid protein is critical for the seeding of amyloid formation: implications for the pathogenesis of Alzheimer's disease, *Biochemistry 32*, 4693-4697.
12. Evans, K. C., Berger, E. P., Cho, C. G., Weisgraber, K. H., and Lansbury, P. T., Jr. (1995) Apolipoprotein E is a kinetic but not a thermodynamic inhibitor of amyloid formation: implications for the pathogenesis and treatment of Alzheimer disease, *Proc Natl Acad Sci U S A 92*, 763-767.
13. Snow, A. D., Mar, H., Nochlin, D., Kimata, K., Kato, M., Suzuki, S., Hassell, J., and Wight, T. N. (1988) The presence of heparan sulfate proteoglycans in

the neuritic plaques and congophilic angiopathy in Alzheimer's disease, *Am J Pathol 133*, 456-463.
14. Castillo, G. M., Ngo, C., Cummings, J., Wight, T. N., and Snow, A. D. (1997) Perlecan binds to the beta-amyloid proteins (A beta) of Alzheimer's disease, accelerates A beta fibril formation, and maintains A beta fibril stability, *J Neurochem 69*, 2452-2465.
15. Gupta-Bansal, R., Frederickson, R. C., and Brunden, K. R. (1995) Proteoglycan-mediated inhibition of A beta proteolysis. A potential cause of senile plaque accumulation, *The Journal of biological chemistry 270*, 18666-18671.
16. Watson, D. J., Lander, A. D., and Selkoe, D. J. (1997) Heparin-binding properties of the amyloidogenic peptides Abeta and amylin. Dependence on aggregation state and inhibition by Congo red, *J Biol Chem 272*, 31617-31624.
17. McLaurin, J., Franklin, T., Zhang, X., Deng, J., and Fraser, P. E. (1999) Interactions of Alzheimer amyloid-beta peptides with glycosaminoglycans effects on fibril nucleation and growth, *Eur J Biochem 266*, 1101-1110.
18. Ariga, T., Miyatake, T., and Yu, R. K. (2010) Role of proteoglycans and glycosaminoglycans in the pathogenesis of Alzheimer's disease and related disorders: amyloidogenesis and therapeutic strategies--a review, *J Neurosci Res 88*, 2303-2315.
19. Castillo, G. M., Lukito, W., Wight, T. N., and Snow, A. D. (1999) The sulfate moieties of glycosaminoglycans are critical for the enhancement of beta-amyloid protein fibril formation, *J Neurochem 72*, 1681-1687.
20. Reed, J., and Reed, T. A. (1997) A set of constructed type spectra for the practical estimation of peptide secondary structure from circular dichroism, *Anal Biochem 254*, 36-40.
21. Kemmer, G., and Keller, S. (2010) Nonlinear least-squares data fitting in Excel spreadsheets, *Nat Protoc 5*, 267-281.
22. Ziegler, A., and Seelig, J. (2004) Interaction of the protein transduction domain of HIV-1 TAT with heparan sulfate: binding mechanism and thermodynamic parameters, *Biophys J 86*, 254-263.
23. van Holde, K. E., Johnson, W. C., and Ho, P. S. (1998) Chemical equilibria involving macromolecules, In *Principles of Physical Biochemistry* (van Holde, K. E., Johnson, W. C., and Ho, P. S., Eds.) 1st ed., pp 605-611, Prentice Hall, Upper Saddle River, NJ.
24. Ziegler, A., and Seelig, J. (2011) Contributions of glycosaminoglycan binding and clustering to the biological uptake of the nonamphipathic cell-penetrating peptide WR9, *Biochemistry 50*, 4650-4664.
25. Rothemund, S., Beyermann, M., Krause, E., Krause, G., Bienert, M., Hodges, R. S., Sykes, B. D., and Sonnichsen, F. D. (1995) Structure effects of double D-amino acid replacements: a nuclear magnetic resonance and circular dichroism study using amphipathic model helices, *Biochemistry 34*, 12954-12962.
26. Privalov, P. L., Dragan, A. I., and Crane-Robinson, C. (2011) Interpreting protein/DNA interactions: distinguishing specific from non-specific and electrostatic from non-electrostatic components, *Nucleic Acids Res 39*, 2483-2491.

27. Fenley, M. O., Russo, C., and Manning, G. S. (2011) Theoretical assessment of the oligolysine model for ionic interactions in protein-DNA complexes, *J Phys Chem B 115*, 9864-9872.
28. Manning, G. S. (1978) The molecular theory of polyelectrolyte solutions with applications to the electrostatic properties of polynucleotides, *Q Rev Biophys 11*, 179-246.
29. Klocek, G., and Seelig, J. (2008) Melittin interaction with sulfated cell surface sugars, *Biochemistry 47*, 2841-2849.
30. Ziegler, A., and Seelig, J. (2007) High affinity of the cell-penetrating peptide HIV-1 Tat-PTD for DNA, *Biochemistry 46*, 8138-8145.
31. Terzi, E., Holzemann, G., and Seelig, J. (1995) Self-association of beta-amyloid peptide (1-40) in solution and binding to lipid membranes, *J Mol Biol 252*, 633-642.
32. Fraser, P. E., Nguyen, J. T., Surewicz, W. K., and Kirschner, D. A. (1991) pH-dependent structural transitions of Alzheimer amyloid peptides, *Biophys J 60*, 1190-1201.
33. Hou, L., Shao, H., Zhang, Y., Li, H., Menon, N. K., Neuhaus, E. B., Brewer, J. M., Byeon, I. J., Ray, D. G., Vitek, M. P., Iwashita, T., Makula, R. A., Przybyla, A. B., and Zagorski, M. G. (2004) Solution NMR studies of the A beta(1-40) and A beta(1-42) peptides establish that the Met35 oxidation state affects the mechanism of amyloid formation, *J Am Chem Soc 126*, 1992-2005.
34. Petkova, A. T., Ishii, Y., Balbach, J. J., Antzutkin, O. N., Leapman, R. D., Delaglio, F., and Tycko, R. (2002) A structural model for Alzheimer's beta -amyloid fibrils based on experimental constraints from solid state NMR, *Proc Natl Acad Sci U S A 99*, 16742-16747.
35. Guo, M., Gorman, P. M., Rico, M., Chakrabartty, A., and Laurents, D. V. (2005) Charge substitution shows that repulsive electrostatic interactions impede the oligomerization of Alzheimer amyloid peptides, *FEBS Lett 579*, 3574-3578.
36. Lindahl, U., and Hook, M. (1978) Glycosaminoglycans and their binding to biological macromolecules, *Annu Rev Biochem 47*, 385-417.
37. Meier, M., and Seelig, J. (2007) Thermodynamics of the coil <==> beta-sheet transition in a membrane environment, *J Mol Biol 369*, 277-289.
38. Cardin, A. D., and Weintraub, H. J. (1989) Molecular modeling of protein-glycosaminoglycan interactions, *Arteriosclerosis 9*, 21-32.
39. McLaurin, J., and Fraser, P. E. (2000) Effect of amino-acid substitutions on Alzheimer's amyloid-beta peptide-glycosaminoglycan interactions, *Eur J Biochem 267*, 6353-6361.
40. van Holde, K. E., Johnson, W. C., and Ho, P. S. (1998) *Principles of Physical Biochemistry*, Prentice Hall, Upper Saddle River, NJ.
41. Rusnati, M., Coltrini, D., Oreste, P., Zoppetti, G., Albini, A., Noonan, D., d'Adda di Fagagna, F., Giacca, M., and Presta, M. (1997) Interaction of HIV-1 Tat protein with heparin. Role of the backbone structure, sulfation, and size, *The Journal of biological chemistry 272*, 11313-11320.
42. Rajendran, L., Honsho, M., Zahn, T. R., Keller, P., Geiger, K. D., Verkade, P., and Simons, K. (2006) Alzheimer's disease beta-amyloid peptides are released in association with exosomes, *Proc Natl Acad Sci U S A 103*, 11172-11177.

43. Walsh, D. M., Tseng, B. P., Rydel, R. E., Podlisny, M. B., and Selkoe, D. J. (2000) The oligomerization of amyloid beta-protein begins intracellularly in cells derived from human brain, *Biochemistry 39*, 10831-10839.

Table 1. Thermodynamic parameters[a)] of Aβ(1-40)-heparin interaction at indicated temperatures and buffer concentrations.

Temperature (°C)	C_{buffer}(mM)	K_d (nM)	stoichiometry ($n_{A\beta}/n_{heparin}$)	$\Delta H°_{A\beta}$(kcal/mol)	$\Delta G°_{A\beta}$(kcal/mol)[b)]	$T\Delta S°_{A\beta}$(kcal/mol)[c)]
18	15	3.0 ± 0.6	14.1 ± 0.7	-4.9 ± 0.2	-11.4 ± 0.1	6.5 ± 0.1
25	15	12.1 ± 5.6	16.1 ± 0.5	-6.3 ± 0.2	-10.9 ± 0.3	4.6 ± 0.4
32	15	18.0 ± 3.1	18.2 ± 0.9	-7.3 ± 0.2	-10.8 ± 0.1	3.6 ± 0.3
25	5	5.6 ± 0.8	14.6 ± 0.9	-7.0 ± 0.4	-11.3 ± 0.1	4.2 ± 0.4
25	15	12.1 ± 5.6	16.1 ± 0.5	-6.3 ± 0.2	-10.9 ± 0.3	4.6 ± 0.4
25	25	7.8 ± 2.4	16.6 ± 0.5	-5.6 ± 0.2	-11.1 ± 0.2	5.5 ± 0.2

[a)] Thermodynamic parameters were derived using the multisite binding model described by equations 2-5.

[b)] The free energy $\Delta G°_{A\beta}$ of peptide binding reaction was calculated according to $\Delta G^0_{A\beta} = RT\ln(K_d)$.

[c)] The entropy $T\Delta S°_{A\beta}$ of the peptide binding reaction was calculated according to $\Delta G^0 = \Delta H^0 - T\Delta S^0$.

Table 2. Thermodynamic binding parameters of Aβ(1-40) and four double d-isomers to heparin at 25 °C.

Peptide	K_d (nM)	stoichiometry ($n_{A\beta}/n_{heparin}$)	$\Delta H°_{A\beta}$(kcal/mol)	$\Delta G°_{A\beta}$(kcal/mol)[a]	$T\Delta S°_{A\beta}$(kcal/mol)[b]
Aβ(1-40)	5.6 ± 0.8	14.6 ± 0.9	-7.0 ± 0.4	-11.3 ± 0.1	4.2 ± 0.4
d5, 6 Aβ(1-40)	2.7 ± 1.3	13.9 ± 3.59	-6.2 ± 2.0	-11.8 ± 0.3	5.6 ± 1.8
d13, 14 Aβ(1-40)	14.0 ± 7.4	12.3 ± 0.8	-4.2 ± 0.2	-10.8 ± 0.3	6.6 ± 0.1
d19, 20 Aβ(1-40)	2.6 ± 0.3	8.6 ± 0.2	-9.3 ± 0.3	-11.7 ± 0.1	2.4 ± 0.3
d35, 36 Aβ(1-40)	1.8 ± 0.6	7.0 ± 0.4	-9.3 ± 0.2	-12.0 ± 0.2	2.8 ± 0.1

[a] The free energy $\Delta G°_{A\beta}$ of peptide binding reaction was calculated according to $\Delta G^0_{A\beta} = RT\ln(K_d)$.

[b] The entropy $T\Delta S°_{A\beta}$ of the peptide binding reaction was calculated according to $\Delta G^0 = \Delta H^0 - T\Delta S^0$.

Figure Captions

Figure 1. (A) Circular dichroism (CD) spectra of Aβ(1-40) dissolved in 5 mM sodium acetate with varying pH values from 3.7 to 4.2. From top to bottom at 198 nm: pH 4.2, 4.1, 4.0, 3.9, 3.8 and 3.7. The spectra were recorded at peptide concentration of 18.3 μM at 25 °C. (B) Content of secondary structure versus the pH of the buffer solution: (■) β-structure and (●) random coil.

Figure 2. Effect of NaCl on conformation of freshly dissolved Aβ(1-40).(A) Circular dichroism (CD) spectra of Aβ(1-40) dissolved in 5 mM sodium acetate (pH 3.7) containing various concentration of NaCl. Spectra from the bottom to the top at 198nm: 0 mM, 5 mM, 10 mM, 15 mM, 20 mM and 100 mM NaCl. The spectra were recorded immediately dissolving the peptide and at a peptide concentration of 18.3 μM at 25 °C. (B) Fraction of secondary structure of Aβ(1-40) are plotted against the NaCl concentration in 5 mM sodium acetate (pH 3.7): (■) β-structure and (●) random coil.

Figure 3. CD spectra of Aβ(1-40) dissolved in sodium acetate (pH 3.7) of varying concentrations (5 mM to 25 mM). Spectra were recorded at a peptide concentration of 18.5 μM at 25°C.

Figure 4. Structural transition of Aβ(1-40) upon binding to heparin monitored by circular dichroism (CD) spectroscopy. All spectra were recorded in 5 mM sodium

acetate (pH 3.7) at 25 °C. Heparin-to-Aβ(1-40) ratio (r) varied between 0 and 0.25. (A) black, r=0; red, r=0.01; blue, r=0.02 and magenta, r=0.05. (B) black, r=0.06; red, r=0.07; blue, r=0.09; magenta, r=0.10 and olive, r=0.12. (C) black, r=0.15; red, r=0.17; blue, r=0.20; magenta, r=0.21; olive, r=0.22; navy, r=0.24 and violet, r=0.25.

Figure 5. (A) Calorimetric trace obtained by titrating 28 μM heparin solution into a 15.3 μM Aβ(1-40) solution (5 mM sodium acetate (pH 3.7)) at 25 °C. Each peak corresponds to an injection of 4 μl heparin solution, occurred at 5 min intervals. (B) Heats of reaction δh_i derived from the ITC experiment above are plotted against the molar ratio of heparin to Aβ(1-40). The solid line corresponds to the best fit of the multisite binding model to the experimentally determined δh_i using the paramters: $K = 3.11 \cdot 10^8 M; n = 13.6; \Delta H^0_{A\beta} = -5.94 kcal / mol$.

Figure 6. Temperature dependence of the molar binding enthalpies of the binding of Aβ(1-40) to heparin . The molar binding enthalpies derived from ITC experiments are plotted against the measuring temperature. Each point corresponds to an ITC measurement. The solid line correspond to the regression line with a slope of $\Delta C^0_{P,A\beta} = -167 cal\, mol^{-1} K^{-1}$.

Figure 7. Temperature dependence of the binding constant of the Aβ(1-40)-heparin interaction. Dots correspond to experimentally measured binding constants (T=18, 25 and 32 °C). Solid line corresponds to the calculated binding constant using vant't

Hoff's law and the temperature dependence of the molar reaction enthalpy as $\Delta H^0_{A\beta}(T) = \Delta H^0_{A\beta}(T_0) + \Delta c^0_P(T - T_0)$.

Figure 8. Circular dichroism (CD) spectra of Aβ(1-40) and four double d-isomers (A) in aqueous solution and (B) in the presence of heparin. black: Aβ(1-40) , red: d5, 6, blue: d13, 14, magenta: d19, 20 and olive:d35, 36. The heparin-to-peptide molar ratio was about 2. Both heparin and Aβ(1-40) were dissolved in 5 mM sodium acetate (pH 3.7) and the spectra were recorded at peptide concentration of 5.4-18 μM.

Figure 9. Salt dependence of the binding constant K of the Aβ(1-40)-heparin interaction at pH 3.7. The solid lines were calculated by equation 6 using z-value of 0.75 (black, experimentally predicted), 2.5 (red, half the nominal net charge) and 5 (blue, nominal net charge).

Figure 10. Aβ(1-40)-heparin interaction at pH 7.4 monitored by circular dichroism (CD) spectroscopy. The following buffers were used: (A-B) 5 mM Hepes (pH 7.4), (C-D) 5 mM Hepes (pH 7.4), 140 mM NaF. CD spectra were recorded at 0 (black), 24 (red), 48 (blue) and 96 hr (olive) at peptide concentration of 15 μM (A, C) and 13 μM (B, C). (A, C) Aβ(1-40) alone, (B, D) Aβ(1-40)-heparin (1:1, m:m).

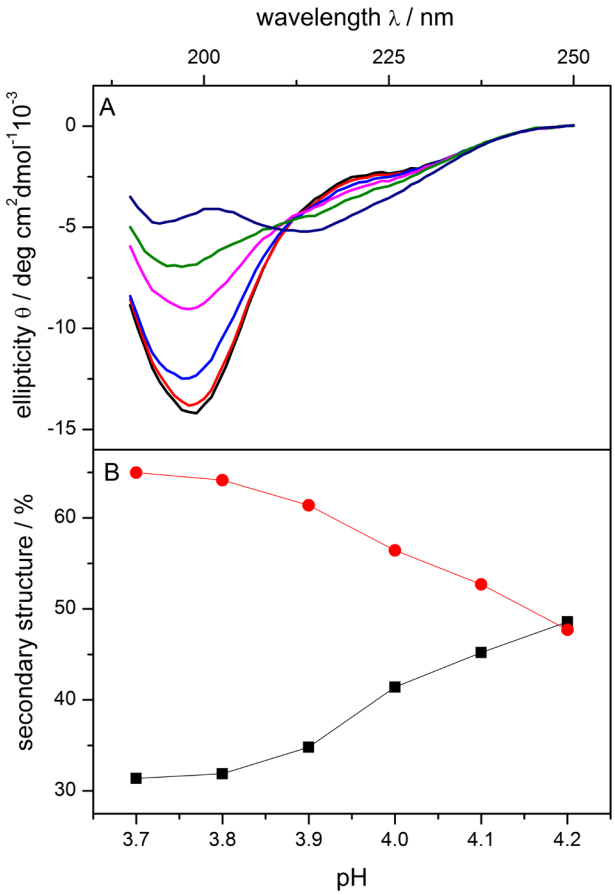
wavelength λ / nm
200
225
250
A
ellipticity θ / deg cm²dmol⁻¹10⁻³
0
-5
-10
-15
B
secondary structure / %
60
50
40
30
3.7
3.8
3.9
4.0
4.1
4.2
pH

Figure 1

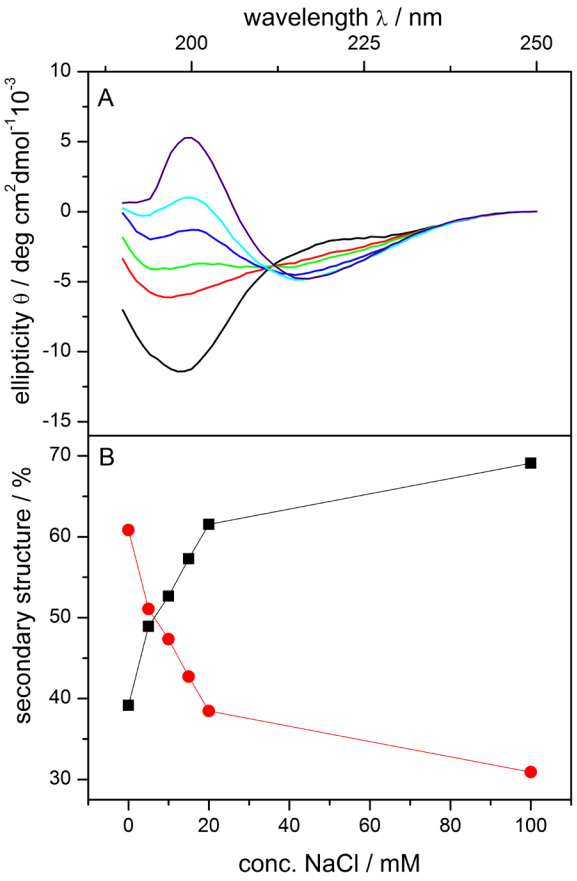
wavelength λ / nm
200
225
250
A
ellipticity θ / deg cm²dmol⁻¹10⁻³
10
5
0
-5
-10
-15
B
secondary structure / %
70
60
50
40
30
0
20
40
60
80
100
conc. NaCl / mM

Figure 2

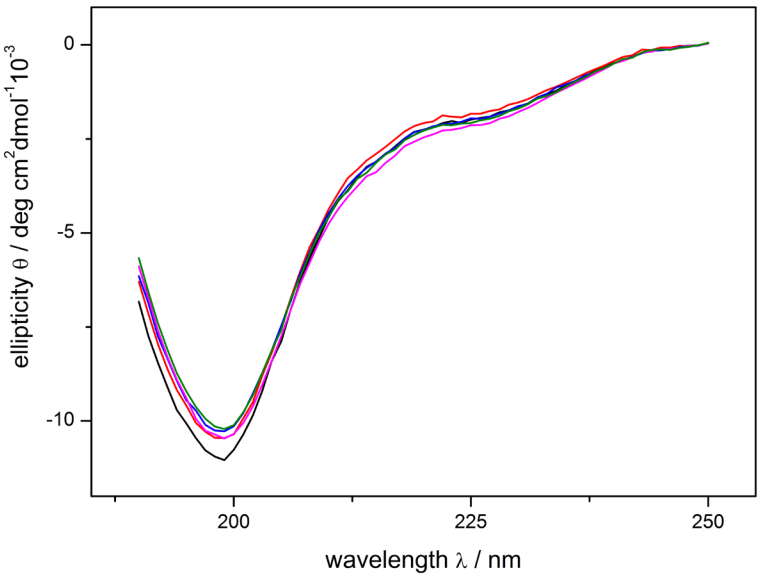
0
-5
-10
ellipticity θ / deg cm²dmol⁻¹10⁻³
200
225
250
wavelength λ / nm

Figure 3

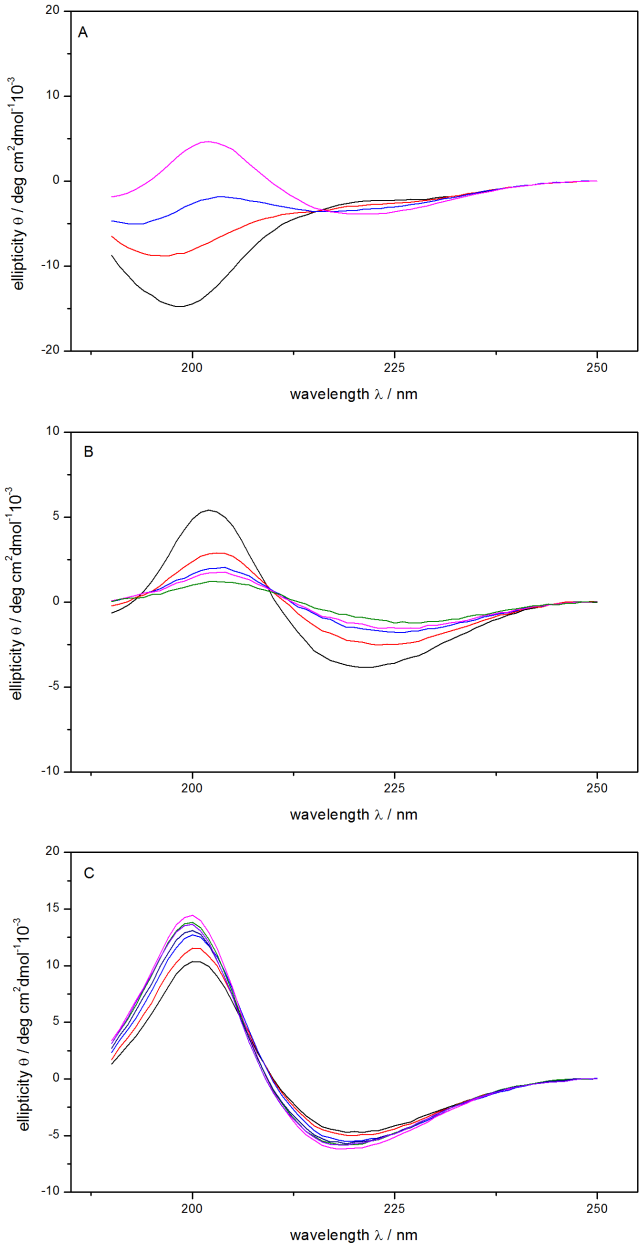
A
ellipticity θ / deg cm²dmol⁻¹10⁻³
wavelength λ / nm
B
ellipticity θ / deg cm²dmol⁻¹10⁻³
wavelength λ / nm
C
ellipticity θ / deg cm²dmol⁻¹10⁻³
wavelength λ / nm

Figure 4

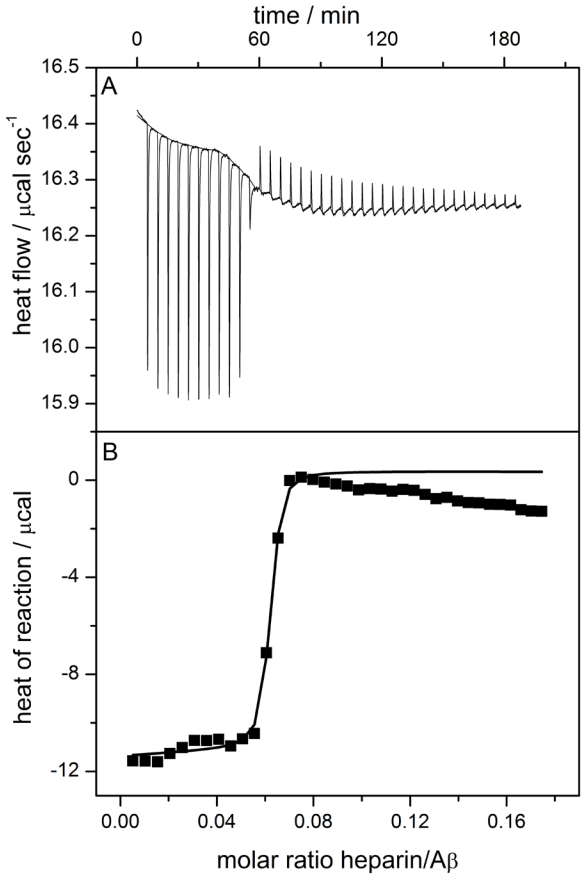
time / min
0
60
120
180
A
heat flow / µcal sec-1
16.5
16.4
16.3
16.2
16.1
16.0
15.9
B
heat of reaction / µcal
0
-4
-8
-12
0.00
0.04
0.08
0.12
0.16
molar ratio heparin/Aβ

Figure 5

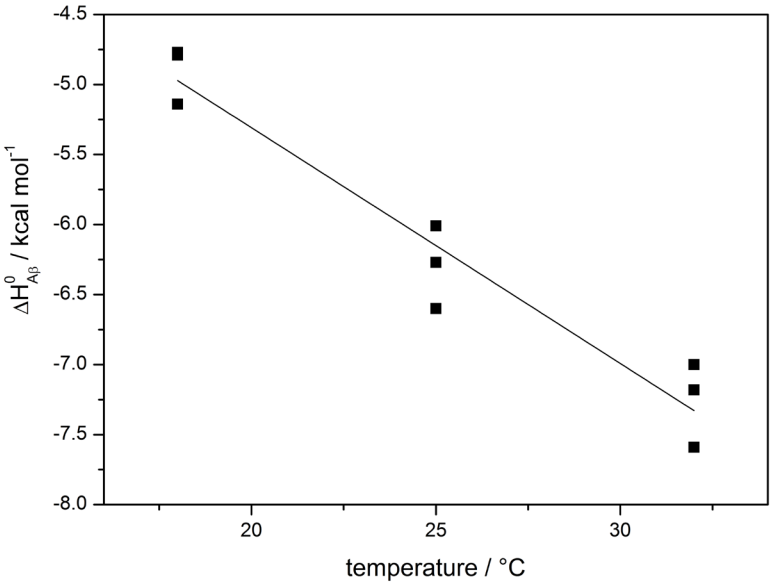
-4.5
-5.0
-5.5
-6.0
-6.5
-7.0
-7.5
-8.0
$\Delta H^0_{A\beta}$ / kcal mol^{-1}
20
25
30
temperature / °C

Figure 6

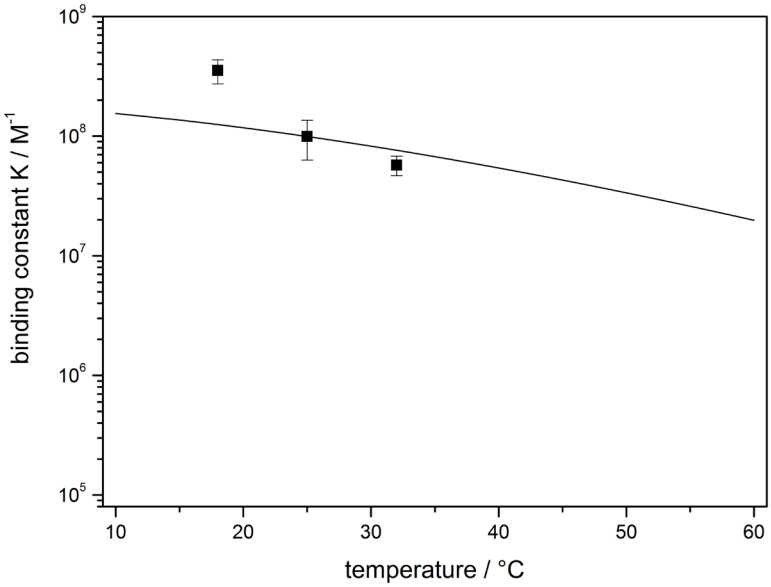
binding constant K / M-1
temperature / °C
10^9
10^8
10^7
10^6
10^5
10
20
30
40
50
60

Figure 7

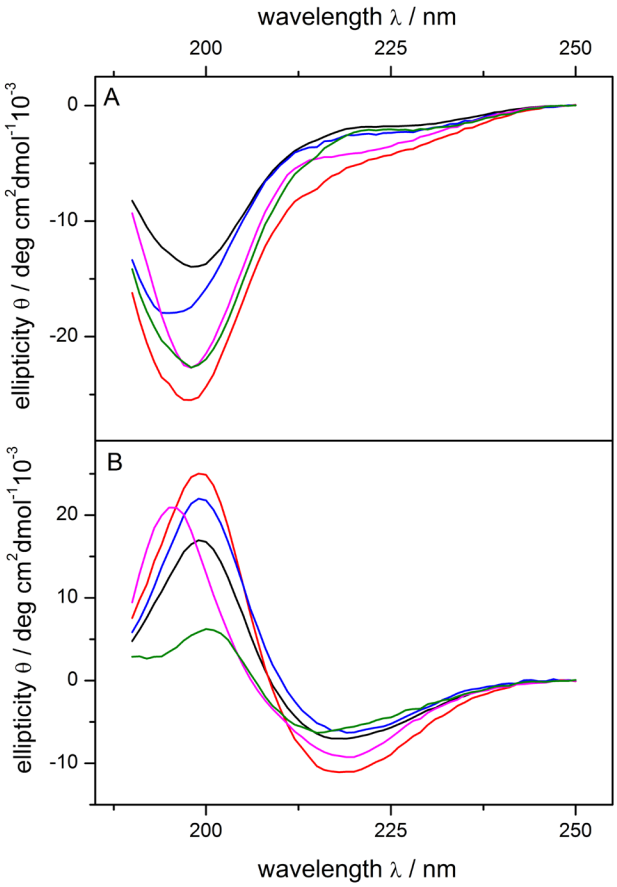
wavelength λ / nm
200
225
250
A
0
-10
-20
ellipticity θ / deg cm²dmol⁻¹10⁻³
B
20
10
0
-10
ellipticity θ / deg cm²dmol⁻¹10⁻³
200
225
250
wavelength λ / nm

Figure 8

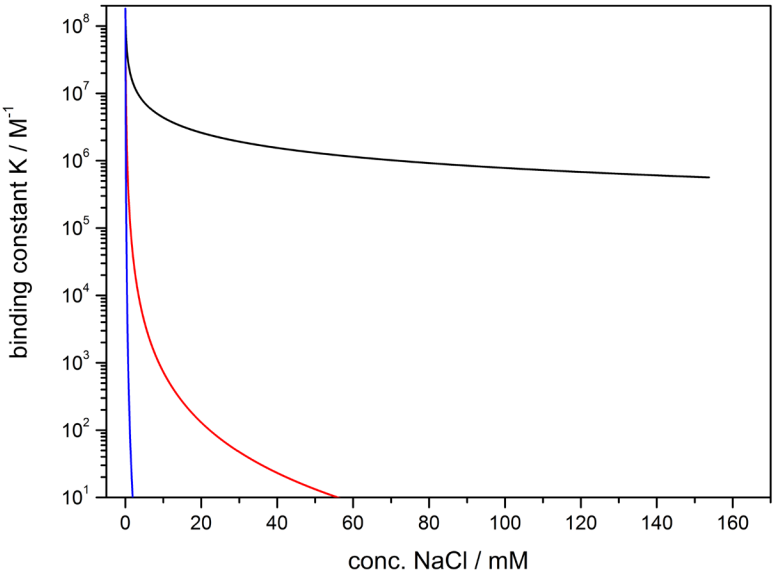
binding constant K / M-1
10^8
10^7
10^6
10^5
10^4
10^3
10^2
10^1
0
20
40
60
80
100
120
140
160
conc. NaCl / mM

Figure 9

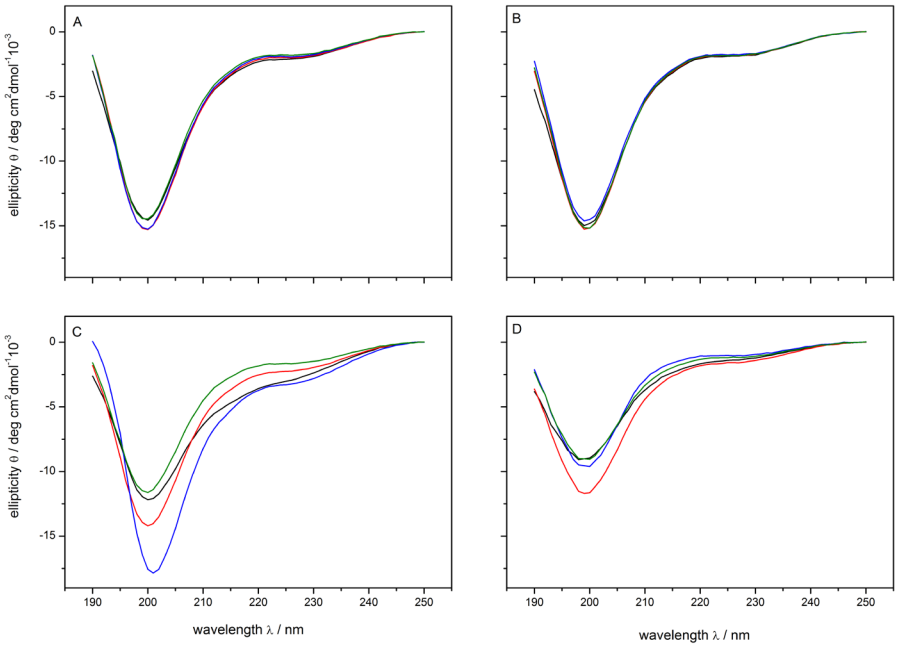
A
B
C
D
ellipticity θ / deg cm²dmol⁻¹10⁻³
0
-5
-10
-15
190
200
210
220
230
240
250
wavelength λ / nm

Figure 10

Appendix

In the previous section, we have studied the thermodynamics of the Aβ(1-40)-heparin interaction at pH 3.7 using isothermal titration calorimetry (ITC). At this pH, Aβ(1-40) is monomeric, which is a prerequisite to determine the binding constant, and therefore the free energy of binding ΔG^0, from the calorimetric data. As previously discussed, Aβ(1-40)-GAG interaction is considered as highly pH dependent. Therefore, we were interested to study the effect of pH on the thermodynamics of the Aβ(1-40)-heparin interaction. However, circular dichroism (CD) spectroscopy revealed that Aβ(1-40) is not monomeric in the pH range of 3.8 to 7, which a priori precludes the determination of binding constants from calorimetric experiments. Nevertheless, we performed CD and ITC measurements in this pH range, namely at pH 4.7 and 6.0. Further, we studied the effect of salt (NaCl) on the thermodynamics of the Aβ(1-40)-heparin interaction at pH 5.0.

Aβ(1-40)-heparin interaction at pH 4.7

The interaction of Aβ(1-40) with heparin has been studied at pH 4.7 in 5 mM sodium acetate. First, CD spectroscopy was applied to examine effect of heparin on the conformation of Aβ(1-40). Figure 1A displays the CD spectra of Aβ(1-40) in buffer and mixed with different amounts of heparin. The heparin-to-Aβ(1-40) molar ratio (r) was increased from 0 to 0.18. The corresponding fractions of secondary structure were evaluated as described before, and are plotted versus r in figure 1B. In buffer, Aβ(1-40) exhibits a major content of β-structure (70%) with minor content of random coil (30%), which demonstrates that Aβ(1-40) is not monomeric. The addition of heparin lead to an increase in β-structure of 15%, whereas the content of random coil is decreased by the same magnitude.

ITC was used to study the thermodynamics of the binding reaction of Aβ(1-40) to heparin at pH 4.7. Figure 2A shows an ITC experiment, in which $4\,\mu l$ aliquots of a $14.3\,\mu M$ heparin solution were injected into the calorimetric cell containing a $21.7\,\mu M$ Aβ(1-40) solution at 25 °C. Integration of the injection peaks yield in the heats of reaction δh_i. As illustrated in figure 2B, δh_i is distinctly exothermic, but decreases with increasing injection number as less and less peptide is available for binding (h_{dilute}). The injection of heparin into pure buffer yielded no significant heats of reaction δh_i (data not shown). The calorimetric data cannot be analyzed using the multisite binding model, as Aβ(1-40) was not in its monomeric state as indicated by the high content of β-structure in the CD spectrum. Therefore, the only thermodynamic parameter, which can be derived from the calorimetric experiment, is the molar heat of reaction, $\Delta H^0_{A\beta}$, obtained by

$$\Delta H^0_{A\beta} = \sum_{i=1}^{n} (\delta h_i - h_{dilute}) / n_{A\beta} \qquad (1)$$

where $n_{A\beta}$ is the total molar amount of Aβ(1-40) in the calorimetric cell. For the Aβ(1-40)-heparin interaction at pH 4.7, we measured a molar heat of reaction of $\Delta H^0_{A\beta} = -3.8 \pm 0.6\,kcal/mol$ (5 experiments), which is distinctly higher compared to the molar binding enthalpy measured for the monomeric Aβ(1-40)-heparin interaction at pH 3.7 ($\Delta H^0_{A\beta} = -5.7\,kcal/mol$).

Aβ(1-40)-heparin interaction at pH 6.0

At pH 6.0, Aβ(1-40)-heparin interaction was studied in 5mM sodium citrate, since sodium acetate can be only used in a pH range of 3.6 to 5.6. CD spectroscopy

measurements showed that presence of heparin ($r = 0.49$) increased the content of β-structure of Aβ(1-40) from 61% to 88% (figure 3). Figure 4A shows the calorimetric experiment, in which $10\mu l$ aliquots of a $26.2\mu M$ heparin solution were injected into the calorimetric cell containing a $15\mu M$ Aβ(1-40) solution at 25 °C. The corresponding heats of reaction are displayed in figure 4B. The heparin-into-buffer titrations revealed no significant heats of dilution. The ITC experiment clearly demonstrated that Aβ(1-40) binds to heparin with a measurable molar heat of reaction of $\Delta H^0_{A\beta} = -4.0 \pm 0.5 kcal/mol$ (2 measurements). Interestingly, the binding enthalpy does not change much in the pH range of 4.7 to 6.0.

Effect of NaCl on the Aβ(1-40)-heparin interaction at pH 5.0

The effect of salt on the Aβ(1-40)-heparin interaction was studied by ITC in 5mM sodium acetate (pH 5.0) at 25°C. For this purpose, the concentration of NaCl was gradually increased in the buffer from 0 to 25 mM. For all concentrations of NaCl, ITC experiments were performed by titrating $10\mu l$ aliquots of a $40\mu M$ heparin solution into a $21.7\mu M$ Aβ(1-40) solution (data not shown). The heparin-into-buffer control experiment revealed no significant heats. The molar heat of reaction $\Delta H^0_{A\beta}$ was derived from the calorimetric data (as described above), and decreased with increasing salt concentration from $-4.3 kcal/mol$ (0 mM NaCl) to $-0.5 kcal/mol$ (25 mM NaCl) as illustrated in figure 5. Linear regression analysis yields a linear dependence of $\Delta H^0_{A\beta}$ on the salt concentration with a correlation coefficient $r = 0.99$ and a slope of $0.14 \pm 0.01 kcalmol^{-1}/mM\ NaCl$. Using the regression equation, we can extrapolate the molar heat of reaction $\Delta H^0_{A\beta}$ to zero, obtaining a NaCl

concentration of $29.3 mM$. However, this does not prove that the Aβ(1-40)-heparin interaction is abolished at this salt concentration under the present experimental conditions.

Appendix figure captions

Appendix figure 1. Structural changes of Aβ(1-40) upon interaction with heparin measured by circular dichroism (CD) spectroscopy. All spectra were recorded in 5 mM sodium acetate (pH 4.7) at 25 °C. (A) The heparin-to-Aβ(1-40) molar ratio (r) is varied from 0 (black), 0.11 (red), 0.13 (blue) and 0.18 (magenta).(B) Fraction of secondary structure plotted versus the corresponding heparin-to-Aβ(1-40) molar ratio: (■) β-structure and (●) random coil. The content of α-helix is below 0.5% for all spectra.

Appendix figure 2. (A) Calorimetric trace obtained by injecting 4 µl aliquots of a 14.3 µM heparin solution into a 21.7 µM Aβ(1-40) solution (5 mM sodium acetate (pH 4.7)) at 25 °C. (B) Heats of reaction δh_i derived from the ITC experiment above are plotted against the injection number n_i.

Appendix figure 3. Conformational change of Aβ(1-40) upon binding to heparin as monitored by circular dichroism (CD) spectroscopy. All spectra were recorded in 5 mM sodium citrate (pH 6.0) at 25 °C. The heparin-to-Aβ(1-40) molar ratio (r) is 0 (black) and 0.49 (red).

Appendix figure 4. (A) Raw data of an ITC experiment, in which 10 µl aliquots of a 26.2 µM heparin solution into a 15 µM Aβ(1-40) solution (5 mM sodium citrate (pH

6.0)) at 25 °C. (B) Heats of reaction δh_i derived from the ITC experiment above are plotted against the injection number n_i.

Appendix figure 5. Effect of salt on the binding reaction of Aβ(1-40) to heparin. The molar heats of reaction, $\Delta H^0_{A\beta}$, are plotted versus the corresponding NaCl concentration in the buffer solution. $\Delta H^0_{A\beta}$ is derived from the calorimetric data as discussed in the text. The solid line corresponds to the regression line with a slope of $0.14 \pm 0.01 kcal mol^{-1} / mM\ NaCl$ and a intercept of $-4.1 \pm 0.1 kcal / mol$.

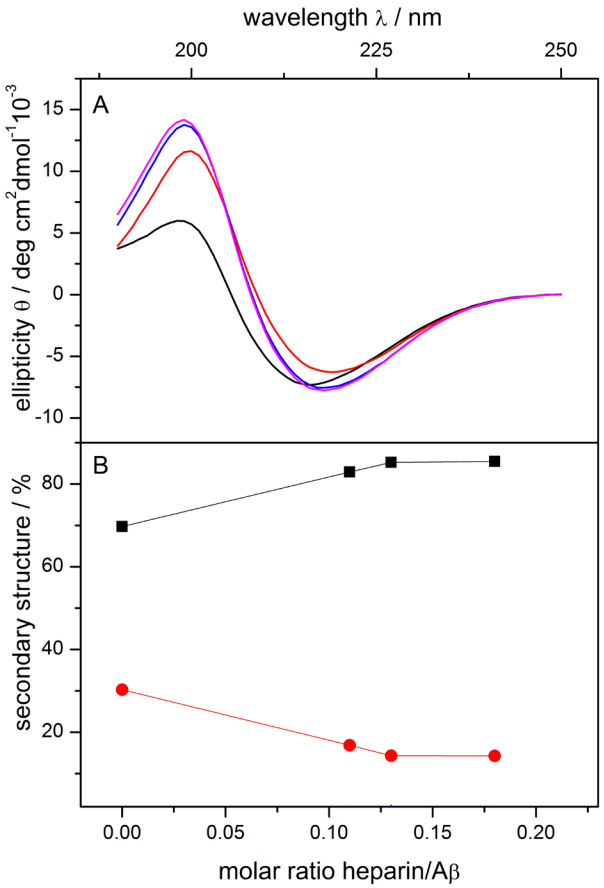

Appendix figure 1

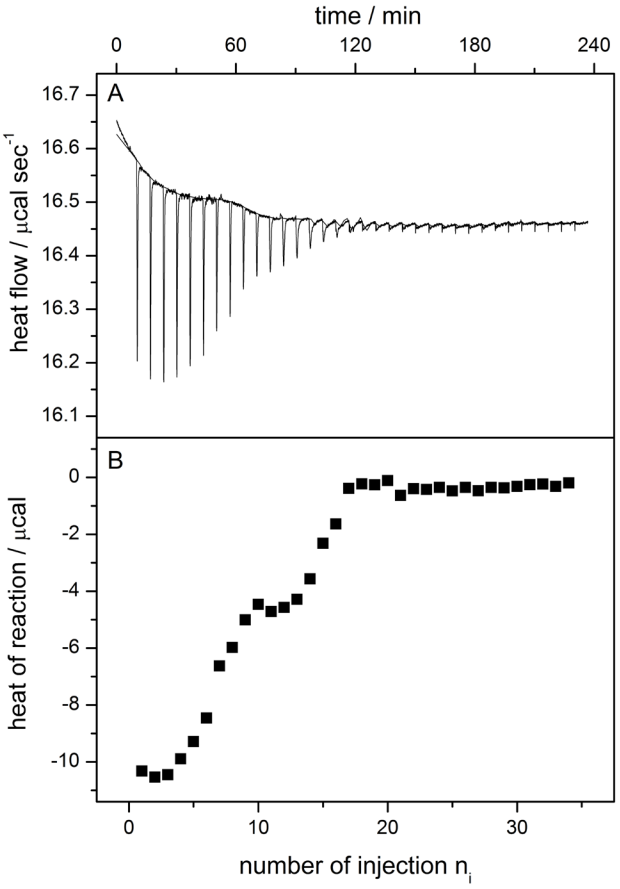

Appendix figure 2

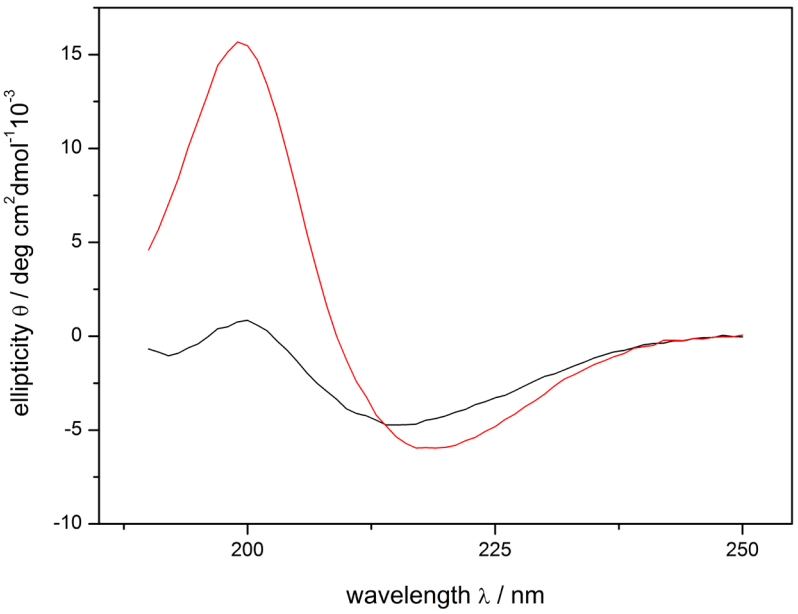

Appendix figure 3

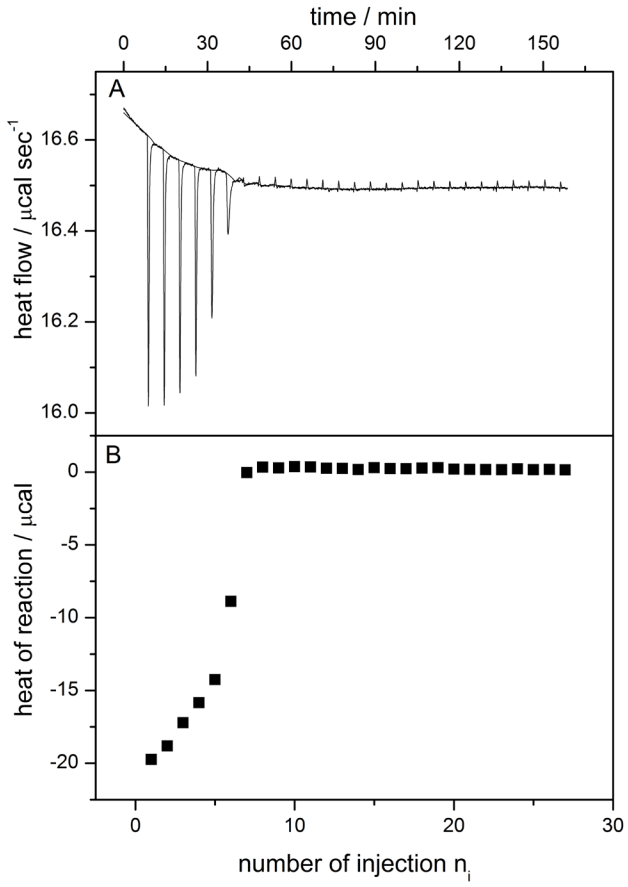

Appendix figure 4

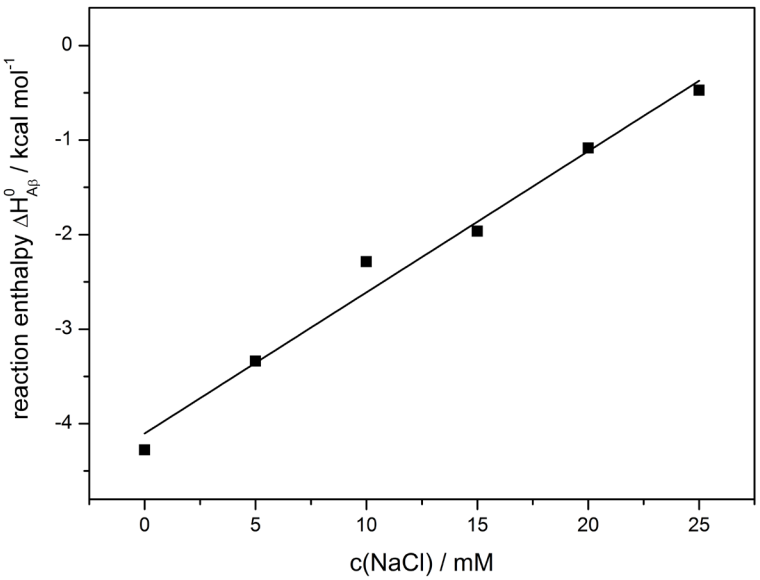

Appendix figure 5

4. Interaction of amyloid-β peptide with cationic lipid membranes

Summary

The amyloid-β peptide (Aβ) is the major component of amyloid plaques, which are a major pathological hallmark of the Alzheimer's disease (AD). AD is major form of dementia with an estimated worldwide prevalence of 25 million. A growing body of evidences indicates that neuronal membranes play an important role in the disease. Particularly, the interaction of Aβ with lipid membranes is considered as a putative mechanism of the Aβ-mediated neurotoxicity.

Here, we have studied the interaction of Aβ(1-40) to cationic small unilamellar vesicles (SUVs) using circular dichroism (CD) spectroscopy, isothermal titration calorimetry (ITC) and dynamic light scattering (DLS). CD spectroscopy reveals two sequential conformational transition of Aβ(1-40) upon binding to cationic lipid vesicles. A random-coil-to-β-structure transition was observed at low lipid-to-peptide molar ratios (L/P), followed by a transition to an α-helical structre at high L/P. The extent of membrane-induced β-structure of Aβ(1-40) was distinctly smaller for cationic lipid vesicles compared to anionic lipid vesicles (at pH 7.2). This is mostly explained by the large difference in the pH value at the membrane surface, which favors Aβ(1-40) aggregation more in the case of anionic lipid vesicles. ITC provides both the molar binding enthalpy ($\Delta H^0 = -2.5\,kcal/mol$) and the binding isotherms, which were analyzed by a model combining a surface partition equilibrium with the Gouy-Chapman theory, revealing a surface partition constant of $K_0 = 0.11 M^{-1}$ and

an effective charge of $z_p = -2.8$ (20 mM Tris-HCl (pH 7.2)) at 25 °C. Further, DLS measurements demonstrates that the interaction of Aβ(1-40) with cationic lipid vesicles leads to vesicle aggregation.

Manuscript: Interaction of amyloid-β peptide with cationic lipid membranes

Introduction

The amyloid-β peptide (Aβ) is one of the most studied peptide with more than 10'000 related articles found in PubMed (National Library of Medicine). The high research activity on Aβ is primarily based on the amyloid-beta hypothesis, which states that the cerebral aggregation of Aβ is the putative cause of the Alzheimer's disease (AD) (*1, 2*). AD is the major form of dementia, affecting 25 million people worldwide (*3*). In the future, the impact of AD will even increase with a predicted 106.8 million people affected in 2050 (*4*). AD is not only a personal tragedy for the patients and their families, but also a major challenge for the society. In particular, the financial costs of the disease are enormous with estimated worldwide costs of $422 billion in 2009 (*5*).

Several line of evidence suggests that the lipid membrane plays an eminent role in the pathology of AD. Thus, it has been shown that the degeneration of the brain cell membrane is accelerated in AD, as observed by the decrease in the content of phospholipids (*6*). Genetic, cell biology and epidemiology studies furthermore indicated that cholesterol is linked to AD. Cholesterol, a normal component of cellular membrane, is highly enriched in the brain (*7*). Controversial results were reported on the cholesterol content in the brain of AD patients. While some reported a

decrease in the cholesterol concentration (*8*), others have observed the opposite (*9*). However, cholesterol is considered to influence the production of Aβ. Aβ is formed by proteolytical cleavage of the amyloid precursor protein (APP) by two proteases called β- and γ-secretases (for review, (*10*)). In an alternative pathway, the non-amyloidogenic pathway, the consecutive action of α- and γ-secretases generates a truncated Aβ peptide called p3, precluding the generation of Aβ. It is noteworthy to mention, that APP and the three secretases are transmembraneproteins. In vitro studies demonstrated that a depletion of cholesterol in neurons lead to inhibition of Aβ generation (*11*), most probably by an increased activity of α-secretase (*12*). Although not fully understood, the effect of cholesterol on the generation of Aβ can be ascribed to the cholesterol-induced changes in membrane properties, such as stiffness and fluidity (*13*).

A variety of biophysical techniques, including circular dichroism (CD) spectroscopy, isothermal titration calorimetry (ITC), atomic force microscopy (AFM) and fluorescence spectroscopy, were applied to study the interaction of Aβ(1-40) with membranes. In general, liposomes composed of different lipids, including phospholipids, cholesterol or gangliosides, were used as membrane-mimicking systems. The binding of Aβ to lipid membranes is mainly driven by electrostatics and therefore dependent on the membrane charge, ionic strength and pH, which mainly effects the net charge of Aβ (see figure 1). Thus most studies reported no interaction when using neutral lipids such as phosphatidylcholine (PC) or sphingomyelin (SM) (*14, 15*). At physiological pH, Aβ binds only at low ionic strength to anionic lipid membranes (*16*), while no binding was observed at physiological salt concentrations (*14, 17*). The presence of anionic lipids induces two sequential structural transitions

of Aβ(1-40) dependent on the lipid-to-peptide molar ratio: a random-coil-to-β-structure transition at low L/P ratios and a β-structure-to-α-helix transition at high L/P molar ratios (*16*). Further, Aβ has been demonstrated to disrupt the lipid membrane, compromising its barrier function (*18*) One explanation is the formation of pores or ion-channels which cause membrane depolarization and disruption of ionic homeostasis (*19, 20*). As an alternative mechanism, it was postulated that Aβ aggregates not fully permeate, but associate the membrane, causing membrane thinning and leakage (*21*).

Here, we have studied the interaction of Aβ(1-40) with cationic small unilamellar vesicles (SUVs) composed of 1,2-dioleoyl-3-trimethylammonium-propane (DOTAP) and 1-palmitoyl-2-oleoyl-sn-glycero-3-phosphocholine (POPC) in a molar ratio of 1:3. The main difference between the two lipids concerns the head group, which lacks a phosphate group in case of DOTAP. In aqueous solution, DOTAP has the ability to forms bilayer structure alone and with other lipids (*22*). For example, ^{31}P-NMR measurements of DOTAP/POPC mixtures (30/70 mol%) revealed a lamellar bilayer architecture (*23*). Cationic lipids such as DOTAP are widely used as transfection agents in gene delivery (*24*). In this respect, DOTAP is probably the most studied cationic lipid, primarily due to its free availability (never protected by patents) and its low cost. In general, cationic lipids do not occur in nature, with the exception of rare examples of phosphatidyllysine and phosphatidylarginine found in bacteria grown under special conditions (*22*). Therefore, the interaction of Aβ(1-40) to cationic lipids is not of physiological relevance. Nevertheless, the study of cationic lipid-Aβ(1-40) interaction might provide new insight for the Aβ(1-40)-lipid membrane interaction. In this study, CD spectroscopy experiments were performed to gain information of the

structural changes of Aβ(1-40) upon binding to cationic lipid vesicles. In addition, isothermal titration calorimetry (ITC) was used to study the thermodynamics of the binding reaction.

Material and Methods

1-palmitoyl-2-oleoyl-sn-glycero-3-phosphocholine (POPC), 1,2-dioleoyl-3-trimethylammonium-propane (DOTAP) and 1-palmitoyl-2-oleoyl-sn-glycero-3-phospho-rac-glycerol (POPG), dissolved in chloroform, were purchased from Avanti Polar Lipids (Alabaster, AL). Aβ(1-40) was from rPeptide (Bogart, GA, USA). All other chemical were purchased from commercial sources at the highest purity and were used without further purification.

Circular dichroism (CD) spectroscopy

CD measurements were carried out with a Chirascan CD spectrometer (Applied Photophysics Ltd., Leatherhead, UK). Spectra were recorded between 190 and 250 nm, with a step size of 1 nm, bandwidth of 1 nm and a time per point of 20 s. For all measurements, a quartz cuvette of 1 mm path length was used. The mean residue molar ellipticity, $[\theta]$, was calculated for each data point according to

$$[\theta]_{MR} = 10^5 \frac{\theta_{obs}}{c \cdot l \cdot n} \tag{1}$$

where θ_{obs} is the observed ellipticity in millidegree, c is the peptide concentration in μM, l is the optical path length in cm and n the number of amino acids of the peptide. The mean molar residue molar ellipticity is given in $\deg cm^2 dmol^{-1}$. The

contents of secondary structure were calculated with a fitting program based on reference spectra determined by Reed and Reed (*25*)

Dynamic light scattering (DLS)

Size and ζ-potential measurements were performed on a Zetasizer Nano ZS instrument (ZEN3600; Malvern Instruments Ltd., Worcestershire, U.K) equipped with a HeNe laser ($633\,nm$) and a backscattering detection (scattering angle of $173°$). Data were analyzed using the built-in software of the instrument.

Preparation of lipid vesicles

Small unilamellar vesicles (SUVs) composed of a binary lipid mixture were prepared as described as follows. A defined amount of lipid was filled into a 4-ml glass vial, with subsequent removal of chloroform with a soft stream of nitrogen and high vacuum overnight. The amount of lipid was weighed and a defined amount of second lipid was added in chloroform and the lipid mixture was dried as described before. 2 ml buffer was added to the dried lipid film and the dispersion was extensively vortexed. The lipid dispersion was sonicated with a G11SP1 Special Ultrasonic Cleaner (Laboratory Supplies CO., Inc) for around 25 min. Metal debris from the titanium tip was removed by simple centrifugation at 14,000 rpm for 4 min using a Eppendorf 5415 C benchtop centrifuge (Vaudaux-Eppendorf AG, Schonenbuch, Switzerland).

Isothermal titration calorimetry (ITC)

Isothermal titration calorimetry (ITC) measurements were performed on a MicroCal VP ITC calorimeter (MicroCal, Northampton, MA). To avoid air bubbles, the solutions were degassed under stirring with a magnet bar for ~10 min (ThermoVac;

Microcal, Northampton, USA). For Aβ(1-40) solution, the buffer were degassed prior peptide dissolvement. Raw data were processed using the Origin software provided with the instrument.

Preparation of Aβ(1-40) solution

Aβ(1-40) samples were prepared as follows. First, the peptide was dissolved in hexafluoroisopropanol (HFIP) at a concentration of 0.5mg/ ml HFIP and equilibrated for one hour at room temperature. The treatment of Aβ(1-40) with HFIP dissolves pre-existing aggregates and define a chemical starting point. Next, a defined amount of Aβ(1-40)-HFIP solution was filled into a 4-ml glass vial. HFIP was removed first by soft stream of nitrogen and subsequently by high vacuum overnight. The samples were then stored at -20°C. Immediately prior to use, Aβ(1-40) was dissolved in the appropriate buffer at a peptide concentration below 30μM. The accurate peptide concentration was obtained by amino acid analysis (University of Bern).

Binding model

Binding isotherms, derived from calorimetric measurements, were analyzed with a surface partition model, in which the degree of peptide binding X_b is related to the peptide concentration c_m immediately above the polar headgroup (*26*)

$$X_b = K_0 \cdot c_m \tag{2}$$

where K_0 is the surface partition constant. This model combines chemical partition equilibration with electrostatic interactions. Charged membrane, be it anionic or cationic, have a surface potential, ψ, which attracts oppositely charged molecules in its vicinity. Thus, if peptide and membrane are oppositely charged, the peptide

concentration is increased in the lipid-water interface compared to bulk solution and can be calculated using the Boltzmann equation:

$$c_m = c_f \cdot \exp(-z_p F_0 \psi_0 / RT) \tag{3}$$

where c_f is the peptide concentration in the aqueous bulk solution, z_p the effective charge of the peptide (normally smaller than the nominal charge), F_0 the Faraday constant, R the universal gas constant and T the absolute temperature. By using the Gouy-Chapman theory, the surface potential, ψ_0, can be connected with the surface charge density, σ, according to (*27, 28*):

$$\sigma^2 = 2000\varepsilon_0\varepsilon_r RT \sum_j c_{j,eq}(e^{-z_j F_0 \psi_0 / RT} - 1) \tag{4}$$

where ε_0 is the electric permittivity of free space, ε_r the dielectric constant of water, $c_{j,eq}$ the concentration of the jth electrolyte in the bulk solution and z_j the signed valence of the jth electrolyte. The membrane surface charge, σ, can now be linked to the degree of binding, X_b, by the following equation (*29*):

$$\sigma = (e_0 / A_L) \cdot \frac{X_{DOTAP}(1 - X_{Cl^-}) + z_p X_b}{1 + (A_p / A_L) X_b} \tag{5}$$

where e_0 is the elementary charge, A_L the surface area of lipid, X_{DOTAP} the molar fraction of DOTAP in the lipid membrane, X_{Cl^-} the mole fraction of bound chloride ions to the headgroups of DOTAP and A_p is the surface area of the inserting peptide (estimated as 50 Å). The term X_{Cl^-} considers that the surface charge is reduced by specific binding of chloride ions to the headgroup of DOTAP. In analogy to the Na^+

binding to POPG (*30, 31*), we assumed that Cl^- binding to DOTAP follows a Langmuir isotherm with a binding constant of $K_{Cl^-} = 0.6 M^{-1}$. Tris-HCl buffer was treated as 1-1 salt. By calculation of the surface potential ψ and the surface peptide concentration c_m for each data point of the binding isotherm, it is possible to determine the surface partition constant K_0 and the effective peptide charge z_p. The knowledge of the binding constant, K_0, allows to calculate the free energy of binding, ΔG^0, according to

$$\Delta G^0 = -RT \ln(55.5 K_0) \tag{6}$$

where the factor 55.5 is the molar concentration of water. In turn, the entropy of binding, ΔS^0, can be calculated by the following equation

$$\Delta G^0 = \Delta H^0 - T\Delta S^0 \tag{7}$$

where ΔH^0 is the molar binding enthalpy, directly derived from the calorimetric experiment.

Calculation of the net charge of Aβ(1-40)

The net charge of Aβ(1-40) at a particular pH corresponds to the sum of charges of all ionizable groups. The charge fraction of the ionizable groups were calculated using the Henderson-Hasselbach equation with the following pKa-values: C-terminus, 3.8; Asp, 4.3; Glu, 4.5; His, 6.5; N-terminus, 7.5; Tyr, 10; Arg, 12.5 (*32*).

Results

Structure of Aβ(1-40) depending on pH, salt and concentration

Circular dichroism (CD) spectroscopy were used to monitor the effect of pH on the secondary structure of freshly dissolved Aβ(1-40). Aβ(1-40) were dissolved in 5 mM phosphate buffer with pH values changing from 6.4 to 8.0 (in 0.2 steps). The corresponding CD spectra are displayed in figure 2. For better visualization, CD spectra were divided into a low pH and a high pH region. Figure 2A displays the CD spectra of Aβ(1-40) at pH 6.4 to 7.2. At pH 7.2, CD spectrum exhibits a minimum at 198 nm which indicates a dominant content of random coil. With decreasing pH values, the ellipiticity at 198 nm is increased. An isosbestic point could be observed at 214 nm indicating a two-state random coil-to-β-structure transition. CD spectra were analyzed as described in the material and methods section, revealing the fraction of secondary structure. In figure 2C, the content of secondary structure were plotted versus the corresponding pH of the buffer solution. The increase in pH from 7.2 to 6.4 leads to a decrease of the content of random coil by 23%, whereas the content of β-structure is increased by nearly the same magnitude. The content of α-helix remains nearly constant at 4%. Figure 2B summarized the CD spectra of Aβ(1-40) recorded in the pH range of 7.2 to 8.0. The obtained CD spectra were almost identical within this pH range, and correspond to mainly random coil (67%).

CD spectroscopy were further employed to examine the effect of salt on the conformation of Aβ(1-40) immediately after dissolving in buffer solution (10 mM sodium phosphate (pH 7.0)) and after 24 hr equilibration. CD spectra were recorded at a peptide concentration of 15 μM at 25 °C. Figure 3A displays the CD spectra of freshly dissolved Aβ(1-40) with varying salt concentrations of 5 to 100 mM NaCl.

All spectra exhibit an ellipticity minimum at 198 nm, which indicates a major content of random coil structure. However, some spectra (especially the spectra with 100 mM NaCl) start to diverge, yielding in ellipticities at 198 nm in the range of $-7380 to -12860 \deg cm^2 dmol^{-1}$. Figure 3B displays the CD spectra of the same Aβ(1-40) solutions after 24 hr equilibration. All spectra reveal the typical characteristics of a predominant random coil structure. In addition, the spectra are identical in the range of 250 nm to 200 nm regardless of the salt concentration.

Analogous experiments were conducted at pH 8.0 (10 mM sodium phosphate), and the corresponding CD spectra are displayed in figure 4. As illustrated in figure 4A and 4B, the presence of salt induced similar effect on the freshly dissolved and equilibrated (24 hr) Aβ(1-40) at pH 8.0 compared to pH 7.0.

Next, we investigated the effect of concentration on the conformation of Aβ(1-40) in 5 mM sodium phosphate at the two pH 7.2 and 8.0. We gradually increased the peptide concentration of the CD samples from 19 to 153 uM. For both pH, the content of β-structure are plotted versus the corresponding peptide concentration, as displayed in figure 5. The increase in peptide concentration leads to an increase of β-structure, which is similar for both conditions.

Structural changes of Aβ(1-40) upon binding to cationic lipid membrane

We have employed CD spectroscopy to monitor structural changes of Aβ(1-40) upon binding to cationic lipid vesicles. CD spectra were recorded of Aβ(1-40) in buffer (10 mM sodium phosphate buffer (pH 7.2)) and mixed with various amounts of small unilamellar vesicles (SUVs) composed of DOTAP/POPC (25/75 mol%). In this way, the lipid-to-peptide molar ratio (L/P) is increased from 0.0 up to 200. No isosbestic

point was observed for all spectra, indicating the involvement of more than two species in the equilibrium. For the sake of better visualization, CD spectra were divided depending on their lipid-to-peptide ratios in a low (figure 6A) and a high lipid region (figure 6B). CD spectra were analyzed as describe in material and methods, and the secondary structure content are plotted versus the lipid-to-peptide ratio as shown in figure 6C. The CD spectra of Aβ(1-40) in buffer exhibits a major content of random coil (63%) with minor content of β-structure (37%). In the low lipid region (L/P= 0 to 27), the addition of cationic lipid vesicles induces a random-coil-to-β-structure transition with an isosbestic point observed at $210\,nm$, as displayed in figure 6A. The addition of cationic lipid vesicles leads to an increase in β-structure by 11%, while the content of random coil is decreased by the same extent. Further addition of cationic lipid vesicles (L/P=40 to 200) leads to an additional structural transition of the peptide from β-structure to α-helix with an observed isosbestic point at $202\,nm$ (figure 6B). The fraction of α-helix is gradually increased to 6% at a lipid-to-peptide ratio of 200.

Analogous experiments were conducted at pH 8.0 (10mM sodium phosphate) in order to study the pH dependence of the conformational changes of Aβ(1-40) upon binding to cationic lipid vesicles. The obtained results were similar to these obtained at pH 7.2 and are shown in figure 7. Here, the addition of cationic lipid vesicles leads to an increase in β-structure of 20%, which is higher compared to pH 7.2. Furthermore, the content of α-helix is increased higher (up to 18%), which can be ascribed to the fact that the measurements were recorded up to higher lipid-to-peptide molar ratios.

Structural changes of Aβ(1-40) upon binding to anionic lipid membrane

To compare the conformational changes of Aβ(1-40) upon binding to cationic lipid membrane with those of anionic lipid membranes, similar CD experiments were performed with SUVs composed of POPC/POPG (25/75 mol%) at the two pH 7.2 and 8.0 (10 mM sodium phosphate). Figure 8 displays the CD spectra of Aβ(1-40) in buffer and in presence of various amounts of anionic lipid vesicles at pH 7.2. An isosbestic point could be observed at 211 nm for all spectra, except for the spectrum with the highest lipid-to-peptide ratio (L/P=555). The addition of anionic lipid vesicles leads to a random-coil-to-β-structure transition with an increase in β-structure of 42% as shown in figure 8B. The further addition of lipid vesicles leads to an additional structural transition of Aβ(1-40) to α-helix (figure 8A).

A different picture was obtained when CD measurements were performed at pH 8.0. For better visualization, the CD spectra were separated into a low (figure 9A) and high lipid region (figure 9B). In the low lipid region (L/P=0 to 44), the addition of anionic lipid vesicles leads first to a shift in the minimum ellipticity from 200 to $204\,nm$ and to a small increase from -13600 to $-12200\,\mathrm{deg}\,cm^2dmol^{-1}$. In the high lipid region (L/P=44 to 533), the minimum is first shifted from 204 to $206\,nm$ and increased from -12200 to $-8800\,\mathrm{deg}\,cm^2dmol^{-1}$, followed by a shift from 206 to $220\,nm$ and an decrease of -8800 to $-11900\,\mathrm{deg}\,cm^2dmol^{-1}$. In figure 9C, the secondary structure content is plotted against the corresponding lipid-to-peptide ratio. As a general trend, the addition of anionic lipid vesicles lead to a decrease in random coil (from 65 to 26%), while the content of β-structure (from 33 to 60%) and α-helix (from 2 to 24%) is increased.

Thermodynamics of the Aβ(1-40) binding reaction to cationic lipid vesicles

Isothermal titration calorimetry (ITC) was used to characterize the thermodynamic properties of the Aβ(1-40) binding reaction to cationic lipid vesicles. By injecting the lipid vesicles into the peptide solution, the ITC experiment provide the binding isotherms, in which the binding ratio, X_b, is expressed as a function of free peptide bulk solution, $c_{pep,f}$, according to,

$$X_b = f\left(c_{pep,f}\right) \tag{8}$$

where X_b is the ratio of bound peptide, $n_{pep,bound}$, to the total molar amount of lipids, $n_{lipids,total}$. A detailed description how the binding isotherm is derived from the calorimetric data is given elsewhere (*33*). Figure 10A shows a typical calorimetric experiment, in which every 300 s 8 µl aliquots of a 20 mM lipid SUV suspension were titrated into a 15 µM Aβ(1-40) solution at 25 °C. Both Aβ(1-40) and lipids were dissolved in 20 mM Tris-HCl (pH 7.2). The calorimetric trace revealed an exothermic reaction for the injection of lipid vesicles into the Aβ(1-40) solution. The heats of reaction h_k were obtained by integration of the injections peaks and were plotted versus the injection number in figure 10B. h_k were initially exothermic and decreased with increasing injection number as less and less peptide was available for binding. At the end of the titration, h_k is nearly constant revealing the heat of dilution of $h_{dil} = -1\mu cal$. As a control experiment, a lipid-into-buffer experiment was conducted, revealing no significant heats of reaction (figure 10C). The molar binding enthalpy, ΔH^0, can be derived directly from the calorimetric experiment and is calculated according to

$$\Delta H^0 = \sum_{k=1}^{n} (h_k - h_{dil}) / n_{pep}^0 \quad (9)$$

where n_{pep}^0 is the molar amount of peptide in the calorimetric cell ($V = 1.4037 ml$). For 20 mM Tris-HCl (pH 7.2), a molar enthalpy of $\Delta H^0 = -2.5 kcal/mol$ was measured for the Aβ(1-40) binding reaction to cationic lipid vesicles. The binding isotherm (figure 10D) was analyzed using the surface partition model described in the material and methods section. The solid line in figure 10D corresponds to the best fit using a $K_0 = 0.11 M^{-1}$ and $z_p = -2.8$. Moreover, additional important thermodynamic binding parameters can be determined, such as the free energy of binding of $\Delta G^0 = -1.1 kcal/mol$ and the entropy of binding of $\Delta S^0 = -4.8 cal/molK$. Peptide binding is therefore driven by the enthalpy ($\Delta H^0 < 0$) and opposed by entropy ($\Delta S^0 < 0$).

Analogous ITC experiments were conducted for two additional buffers (Hepes and Mops) at pH 7.2. For Mops buffer (20 mM), figure 11A shows the ITC experiment obtained by injecting cationic lipid vesicles into a Aβ(1-40) solution at 25 °C. The injection of lipid vesicles caused an endothermic reaction as shown by the calorimetric trace. Heat of reactions h_k were decreased with increasing injection number and reached a constant heats of dilution of $h_{dil} = 3 \mu cal$. As a control experiment, a lipid-into-buffer control experiment was conducted and is shown in figure 11B. With the exception of the first injection ($\sim -5 \mu cal$), the heats of reaction were endothermic, with decreasing values from $8 \; to \; 6 \mu cal$ with increasing injection number. An overlay of the heats of reaction h_k obtained from the lipid titrations into

buffer and Aβ(1-40) solution (figure 11C) illustrates that the decrease in h_k is so similar that it cannot be clearly distinct between the two types of experiments. Therefore, it is not appropriate to derive neiter the molar binding enthalpy, ΔH^0, nor the binding isotherm from the calorimetric data.

In the case of Hepes buffer (20 mM), the lipid-into-peptide titration experiment at 25 °C is shown in figure 12A. Here, the heats of reaction h_k were at first endothermic, became exothermic and then gradually changed to endothermic again with heats of dilution of $h_{dilute} = 1.5 \mu cal$ (figure 12B). The lipid-into-buffer injections revealed constant heats of reaction of $h_k = 7 \mu cal$ (figure12C). Because these h_k are considerably higher than the obtained heats of dilution, it is not appropriate to calculate the molar binding enthalpy. In addition, the binding isotherm could not be fitted using the surface partition model described above. Therefore, any thermodynamic binding parameter could be derived from the calorimetric data in Hepes buffer.

DLS measurements with cationic lipid membrane

Dynamic light scattering (DLS) is straightforward method to determine the size and ζ-potential of colloid particles, such as lipid vesicles. The determined ζ-potential corresponds to the electric potential at the plane of shear. However, the ζ-potential can be used to calculate the surface potential if the location of the plane of shear is either known or assumed (*34*). Here, dynamic light scattering (DLS) were used to obtain information about the effect of Aβ(1-40) on the size and ζ-potential of cationic SUVs composed of DOTAP/POPC (25:75 mol%). All DLS samples contain $20 \mu M$ cationic lipid vesicles, which were mixed with various amounts of Aβ(1-40). In this

way, the peptide concentrations were gradually increased from $0\ to\ 14.8\,\mu M$, yielding peptide-to-lipid ratios in the range of 0 to 1.49. In Figure 13, both the size and the ζ-potential of cationic lipid vesicles were plotted versus their corresponding concentration of Aβ(1-40). In absence of Aβ(1-40), the lipid vesicles have a size of $58\,nm$ and a ζ-potential of $29\,mV$. As illustrated in figure 13A, even low concentrations of Aβ(1-40) ($1.3\,\mu M$) lead to 2-fold increase in the particle size from $58\ to 124\,nm$. Interestingly, a moderate increase in the particles size from $124\ to\ 162\,nm$ could be observed in the added peptide concentration range of 1.3 to 6 μM. At higher peptide concentration, the size of the particles sharply increase to a size of $>1\,\mu m$. Figure 13B shows the effect of Aβ(1-40) on the ζ-potential of the cationic lipid vesicles. An increase in the peptide concentration leads to a decrease in the ζ-potential from 29 mV to 14 mV. However, electrical neutrality has not been observed in the studied peptide range.

Discussion

Structure of Aβ(1-40) influenced by salt, pH and concentration

CD spectroscopy measurements demonstrate that the Aβ(1-40) fibrillization is favored with decreasing pH from 7.2 to 6.4, as indicated by the increase of β-structure content of the freshly dissolved peptide. On the other hand, the CD spectra of freshly dissolved Aβ(1-40) are constant in the pH range of 7.2 to 8.0, which suggests a minor effect of pH on the fibrillization process in this pH range. These results are in line with previous reports on an Aβ aggregation maximum between pH 4 to 7 (*35, 36*). For reason of exactness it is noteworthy to mention, that the ionic strength of a buffer solution of constant concentration varies with varying pH values. However, in case of

10 mM sodium phosphate, the ionic strength is decreased from 0.028 M at pH 7.2 to 0.013 M at pH 6.4, and can therefore be omitted as an explanation for the pH induced structural transition. Further, the presence of salt induces no conformational change in Aβ(1-40) within 24 hrs as showed in figure 3 and 4 at pH 7.0 and 8.0, respectively. However, small changes in the CD spectrum was observed for freshly dissolved peptide at high salt concentrations (especially 100 mM) compared to the corresponding spectra recorded under low ionic strength conditions. This effect, which disappeared after 24 hr of equilibration, is not a change in conformation, but can be best explained by a salt-induced decrease in the peptide solubility. As outlined in the material and methods section, CD spectra were initially recorded in mdeg, but converted to mean residue molar ellipticity, $[\theta]$, in $\deg cm^2 dmol^{-1}$. The conversion equation requires the knowledge of the peptide concentration. By using a lower peptide concentration than the nominal concentration $(15\mu M)$, CD spectra recorded at high ionic strength conditions perfectly overlay with those at low ionic strength. At 100 mM NaCl, the difference between the actual $(\sim 5.8\mu M)$ and nominal peptide concentration is 300%. This is a serious source of error, as the Aβ(1-40) concentration cannot be determined directly (e.g by UV absorbance at 280 nm). In general, salt affects the peptide solubility in addition with other factors, such as the peptide length, amino acid composition, pH and temperature (*37*).

Further, CD spectroscopy have demonstrated that the increase of peptide concentration cause an increase in β-structure, which was similar at pH 7.0 to 8.0. This was previously demonstrated for slightly different conditions (5 mM Mops, pH 7.4) (*14*). Differences with respect to concentration-induced β-structure might be

ascribed due to differences in buffer, sample preparation and chemical history of the peptide.

Structural changes of Aβ(1-40) upon binding to cationic lipid vesicles

CD spectroscopy demonstrates that the interaction of Aβ(1-40) to cationic lipid vesicles induces first a transition from random-coil to β-structure, followed by a transition to α-helix at high lipid-to-peptide molar ratios. The interaction of Aβ(1-40) to negatively charged lipid membranes has been previously studied at pH 7.4, revealing first a lipid-induced random-coil to β-structure, followed by a transition to α-helix at high lipid-content (*16*). These experiments were repeated for phosphate buffer at pH 7.2 and 8.0, in order to avoid differences due to different buffer, peptide sample preparation and pH. At pH 7.2, CD measurements revealed lipid-induced structural transition of Aβ(1-40) as previously reported (*16*). However, large differences were observed for measurements at pH 8.0 (figure 9). Here, we observed a simultaneously increase of β-structure and α-helix, while the content of random coil is decreased. Why these results at pH 8.0 were so different to those obtained at pH 7.2 and 7.4, is not understood.

However, our focus lies on the lipid-induced increase in β-structure of Aβ(1-40). The results obtained for the 4 conditions (charged lipid (DOTAP vs. POPG), pH (7.2 vs. 8.0) are summarized in figure 14. The highest increase in β-structure was observed for anionic lipid vesicles at pH 7.2. The membrane-induced increase in β-structure of Aβ(1-40) has its molecular origin in the combined effects of electrostatic attraction, the increase in peptide concentration at the membrane surface and aggregation (*38*). Lipid vesicles containing either positively or negatively charged lipids have a surface membrane potential ψ, which attracts oppositely charged residues of Aβ(1-40) to the

membrane surface, leading to an increase in peptide concentration at the membrane surface. The peptide concentration at the membrane surface, c_m, can be calculated using the Boltzmann equation (see equation 3) with the knowledge of the membrane surface potential, ψ, and the charge of the peptide, z_p. By using equation 4 and 5, the surface potential can be estimated at low ionic strength as $\pm 150 mV$ for the two lipid systems. Calculations of the net charge revealed that Aβ(1-40) is negative at pH 7.2 (–2.8) and pH 8.0 (–3.6) as displayed in figure 1. Therefore, it seems even surprising that Aβ(1-40) can bind to anionic lipid membranes at the two pH. However, it can be postulated that the net charge is not solely decisive, but that the electrostatic interactions are mediated by a basic cluster of amino acids (His_{13}-His_{14}-Lys_{16}) of Aβ(1-40). Further, the pH at the surface of charged lipid vesicles is changed compared to the bulk value (by 2.5 Unit for $\psi = \pm 150 mV$), due to the attraction of protons or hydroxyl ions in its vicinity. For anionic lipid vesicles at a bulk pH of 7.2, the surface pH is therefore lowered to 4.7 and leads to a positive net charge of Aβ(1-40) in the membrane vicinity. However, the surface pH of cationic lipid vesicles is increased to a value of 9.7, which leads to an even more negative net charge of Aβ(1-40). We can therefore conclude that the electrostatic attraction and, in turn, the peptide concentration at the membrane surface, is at least equal, if not higher in case of cationic lipid vesicles. However, the increased peptide concentration at the membrane surface leads to peptide aggregation, as indicated by the spectral change to β-structure. The aggregation of Aβ(1-40) is dependent on several factors, such as peptide concentration (*14*), pH (*35, 36*), temperature (*39*) and salt (*40*). With regard to pH, an aggregation maximum was reported in the pH range of 4 to 7 (*35, 36*). As discussed above, anionic lipid vesicles have under the given experimental conditions

a surface pH of 4.7, which is in the reported aggregation maximum. This explains the higher membrane-induced β-structure for anionic lipid vesicles in comparison to cationic lipid vesicles.

Thermodynamic of the lipid-peptide interaction

Isothermal titration calorimetry (ITC) is a useful tool to study thermodynamics of peptide-lipid interactions, such as the binding of Aβ(1-40) to cationic lipid vesicles. Calorimetric measurements conducted in Tris-HCl buffer directly revealed the molar bindings enthalpy of $\Delta H^0 = -2.5 kcal/mol$ and the bindings isotherm, which was analyzed with a surface partition model, yielding a surface partition constant of $K_0 = 0.11 M^{-1}$ and an effective peptide charge of $z_p = -2.8$. Analogous calorimetric experiments were previously conducted for anionic lipid vesicles at 28 °C, revealing a molar binding enthalpy of $\Delta H^0 = -7.3 kcal/mol$ (10 mM Tris-HCl (pH 7.4)), a surface partition constant of $K_0 = 0.28 M^{-1}$ and an effective peptide charge of $z_p = 2$ (the latter two parameters determined for Mops (pH 7.4)) (*14*). Although the thermodynamic binding parameters are often temperature-dependent, the slight temperature difference (25 to 28 °C) between the two data sources can be neglected. The large difference between the molar binding enthalpies can be mainly explained by the lower membrane-induced increase in β-structure of Aβ(1-40) upon binding to cationic lipid vesicles. Studies with double d-isomers of Aβ(1-40) revealed the thermodynamics of the β-structure formation of Aβ(1-40). Membrane-induced β-structure formation has an enthalpy of $\Delta H_\beta = -1.0 kcal/mol\ per\ residue$, which constitutes the major contribution to the molar binding enthalpy (chapter 2). However, the two surface partition constants are in a similar range, which can be

expected, as K_0 denotes for the transfer of the peptide from the plane of binding (peptide concentration c_m) into the lipid bilayer surface. Moreover, the two peptide charges are in the expected range.

The binding of Aβ(1-40) to cationic lipid membrane is likely to be associated with the release or absorption of protons, as it was previously observed for the binding to anionic membranes (*14*). Protonation (or deprotonation) reactions can be directly measured with isothermal titration calorimetry by studying the binding reactions in buffers with different dissociation enthalpies (*41*). In addition to Tris-HCl ($\Delta H_{Diss} = 11.51 kcal/mol$), the binding of Aβ(1-40) to cationic lipid vesicles were also studied in Mops ($\Delta H_{Diss} = 5.29 kcal/mol$) and in Hepes ($\Delta H_{Diss} = 5.02 kcal/mol$) (*42*). As illustrated in corresponding figures 10, 11 and 12, the use of different buffers had a tremendous effect on the calorimetric experiments. Unfortunately, the use of Mops and Hepes also affected the lipid-into-buffer titrations, which were designed as a control experiment. For this type of experiments, the heats of reaction are normally in the range of $\pm 2 \mu cal$ (as for Tris-HCl). However, for both Hepes and Mops, heats of reaction of $+7 \mu cal$ were measured. A possible explanation for these unusual findings comes from specific interactions of buffer molecules to the headgroup of DOTAP. Since the molar binding enthalpy could not be derived from the calorimetric measurements in Hepes and Mops, the uptake/release of protons associated with the Aβ(1-40) binding reaction to cationic membrane could not be determined.

Furthermore, dynamic light scattering (DLS) was applied to study the effect of Aβ(1-40) on the size and the ζ-potential of cationic lipid vesicles. As illustrated in figure

14, DLS measurements demonstrates that the binding of Aβ(1-40) to cationic lipid vesicles leads to vesicle aggregation, as previously observed for anionic lipid vesicles (*43*).

References

1. Hardy, J. A., and Higgins, G. A. (1992) Alzheimer's disease: the amyloid cascade hypothesis, *Science 256*, 184-185.
2. Hardy, J., and Selkoe, D. J. (2002) The amyloid hypothesis of Alzheimer's disease: progress and problems on the road to therapeutics, *Science 297*, 353-356.
3. Ferri, C. P., Prince, M., Brayne, C., Brodaty, H., Fratiglioni, L., Ganguli, M., Hall, K., Hasegawa, K., Hendrie, H., Huang, Y., Jorm, A., Mathers, C., Menezes, P. R., Rimmer, E., and Scazufca, M. (2005) Global prevalence of dementia: a Delphi consensus study, *Lancet 366*, 2112-2117.
4. Brookmeyer, R., Johnson, E., Ziegler-Graham, K., and Arrighi, H. M. (2007) Forecasting the global burden of Alzheimer's disease, *Alzheimers Dement 3*, 186-191.
5. Wimo, A., Winblad, B., and Jonsson, L. (2010) The worldwide societal costs of dementia: Estimates for 2009, *Alzheimers Dement 6*, 98-103.
6. Nitsch, R. M., Blusztajn, J. K., Pittas, A. G., Slack, B. E., Growdon, J. H., and Wurtman, R. J. (1992) Evidence for a membrane defect in Alzheimer disease brain, *Proc Natl Acad Sci U S A 89*, 1671-1675.
7. Simons, M., Keller, P., Dichgans, J., and Schulz, J. B. (2001) Cholesterol and Alzheimer's disease: is there a link?, *Neurology 57*, 1089-1093.
8. Mason, R. P., Shoemaker, W. J., Shajenko, L., Chambers, T. E., and Herbette, L. G. (1992) Evidence for changes in the Alzheimer's disease brain cortical membrane structure mediated by cholesterol, *Neurobiol Aging 13*, 413-419.
9. Xiong, H., Callaghan, D., Jones, A., Walker, D. G., Lue, L. F., Beach, T. G., Sue, L. I., Woulfe, J., Xu, H., Stanimirovic, D. B., and Zhang, W. (2008) Cholesterol retention in Alzheimer's brain is responsible for high beta- and gamma-secretase activities and Abeta production, *Neurobiol Dis 29*, 422-437.
10. Haass, C., Kaether, C., Thinakaran, G., and Sisodia, S. (2012) Trafficking and Proteolytic Processing of APP, *Cold Spring Harb Perspect Med 2*, a006270.
11. Simons, M., Keller, P., De Strooper, B., Beyreuther, K., Dotti, C. G., and Simons, K. (1998) Cholesterol depletion inhibits the generation of beta-amyloid in hippocampal neurons, *Proc Natl Acad Sci U S A 95*, 6460-6464.
12. Kojro, E., Gimpl, G., Lammich, S., Marz, W., and Fahrenholz, F. (2001) Low cholesterol stimulates the nonamyloidogenic pathway by its effect on the alpha -secretase ADAM 10, *Proc Natl Acad Sci U S A 98*, 5815-5820.
13. Shobab, L. A., Hsiung, G. Y., and Feldman, H. H. (2005) Cholesterol in Alzheimer's disease, *Lancet Neurol 4*, 841-852.
14. Terzi, E., Holzemann, G., and Seelig, J. (1995) Self-association of beta-amyloid peptide (1-40) in solution and binding to lipid membranes, *J Mol Biol 252*, 633-642.
15. Matsuzaki, K., and Horikiri, C. (1999) Interactions of amyloid beta-peptide (1-40) with ganglioside-containing membranes, *Biochemistry 38*, 4137-4142.
16. Terzi, E., Holzemann, G., and Seelig, J. (1997) Interaction of Alzheimer beta-amyloid peptide(1-40) with lipid membranes, *Biochemistry 36*, 14845-14852.
17. Ikeda, K., and Matsuzaki, K. (2008) Driving force of binding of amyloid beta-protein to lipid bilayers, *Biochem Biophys Res Commun 370*, 525-529.
18. McLaurin, J., and Chakrabartty, A. (1996) Membrane disruption by Alzheimer beta-amyloid peptides mediated through specific binding to either

phospholipids or gangliosides. Implications for neurotoxicity, *J Biol Chem 271*, 26482-26489.
19. Arispe, N., Pollard, H. B., and Rojas, E. (1993) Giant multilevel cation channels formed by Alzheimer disease amyloid beta-protein [A beta P-(1-40)] in bilayer membranes, *Proc Natl Acad Sci U S A 90*, 10573-10577.
20. Butterfield, S. M., and Lashuel, H. A. (2010) Amyloidogenic protein-membrane interactions: mechanistic insight from model systems, *Angew Chem Int Ed Engl 49*, 5628-5654.
21. Sokolov, Y., Kozak, J. A., Kayed, R., Chanturiya, A., Glabe, C., and Hall, J. E. (2006) Soluble amyloid oligomers increase bilayer conductance by altering dielectric structure, *J Gen Physiol 128*, 637-647.
22. Simberg, D., Weisman, S., Talmon, Y., and Barenholz, Y. (2004) DOTAP (and other cationic lipids): chemistry, biophysics, and transfection, *Crit Rev Ther Drug Carrier Syst 21*, 257-317.
23. Mitrakos, P., and Macdonald, P. M. (2000) Nucleotide chain length and the morphology of complexes with cationic amphiphiles: (31)P-NMR observations, *Biochim Biophys Acta 1463*, 355-373.
24. Felgner, P. L., Gadek, T. R., Holm, M., Roman, R., Chan, H. W., Wenz, M., Northrop, J. P., Ringold, G. M., and Danielsen, M. (1987) Lipofection: a highly efficient, lipid-mediated DNA-transfection procedure, *Proc Natl Acad Sci U S A 84*, 7413-7417.
25. Reed, J., and Reed, T. A. (1997) A set of constructed type spectra for the practical estimation of peptide secondary structure from circular dichroism, *Anal Biochem 254*, 36-40.
26. Beschiaschvili, G., and Seelig, J. (1990) Peptide binding to lipid bilayers. Binding isotherms and zeta-potential of a cyclic somatostatin analogue, *Biochemistry 29*, 10995-11000.
27. McLaughlin, S. (1977) Electrostatic potentials at membrane-solution interfaces, *Curr. Top. Membr. Transport*, 71-144.
28. Aveyard, R. H., D. A. (1973) *An Introduction to the Principles of Surface Chemistry*, Cambridge University Press, London.
29. Beschiaschvili, G., and Seelig, J. (1990) Melittin binding to mixed phosphatidylglycerol/phosphatidylcholine membranes, *Biochemistry 29*, 52-58.
30. Eisenberg, M., Gresalfi, T., Riccio, T., and McLaughlin, S. (1979) Adsorption of monovalent cations to bilayer membranes containing negative phospholipids, *Biochemistry 18*, 5213-5223.
31. Macdonald, P. M., and Seelig, J. (1987) Calcium binding to mixed phosphatidylglycerol-phosphatidylcholine bilayers as studied by deuterium nuclear magnetic resonance, *Biochemistry 26*, 1231-1240.
32. Ma, K., Clancy, E. L., Zhang, Y. B., Ray, D. G., Wollenberg, K., and Zagorski, M. G. (1999) Residue-specific pK(a) measurements of the beta-peptide and mechanism of pH-induced amyloid formation, *J Am Chem Soc 121*, 8698-8706.
33. Seelig, J. (1997) Titration calorimetry of lipid-peptide interactions, *Biochim Biophys Acta 1331*, 103-116.
34. Cohen, J. A. (2003) Electrophoretic characterization of liposomes, *Methods Enzymol 367*, 148-176.

35. Wood, S. J., Maleeff, B., Hart, T., and Wetzel, R. (1996) Physical, morphological and functional differences between ph 5.8 and 7.4 aggregates of the Alzheimer's amyloid peptide Abeta, *J Mol Biol 256*, 870-877.
36. Huang, T. H., Yang, D. S., Plaskos, N. P., Go, S., Yip, C. M., Fraser, P. E., and Chakrabartty, A. (2000) Structural studies of soluble oligomers of the Alzheimer beta-amyloid peptide, *J Mol Biol 297*, 73-87.
37. Rohl, C. A., and Baldwin, R. L. (1998) Deciphering rules of helix stability in peptides, *Methods Enzymol 295*, 1-26.
38. Seelig, J. (2004) Thermodynamics of lipid-peptide interactions, *Biochim Biophys Acta 1666*, 40-50.
39. Gursky, O., and Aleshkov, S. (2000) Temperature-dependent beta-sheet formation in beta-amyloid Abeta(1-40) peptide in water: uncoupling beta-structure folding from aggregation, *Biochim Biophys Acta 1476*, 93-102.
40. Klement, K., Wieligmann, K., Meinhardt, J., Hortschansky, P., Richter, W., and Fandrich, M. (2007) Effect of different salt ions on the propensity of aggregation and on the structure of Alzheimer's abeta(1-40) amyloid fibrils, *J Mol Biol 373*, 1321-1333.
41. Morin, P. E., and Freire, E. (1991) Direct calorimetric analysis of the enzymatic activity of yeast cytochrome c oxidase, *Biochemistry 30*, 8494-8500.
42. Hanson, W. M., Domek, G. J., Horvath, M. P., and Goldenberg, D. P. (2007) Rigidification of a flexible protease inhibitor variant upon binding to trypsin, *J Mol Biol 366*, 230-243.
43. Lee, G., Pollard, H. B., and Arispe, N. (2002) Annexin 5 and apolipoprotein E2 protect against Alzheimer's amyloid-beta-peptide cytotoxicity by competitive inhibition at a common phosphatidylserine interaction site, *Peptides 23*, 1249-1263.

Captions to figures

Figure 1. The net charge of Aβ(1-40) dependent on the pH of the buffer solution. As described in the material and method section, net charge was calculated using the Henderson-Hasselbach equation with the corresponding pKa-values.

Figure 2. Effect of pH on the conformation of the freshly dissolved Aβ(1-40). (A) Circular dichroism (CD) spectra of Aβ(1-40) dissolved in 5 mM phosphate buffer with varying pH values from 6.4 to 7.2 (in 0.2 steps). From bottom to the top at 198 nm: pH 7.2, 7.0, 6.8, 6.6 and 6.4. The spectra were recorded at a peptide concentration of 15 μM at 25 °C. (B) CD spectra of freshly dissolved Aβ(1-40) with varying pH values from 7.2 to 8.0. (C) Content of secondary structure versus the pH of the buffer solution: (■) β-structure, (●) random coil and (▲) α-helix.

Figure 3. Effect of NaCl on the conformation of freshly dissolved and 24 hr equilibrated Aβ(1-40) at pH 7.0. (A) CD spectra of Aβ(1-40) freshly dissolved in 10 mM sodium phosphate buffer containing various concentration of NaCl. Spectra from bottom to the top at 198 nm: 0 mM, 15 mM, 5 mM, 25 mM, 10 mM, 20 mM and 100 mM NaCl. The spectra were recorded immediately after dissolving the peptide and at a peptide concentration of 15 μM at 25 °C. (B) CD spectra of the corresponding Aβ(1-40) solutions (see (A)) equilibrated for 24 hr.

Figure 4. (A) CD spectra of Aβ(1-40) freshly dissolved in 10 mM sodium phosphate buffer (pH 8.0) containing various concentration of NaCl. Spectra from bottom to the top at 198 nm: 0 mM, 10 mM, 5 mM, 20 mM, 25 mM and 100 mM NaCl. The spectra were recorded immediately after dissolving the peptide and at a peptide concentration of 15 μM at 25 °C. (B) CD spectra of the corresponding Aβ(1-40) solutions (see (A)) equilibrated for 24 hr.

Figure 5. Concentration-induced conformational change of Aβ(1-40) monitored by CD spectroscopy at pH 7.2 (●) and 8.0 (■) in 5 mM sodium phosphate . Spectra were recorded at varying peptide concentrations of 19 to 153 uM at 25 °C.

Figure 6. Conformational change of Aβ(1-40) upon binding to SUVs composed of DOTAP/POPC (25/75 mol%) monitored by CD spectroscopy. Spectra were recorded in 10 mM sodium phosphate (pH 7.2) at 25 °C. Lipid-to-peptide molar ratios of the spectra varied between 0 and 200. (A) black, L/P=0; magenta, L/P=7; blue, L/P=13 and red, L/P=27. (B) black, L/P=40; red, L/P=53; blue, L/P=67; magenta, L/P=100 and olive, L/P=200. (C) Fraction of secondary structure was plotted vs. the corresponding lipid-to-peptide ratio: (■) β-structure, (●) random coil and (▲) α-helix.

Figure 7. Structural transition of Aβ(1-40) upon binding to positively charge SUVs DOTAP/POPC (25/75 mol%) as measured by CD spectroscopy. All Spectra were recorded in 10 mM sodium phosphate (pH 8.0) at 25 °C. Lipid-to-peptide molar ratios

of the spectra varied between 0 and 348. (A) black, L/P=0; red, L/P=6 and blue, L/P=14. (B) black, L/P=29; red, L/P=44; blue, L/P=116; magenta, L/P=174 and olive, L/P=348. (C) Fraction of secondary structure was plotted vs. the corresponding lipid-to-peptide ratio: (■) β-structure, (●) random coil and (▲) α-helix.

Figure 8. Conformational change of Aβ(1-40) upon binding to negatively charged SUVs composed of POPG/POPC (25/75 mol%) as measured by CD spectroscopy. Spectra were recorded in 10 mM sodium phosphate (pH 7.2) at 25 °C. Lipid-to-peptide molar ratios varied between 0 and 533. (A) black, L/P=0; red, L/P=22; blue, L/P=44; navy, L/P=89; magenta, L/P=178; olive, L/P=266 and violet, L/P=533. (B) Plot of fraction of secondary structure vs. the corresponding lipid-to-peptide ratio: (■) β-structure, (●) random coil and (▲) α-helix.

Figure 9. Structural change of Aβ(1-40) upon binding to anionic SUVs composed of POPC/POPC (25/75 mol%) as measured by CD spectroscopy at pH 8.0. Spectra were recorded in 10 mM sodium phosphate at 25 °C. Lipid-to-peptide molar ratios of the spectra are in the range of 0 to 533. (A) black, L/P=0; red, L/P=9 ; blue, L/P=13 and magenta, L/P=44. (B) magenta, L/P=44; black, L/P=89; red, L/P=178; blue, L/P=267and olive, L/P=533. (C) Fraction of secondary structure was plotted versus the corresponding lipid-to-peptide molar ratio: (■) β-structure, (●) random coil and (▲) α-helix.

Figure 10. The binding of Aβ(1-40) to cationic SUVs in 20mM Tris-HCl (pH 7.2) as observed by isothermal titration calorimetry. (A) Experimental heat flow as obtained by the injection of cationic SUVs (DOTAP/POPC (25/75 mol%)) into a 15 μM Aβ(1-40) solution at 25 °C. (B) Heats of reaction h_k were plotted vs. the injection number n_k. (C) Heat flow obtained by the injection of cationic SUVs into pure buffer at 25 °C. (D) Binding isotherm derived from the calorimetric experiment displayed in (A). The solid line corresponds to the best fit of the surface partition model with a $K_0 = 0.11 M^{-1}$ and $z_p = -2.9$.

Figure 11. ITC experiment of the Aβ(1-40) binding reaction to cationic SUVs in 20 mM Mops (pH 7.2). (A) Calorimetric trace obtained by the injection of cationic SUVs (DOTAP/POPC (25/75 mol%)) into a 15 μM Aβ(1-40) solution at 25 °C. (B) Heat flow obtained by the injection of cationic SUVs into pure buffer at 25 °C. (C) Heats of reaction h_k of (A) and (B) were plotted vs. the injection number n_k.

Figure 12. ITC experiment of the Aβ(1-40) binding to cationic SUVs in 20 mM Hepes (pH 7.2). (A) Experimental heat flow obtained by the injection of cationic SUVs (DOTAP/POPC (25/75 mol%)) into a 15 μM Aβ(1-40) solution at 25 °C. (B) Heat flow obtained by the injection of cationic SUVs into pure buffer at 25 °C. (C) Heats of reaction h_k were plotted vs. the injection number n_k.

Figure 13. Effect of Aβ(1-40) on the size and ζ-potential of SUVs composed of DOTAP/POPC (25/75 mol%) measured by dynamic light scattering (DLS). The total lipid concentration was 20 μM, and the peptide concentration was increased from 0 to 14.8 μM. Both Aβ(1-40) and the lipid vesicles were dissolved in 10 mM phosphate (pH 7.2). All measurements were conducted at 25 °C. (A) Vesicle size was plotted vs. the concentration of Aβ(1-40). (B) ζ-potential of vesicles dependent on the peptide concentration.

Figure 14. Dependence of the membrane-induced β-structure formation of Aβ(1-40) on the charge of lipid vesicles and pH of buffer solution. Data were taken from figure 7, 8, 9 and 10. The corresponding fraction of β-structure was plotted vs. the lipid-to-peptide ratios: (■) DOTAP, pH 7.2, (●) DOTAP, pH 8.0, (▲) POPG, pH 7.2 and (▼) POPG, pH 8.0

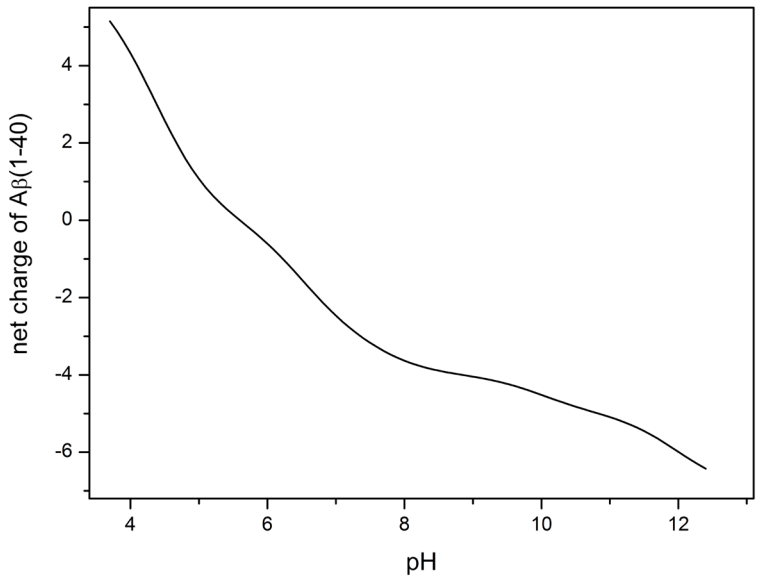

Figure 1

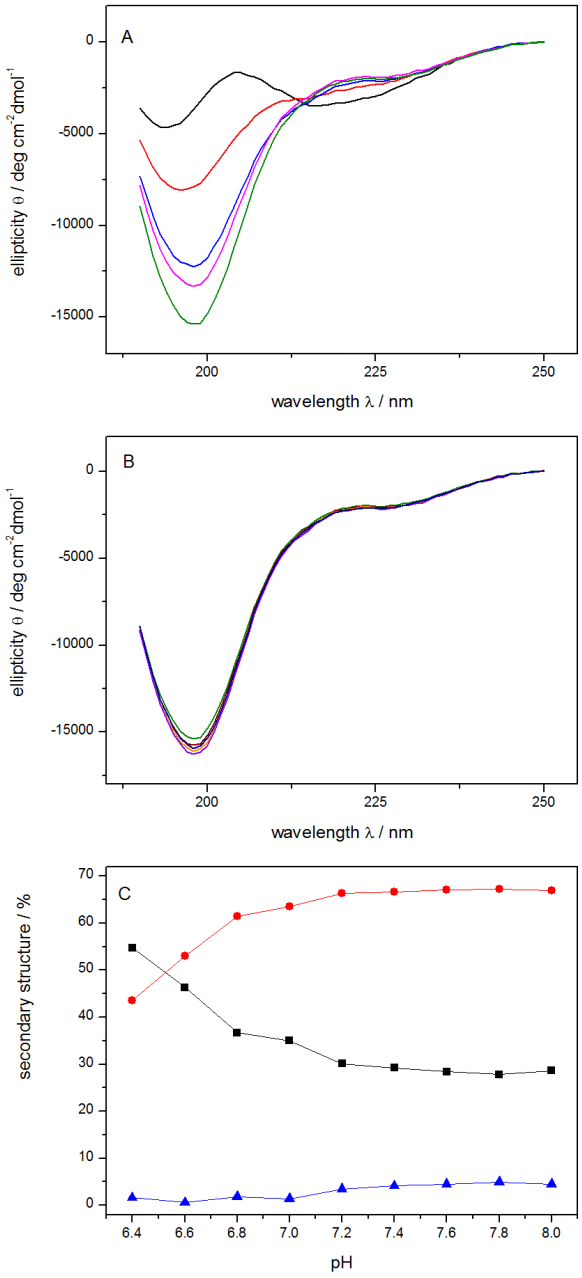
A
ellipticity θ / deg cm^{2}dmol^{-1}
0
-5000
-10000
-15000
200
225
250
wavelength λ / nm
B
ellipticity θ / deg cm^{2}dmol^{-1}
0
-5000
-10000
-15000
200
225
250
wavelength λ / nm
C
secondary structure / %
70
60
50
40
30
20
10
0
6.4
6.6
6.8
7.0
7.2
7.4
7.6
7.8
8.0
pH

Figure 2

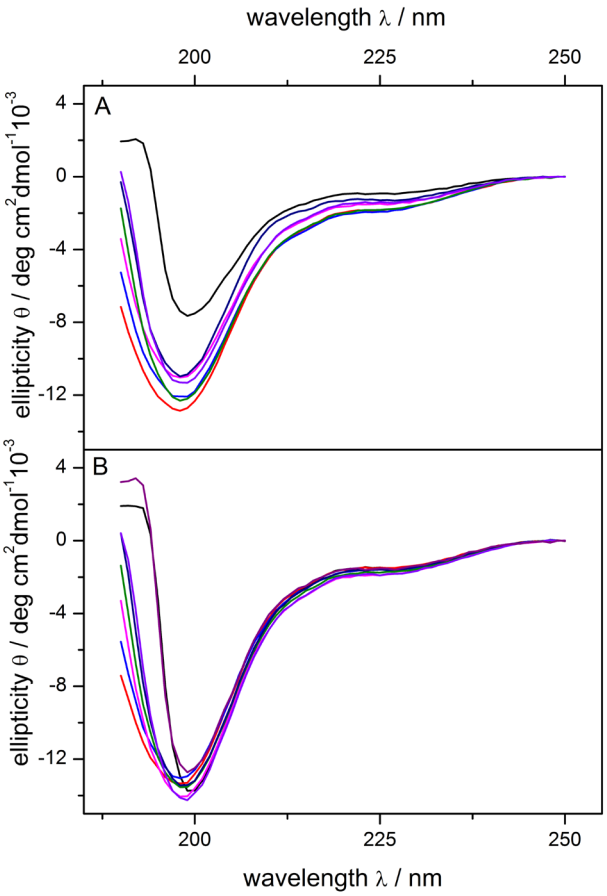
wavelength λ / nm
200
225
250
A
B
4
0
-4
-8
-12
ellipticity θ / deg cm²dmol⁻¹10⁻³

Figure 3

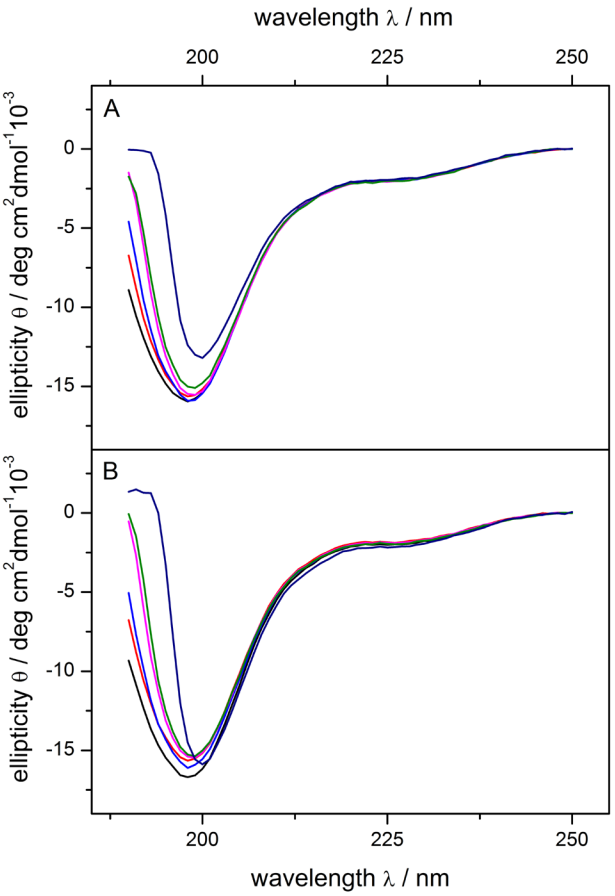
wavelength λ / nm
200
225
250
A
B
0
-5
-10
-15
ellipticity θ / deg cm²dmol⁻¹10⁻³
ellipticity θ / deg cm²dmol⁻¹10⁻³
200
225
250
wavelength λ / nm

Figure 4

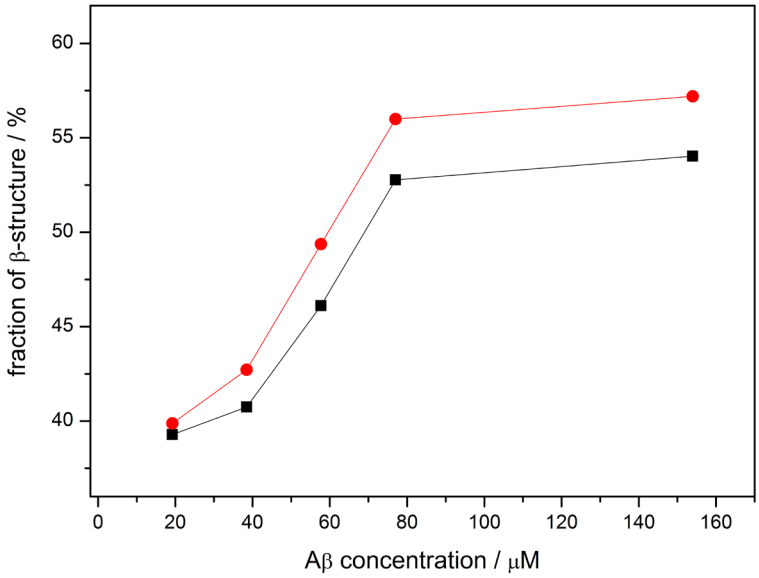
fraction of β-structure / %
60
55
50
45
40
0
20
40
60
80
100
120
140
160
Aβ concentration / μM

Figure 5

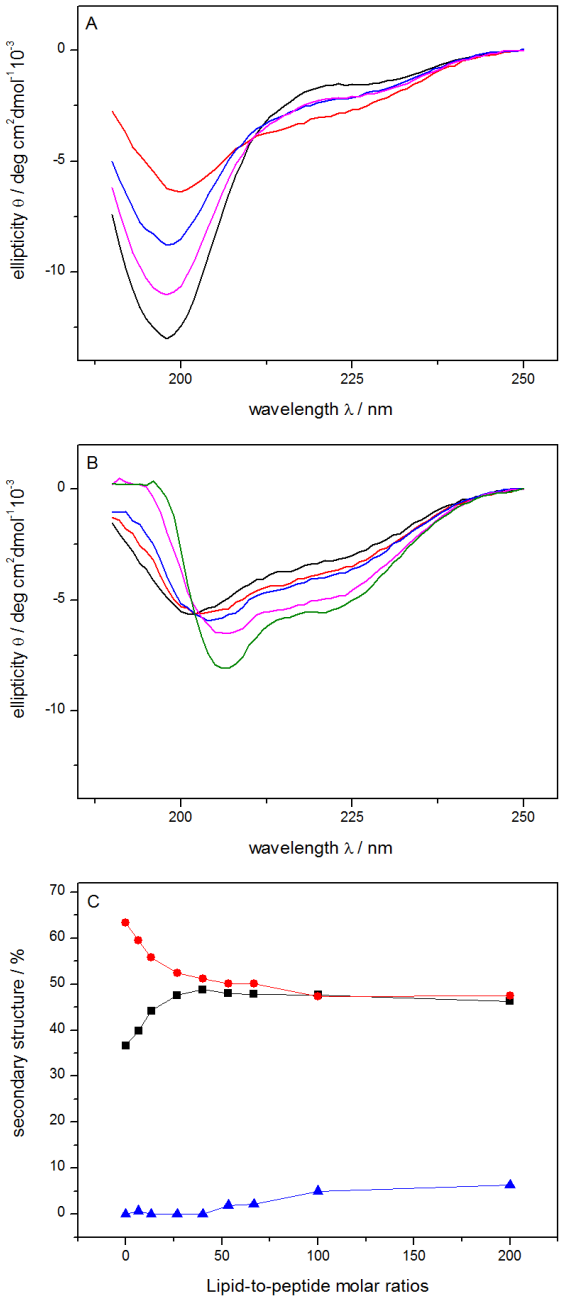
A
ellipticity θ / deg cm²dmol⁻¹10⁻³
0
-5
-10
200
225
250
wavelength λ / nm
B
ellipticity θ / deg cm²dmol⁻¹10⁻³
0
-5
-10
200
225
250
wavelength λ / nm
C
secondary structure / %
70
60
50
40
30
20
10
0
0
50
100
150
200
Lipid-to-peptide molar ratios

Figure 6

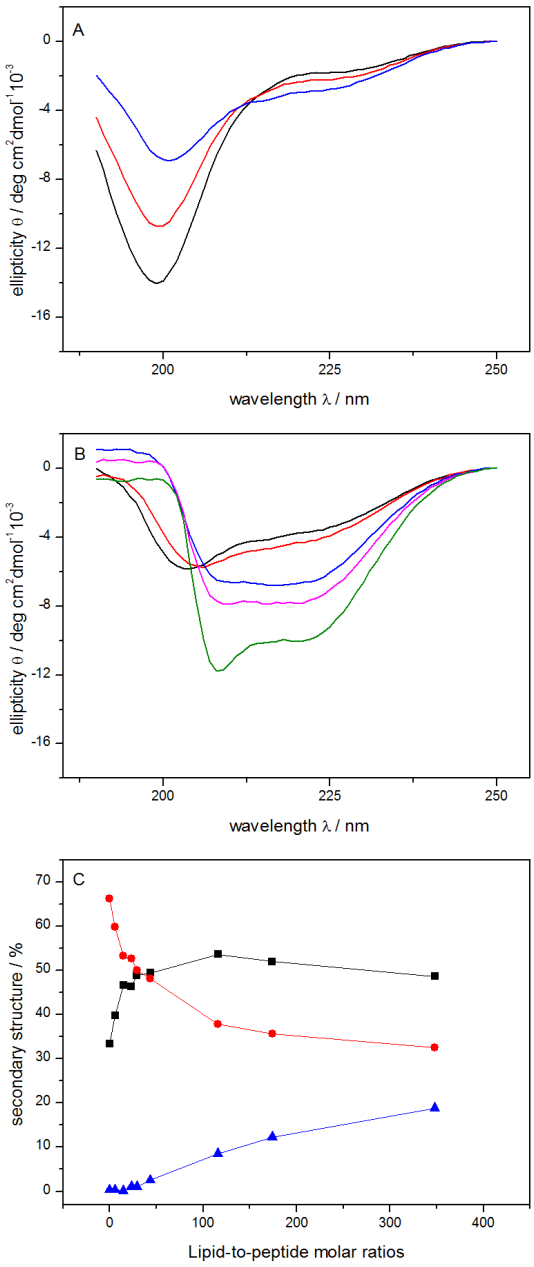
A
ellipticity θ / deg cm²dmol⁻¹10⁻³
0
-4
-8
-12
-16
200
225
250
wavelength λ / nm
B
ellipticity θ / deg cm²dmol⁻¹10⁻³
0
-4
-8
-12
-16
200
225
250
wavelength λ / nm
C
secondary structure / %
70
60
50
40
30
20
10
0
0
100
200
300
400
Lipid-to-peptide molar ratios

Figure 7

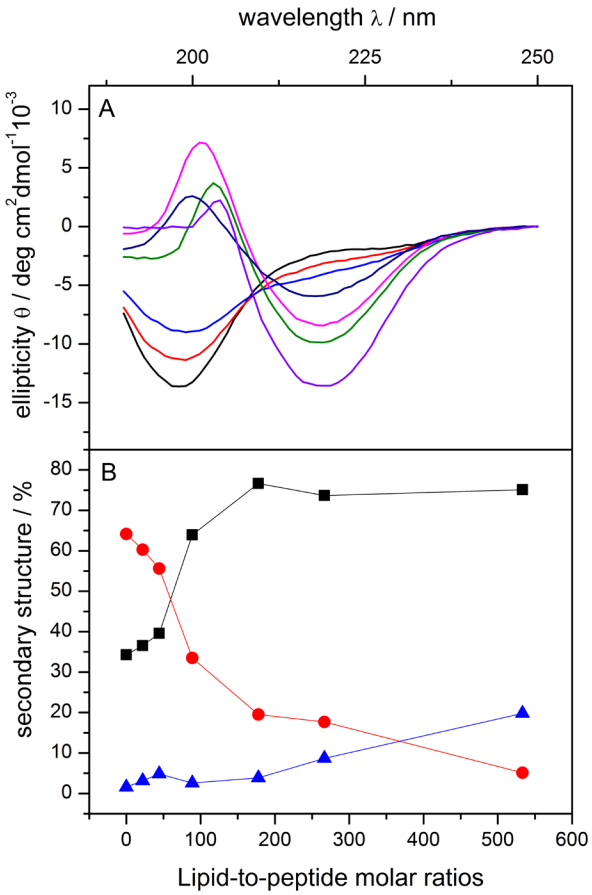
wavelength λ / nm
200
225
250
A
ellipticity θ / deg cm²dmol⁻¹10⁻³
10
5
0
-5
-10
-15
B
secondary structure / %
80
70
60
50
40
30
20
10
0
0
100
200
300
400
500
600
Lipid-to-peptide molar ratios

Figure 8

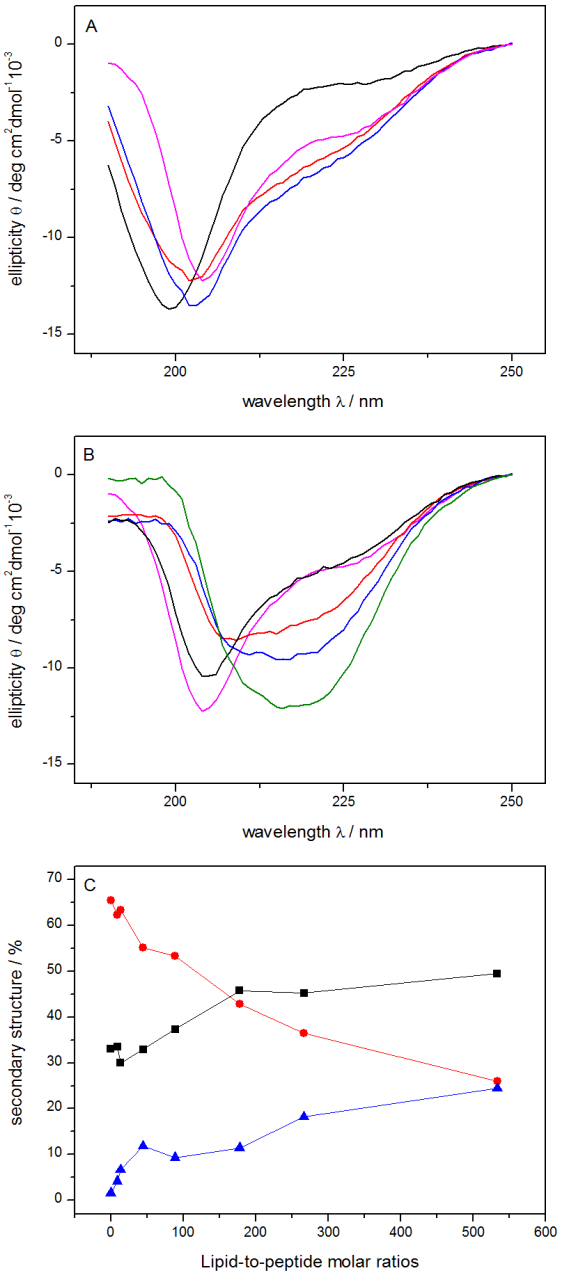
A
ellipticity θ / deg cm²dmol⁻¹10⁻³
0
-5
-10
-15
200
225
250
wavelength λ / nm
B
ellipticity θ / deg cm²dmol⁻¹10⁻³
0
-5
-10
-15
200
225
250
wavelength λ / nm
C
secondary structure / %
70
60
50
40
30
20
10
0
0
100
200
300
400
500
600
Lipid-to-peptide molar ratios

Figure 9

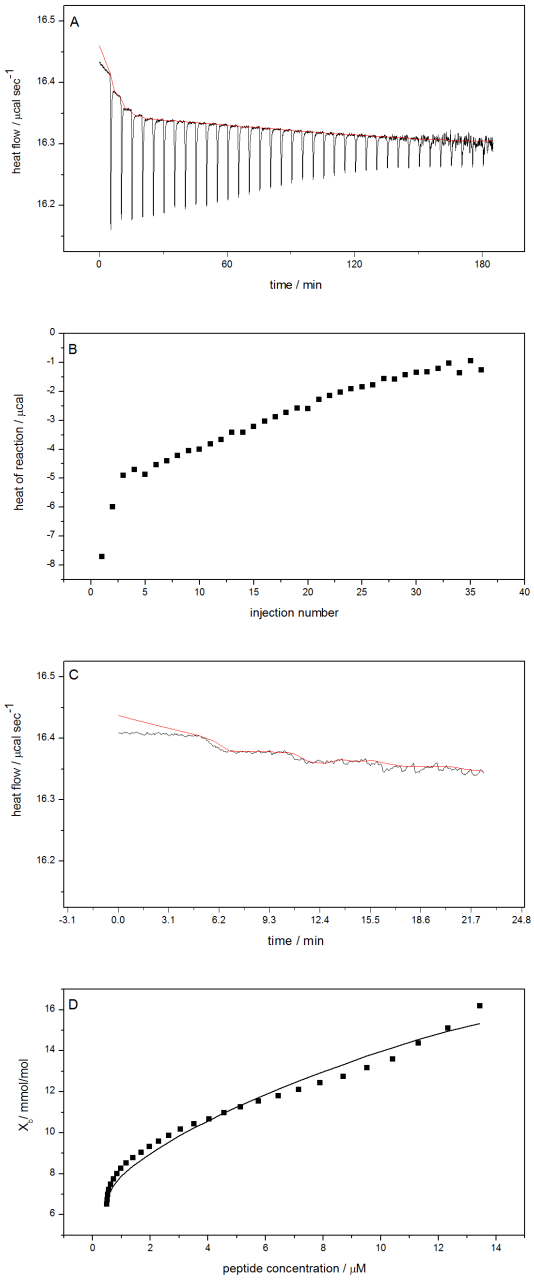
A
heat flow / µcal sec^{-1}
time / min
B
heat of reaction / µcal
injection number
C
heat flow / µcal sec^{-1}
time / min
D
X_2 / mmol/mol
peptide concentration / µM

Figure 10

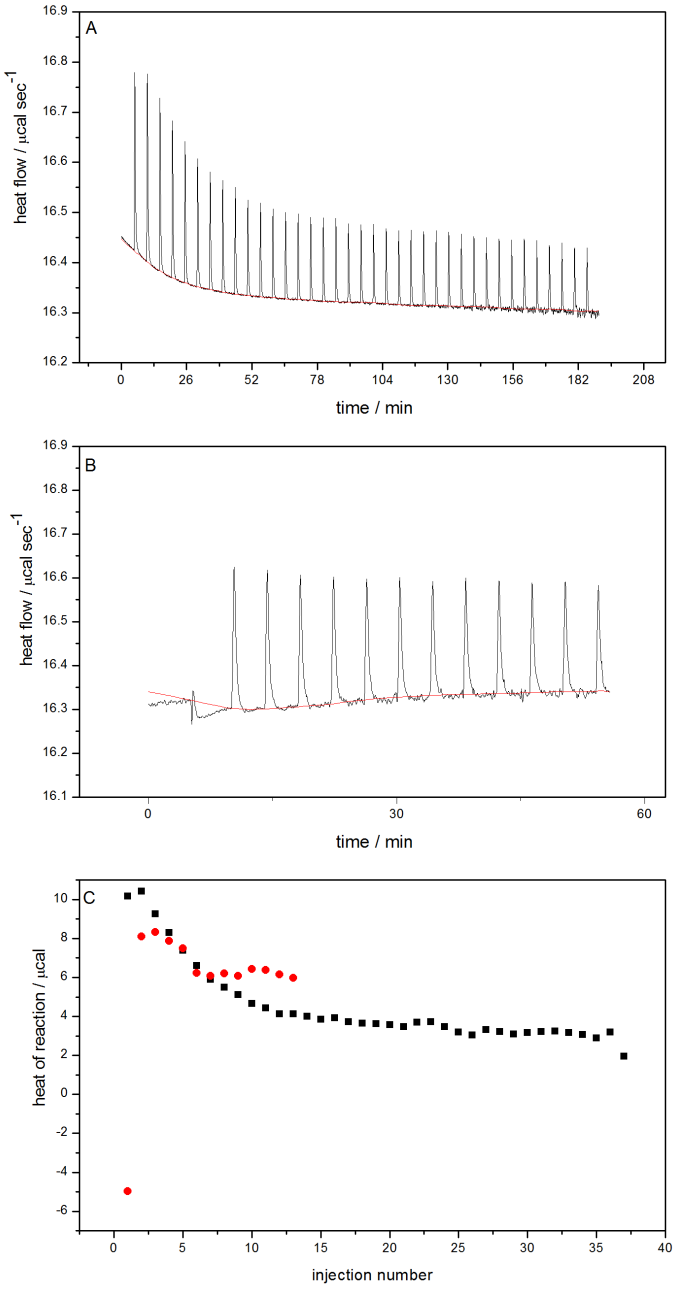
A
heat flow / µcal sec-1
time / min
B
heat flow / µcal sec-1
time / min
C
heat of reaction / µcal
injection number

Figure 11

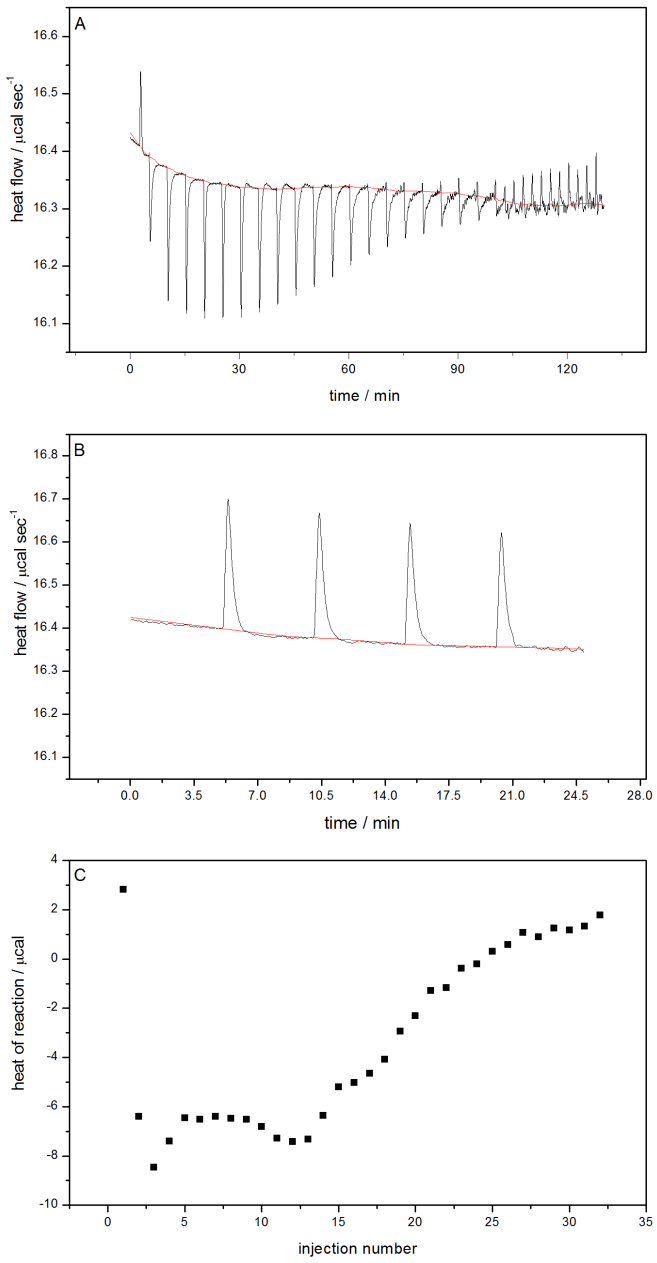
A
heat flow / µcal sec-1
time / min
B
heat flow / µcal sec-1
time / min
C
heat of reaction / µcal
injection number

Figure 12

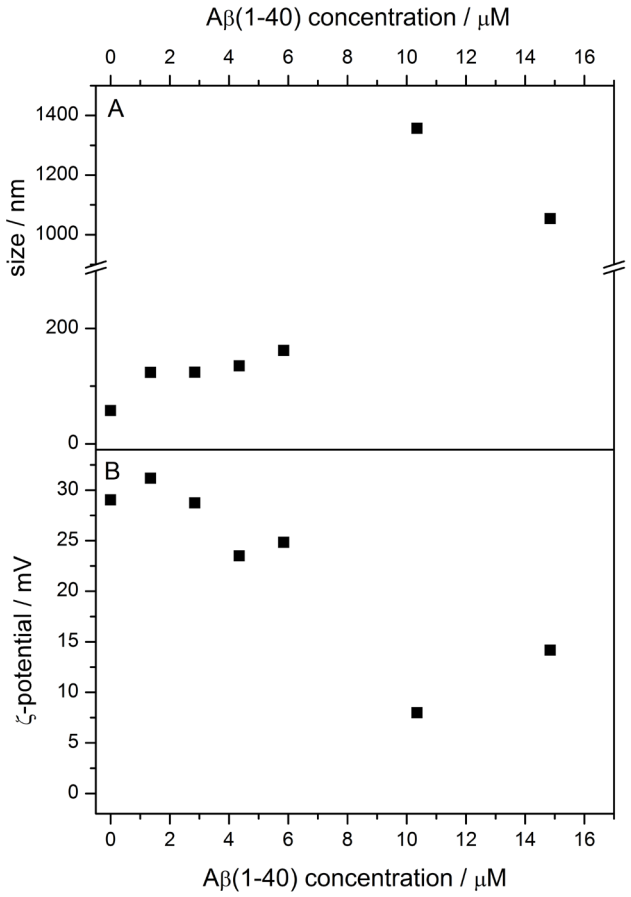
Aβ(1-40) concentration / μM
A
size / nm
B
ζ-potential / mV
Aβ(1-40) concentration / μM

Figure 13

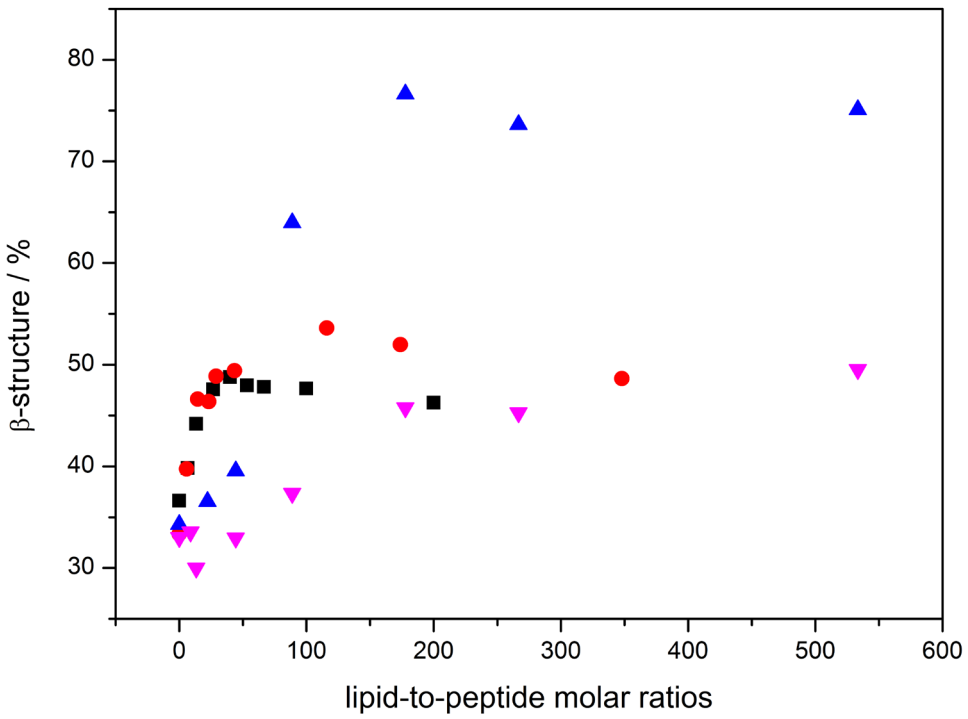
β-structure / %
80
70
60
50
40
30
0
100
200
300
400
500
600
lipid-to-peptide molar ratios

Figure 14

5. Summary

The aim of the thesis is a better understanding of the thermodynamics and structural aspects of the interaction of Aβ(1-40) with lipid membranes and glycosaminoglycans (GAGs). We investigate the thermodynamic driving forces of the random-coil-to-β-structure transition of Aβ(1-40) in a membrane environment. In contrast to previous reports, we use anionic lipid vesicles coated with the polymer poly(ethylenglycol) (PEG), which prevents vesicle aggregation. Circular dichroism (CD) spectroscopy demonstrate that PEGylated vesicles induce a random-coil-to-β-structure transition with a defined conformational endpoint in Aβ(1-40) and four double d-isomers. The additional transition to α-helix of Aβ(1-40), reported in earlier studies for high lipid-to-peptide molar ratios of non-PEGylated anionic vesicles, was diminished. Hence, the defined conformational endpoint allows for the quantification of the membrane-induced β-structure, which is dependent on the location of the double-d substitution in the peptide sequence. Isothermal titration calorimetry (ITC) reveals the thermodynamic binding parameters for the studied peptides. The thermodynamic parameters of the β-structure formation are deduced by correlating the structural data with the thermodynamic binding parameters. In addition, we study the effect of pH on the thermodynamic binding parameters of Aβ(1-40).

In order to elucidate the role of GAGs in the Aβ(1-40) fibrillization process, we investigate the interaction of Aβ(1-40) with heparin. First, CD measurements demonstrate the effect of physico-chemical parameters, including pH, ionic strength and temperature, on the conformational state of Aβ(1-40). These measurements lead to experimental conditions, in which the interaction of monomeric Aβ(1-40) with

heparin can be studied. The monomeric state of Aβ(1-40) is a prerequisite for a full thermodynamic characterization of the interaction by ITC. Under the given conditions, ITC experiments demonstrate that Aβ(1-40) interacts with high affinity with heparin. CD spectroscopy reveals a structural transition of Aβ(1-40) from random-coil to β-structure. By studying the double-d isomers of Aβ(1-40), we identify a molecular pattern of the Aβ(1-40)-heparin interaction. We predict the binding constant for the Aβ(1-40)-heparin interaction at physiological ionic strength by using the oligolysine model. Finally, CD measurements reveal that GAGs do not induce a structural transition of Aβ(1-40) at physiological pH.

In the last part of the thesis, the interaction of Aβ(1-40) to cationic lipid vesicles is studied. CD spectroscopy measurements demonstrat that Aβ(1-40) undergoes two sequential structural transitions upon the binding to cationic membranes. First, a random-coil to β-structure transition is observed, followed by a transition to an α-helix at high lipid-to-peptide molar ratios. Compared to anionic lipid vesicles, the membrane-induced β-structure of Aβ(1-40) is less pronounced for cationic membranes, mainly due to the higher pH value at the membrane surface. The thermodynamics of the Aβ(1-40) membrane binding is studied with ITC for three buffer conditions, namely Tris-HCl, Mops and Hepes. Dynamic light scattering measurements show that the binding of Aβ(1-40) induces the formation of large aggregates.

6. Acknowledgment

This work was carried out from March 2008 until June 2012 in the laboratory of Prof. Dr. Joachim Seelig in the Division of Biophysical Chemistry at the Biozentrum of the University of Basel.

First of all I would like to express my sincere gratitude to my doctoral supervisor, Prof. Joachim Seelig, for offering me the opportunity to work on this interesting project. I particularly appreciate his guidance and constant support throughout this thesis.

I also want to thank Prof. Dr. Anna Seelig for her encouragement and for several discussions concerning the thesis.

I am very grateful to Prof. Dr. J. Huwyler for serving as a referee for this thesis.

My warm thanks go to Dr. André Ziegler for his scientific and private advice and for answering my innumerable questions.

I am very grateful to Therese Schulthess for several contributions concerning this thesis and her continuous advice and support with experiments.

I also want to thank Susanna Notz for her support in administrative matters and numerous encouragements.

Furthermore, I am very grateful to Leo Faletti and Simon Saner for their support whenever technical problems appeared.

I also want to thank my other present and former colleagues of the Seeligs' lab and the floor mates for the inspiring working environment: Dr. Päivi Äanisma, Frauke Assmus, Maria de Fatima Leite dos Reis, Christine Egger, Estefania Egido de Frutos, Dr. Cinzia Espostio, Dr. Sarah Güthe, Angie Klarer, Dr. Gabriela Klocek, Beatrix Lang, Dr. Caroline Loew, Xiaochum Li Blatter, Dr. Christian Maag, Rita Müller, Dr. Samantha Perspicace, Corinne Salvisberg, Dr. Andreas Beck, Dr. Andreas Bruns, Dr. Georg Funk, Dr. Michael Hayley, Dr. Matthias Meier, Koji Mochizuki, Reto Sauder, Dr. Timothy Sharpe, Dr. Fabian Zehender, Dr. Matthias Zwick.

Last but not least I owe my loving thanks to my family and friends.